Thermochromic properties of VO_2 nano-coatings by inverted cylindrical magnetron sputtering

by

Itani Given Madiba

Dissertation submitted in part fulfilment of the requirements

for the degree of

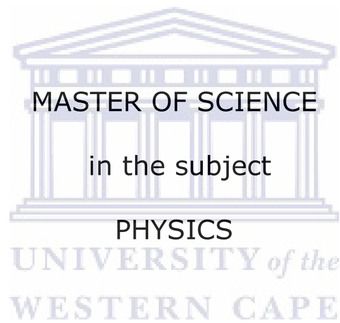

MASTER OF SCIENCE

in the subject

PHYSICS

at the

UNIVERSITY OF WESTERN CAPE

SUPERVISOR:

PROF M MAAZA (iThemba LABS)

CO-SUPERVISORS:

Dr B. D. NGOM (Nanoafnet-iThemba LABS)

PROF. M.T TSCHOKONTE (UWC)

August 2012

I, Itani Given Madiba declare that this is my work. It is being submitted in part fulfilment of the requirement for the degree of Master of Science at the University of Western Cape. It has not been submitted before for any degree or examination, at any other university.

Signature: .... Date: ....

ACKNOWLEDGEMENTS

WITH GOD NOTHING IS IMPOSSIBLE

I would like to thank God; the all mighty for being with me all the way through all the challenges and difficulties. It has been a rough journey but the power of his name kept me going, there are times where I thought I should quit and can't make it at all but his word kept on telling me that's where your destiny lies. Thank u lord.

I express my sincere gratitude and appreciate the financial support that I received from NSFAS through all my undergraduate degree. The support that I got was unbelievable as coming from grade 12; I had no single cent to land me in university. The 100% financial assistance I received gave me hope, worked harder in a way that the road to my destiny got wide open. I couldn't ask more than the help I was getting and may the same assistance lands to the upcoming needy young stars like me.

I would also like to sincerely acknowledge Ithemba labs and NRF to give me the opportunity to explore myself deeper into research and science straight away from honors degree. It was not going to be possible for me to move from Limpopo to study in Capetown but that all came possible through the support from ithemba and NRF. In particular I deeply appreciate the comfort welcome I received from ithemba labs into their research facilities.

UNIVERSITY of the
WESTERN CAPE

I never had a clue how I will make it at masters but through the help, words of encouragement, advice, and leadership I got from my supervisor I started to have light and gain strong belief in myself. Prof Malik Maaza has been everything that I could ask for; he was a father figure who was always there to show me the way even if it means he has to stay in the laboratory assisting me in experiments. May God bless him.

I greatly appreciated the support from my co-supervisors Dr B.D Ngom and Prof. M.T Tschokonte for giving me the opportunity to work with them, giving me direction, help in almost every aspect of my thesis. I feel blessed to have worked with you.

I also would like to thank the management and colleagues from ithemba labs who helped me in my work;

UNIVERSITY of the
WESTERN CAPE

- Dr. R. Nemutudi, HOD of Materials Research Department, iThemba LABS-Cape Town, for warm welcome and making the facilities at MRD available for some of the experiments.
- Mr. P. Sechogela, for being a kind office mate and helping me with RBS measurements
- Prof Carlos pineda and Dr Mandla Msimanga for their patience and helping me with RBS and ERDA measurements.
- Dr. R. Butcher, for helping me with XRD measurements.
- Dr. M. Nkosi, for helping in AFM imaging.
- Dr J.B Kana Kana, for helping in UV-Visible for his advice and direction on VO_2 study.

- Prof. O. Nemraoui, for helping me in synthesizing the samples.
- Dr L. Kotsedi for helping in some experimental work.

I would also like to acknowledge fellow students who on daily basis were an integral part of my study; Mr N. Nyangiwe, MR Z. Khumalo, Mrs Alien simo, Mr B. Sone, Mr S.Khamlich.

Friends were there to socialize, advise and moral support, i would like to acknowledge; Makhado Ramovha, KanaKana Muofhe, Mashudu Raphunga, Itani Tshihatu, Herbet Kutama, Nemulodi fhumulani, Sfiso Khanyile, Samuel Maliaga, Bob Cheuene and Albert Ramashia. The love and support from my friends gave me courage in everything I faced.

UNIVERSITY of the
WESTERN CAPE

Lastly I would like to humble myself give thanks to all that my family has done for me through this entire difficult journey; my grandmother, my brother, my uncles, my Mother, Mr and Mrs Madia and their whole family, and my extended family. It was not easy at all but with the litte that we had, it became possible for me to be here today. THANK YOU! Ndaa

I dedicate this thesis to my family for their undying support and love.

ABSTRACT

Vanadium dioxide (VO_2) films have been known as the most feasible thermochromic nano-coatings for smart windows which self control the solar radiation and heat transfer for energy saving and comfort in houses and automotives. Such an attractive technological application is due to the fact that VO_2 crystals exhibit a fast semiconductor-to-metal phase transition at a transition temperature T_M of about 68°C, together with sharp optical changes from high transmitive to high reflective coatings in the IR spectral region. The phase transition has been associated to the nature of the microstructure, stoichiometry and some other surrounding parameters of the oxide. This study reports on the effect of the crystallographic quality controlled by the substrate temperature on the thermochromic properties of VO_2 thin films synthesized by inverted cylindrical magnetron sputtering. Vanadium dioxide thin films were deposited on glass substrate, at various temperatures between 350 to 600 ^{0}C, deposition time kept constant at 1 hour. Prior the experiment, deposition conditions such as base pressure, oxygen pressure, rf power and target-substrate distance were carefully optimized for the quality of VO_2 thin films. The reports results are based on AFM, XRD, RBS, ERDA and UV-VIS. The atomic force microscopy (AFM) was used to study the surface roughness of the thin films. Microstructures and orientation of grain size within the VO_2 thin films were investigated by the use of X-ray diffraction technique. The stoichiometry and depth profiles of the films were all confirmed by RBS and ERDA respectively. The optical properties of VO_2 were observed using the UV-Vis spectrophotometer.

Keywords: Vanadium dioxide; Transition temperature; microstructure; Thermochromic; Substrate temperature; Sputtering; Optical properties; Thin films.

UNIVERSITY of the
WESTERN CAPE

TABLE OF CONTENT

ACKNOWLEDGMENTS III

ABSTRACT Vii

TABLE OF CONTENTS Viii

LIST OF TABLES Xi

LIST OF FIGURES Xii

CHAPTTER ONE **1**

1.1 Introduction **1**

Motivation and objectives **3**

Aims **4**

Thesis outline **4**

1.2 Literature review on VO_2 **5**

1.2.1 Electronic and Structure on VO_2 **10**

1.2.2 Optical properties of VO_2 **20**

1.2.3 Electrical Properties of VO_2 **23**

1.2.4 VO_2: Phase transition characteristics **24**

1.2.5 VO_2: Deposition techniques **25**

1.3 Reference **26**

CHAPTER TWO **33**

2 OVERVIEW ON SPUTTERING **33**

2.1 INTRODUCTION AND PRINCIPLES OF SPUTTERING **33**

2.1.1 Inroduction **33**

2.1.2 Principles of sputtering **34**

2.1.3 Sputtering parameters **36**

2.2 Different methods of sputtering **37**

UNIVERSITY of the
WESTERN CAPE

2.2.1 Reactive sputtering 37

2.2.2 Direct DC Sputtering 39

2.2.3 Magnetron Sputtering 40

2.2.4 Radiofrequency (RF) sputtering 41

2.3 Choice of deposition methods 43

2.4 Radiofrequency inverted cylindrical magnetron sputtering 44

2.5 Modes of thin films 47

2.6 References 51

CHAPTER THREE 54

3 CHARACTERIZATION TECHNIQUES 54

3.1 Atomic force microscopy (AFM) 54

3.1.1 Principles of AFM 54

3.1.2 Modes of operation 56

3.2 X ray diffraction technique 61

3.2.1 Fundamental principles 61

3.2.2 Principle of operation 63

3.3 Rutherford backscattering spectrometry (RBS) 66

3.3.1 Kinematic factor 67

3.3.2 Scattering cross section 69

3.3.3 Stopping power 70

3.4 Elastic recoil detection analysis 71

3.4.1 Introduction 71

3.4.2 Principles of ERDA 72

3.4.3 Depth profiling 73

3.4.4 Depth resolution 74

UNIVERSITY of the
WESTERN CAPE

3.5 UV-Visible spectrophotometer **75**

3.5.1 Basic principles of the UV-Vis **75**

3.6 References **78**

CHAPTER FOUR **80**

4 RESULTS AND DISCUSSIONS

4.1 Synthesis and experimental details **80**

4.1.1 Synthesizing of thin films **80**

4.1.2 Thin films analysis **80**

4.2 Results and discussions **83**

4.2.1 XRD- structure analysis **83**

4.2.2 Surface morphology **87**

4.2.3 Stoichiometry and composition of thin films **93**

4.2.4 Elemental analysis and depth profiling of thin films **99**

4.2.5 Optical properties **105**

4.2.6 References **110**

CHAPTER FIVE **110**

5.1 Conclussions **111**

5.2 Future work **111**

UNIVERSITY of the
WESTERN CAPE

LIST OF TABLES

1.1 Anderson crystal structure parameters of M1-VO2 **16**

1.2 Crystal structure parameters given by longo and Kierkegaard **16**

1.3 Crystal structure parameters of M_1 VO_2 given by wentzcovitch **17**

4.1 Thickness and composition of VO_2 thin films at different substrate temperatures obtained from the RBS simulations **98**

4.2 Comparison of ERDA and RBS thickness **104**

LIST OF FIGURES

1.1	Crystallographic structures of vanadium dioxide (VO_2)	**8**
1.2	Variation of VO_2 electrical resistivity with temperature	**9**
1.3	Phase diagram for the vanadium-oxygen system	**11**
1.4	VO_2 unit cells above and below the phase transition	**14**
1.5	Orientation and dimensions of tetragonal/rutile unit cells of VO_2	**15**
1.6	Energy-level diagram of VO_2	**19**
1.7	Optical switching mechanism of VO_2 thin films between semiconductor and metal state	**21**
2.1	Sputter deposition systems	**35**
2.2	Schematic of the inverted cylindrical magnetron sputter gun	**45**
2.3	island growth (volmer-weber)	**50**
2.4	layer by layer growth	**50**
2.5	layer plus island formation	**50**
3.1	Principles of atomic force microscopy	**57**
3.2	Morphology of a 3D image of a VO_2 thin film grown on glass substrate	**60**
3.3	Bruker's X-ray Diffraction D8-Discover instrument at iThemba LABS	**65**
3.4	Illustration of the electromagnetic spectrum	**76**
4.1	XRD spectra of VO_2 thin films	**86**
4.2	(a) Evolution of the (011) plan of VO_2 thin films at different substrate temperature. (b): dependence of crystalline grain size on substrate temperature of VO_2 thin films along (011) plan	**87**
4.3	3D AFM image of VO_2 at 350°c	**88**
4.4	3D AFM image of VO2 at 400°C (top) and 450°c (bottom)	**89**
4.5	3D AFM image of VO2 at 500°C (top) and 550°c (bottom)	**90**

UNIVERSITY of the
WESTERN CAPE

4.6	3D AFM image of VO2 thin film at 600°C	**91**
4.7	Dependence of roughness on substrate temperature of VO_2 thin films	**92**
4.8	RBS spectrum of VO_2 at 350°C	**95**
4.9	RBS spectrum of VO_2 at 500°C	**96**
4.10	RBS spectrum of VO2 at 600°C	**97**
4.11	Vanadium edge fit (701±110) x 10^{15} at/cm^2 of VO_2 film at 350^{0}C	**101**
4.12	Vanadium edge fit (450±90) x 10^{15} at/cm^2 of VO_2 film at 500^{0}C	**102**
4.13	Vanadium edge fit (557±120) x 10^{15} at/cm^2 of VO_2 film at 600^{0}C	**103**
4.14	Spectral transmission of VO_2 films at 350-600°C	**106**
4.15	Cycling branches of VO_2 between heating and cooling at steps of 5°c using λ=1100 nm from 25°C to 100°C	**107**
4.16	Trend of the transition temperature (T_{tr}) with the substrate temperature	**108**

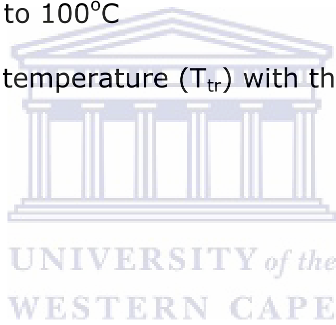
UNIVERSITY of the
WESTERN CAPE

CHAPTER 1

1-INTRODUCTION AND LITERATURE REVIEW ON VO_2

1.1 INTRODUCTION

Smart materials have shown a subject of great interest in the past decade, arising from research in many different areas, with large overlap in nanotechnology. Initial nanotechnology influenced improvements to smart materials with simple changes to existing technologies. The future however holds possibilities for extremely complex solutions for producing not only smart materials but ones that are highly intelligent. These materials applications may incorporate nano-sensors, nano-computers and nano-machines into their structure. This will enable them to sense changes in the environment around them and respond in a predictable way rather than make simple changes caused by the environment. Some types of smart materials include piezoelectric materials; those that either produce a voltage when stressed or alter shape under the influence of an electric charge. Thermochromic materials change color in response to changes in temperature, and those that change color due to light conditions are known as photochromic. A wide range of applications of these smart photochomic materials is observed in areas like energy conservation with highly efficient batteries and smart textiles that can change colour and pattern

UNIVERSITY of the
WESTERN CAPE

upon the appearance of the surrounding environment, and Surveillance using "smartdust" and "smartdust motes" that are nano-sized machines housing a range of sensors and wireless communication devices. This work focuses entirely on the thermochromic "smart material" called Vanadium dioxide.

Vanadium dioxide is one of the most interesting and studied oxide of the vanadates family. It undergoes a reversible first order phase transition, which shows the transformation of two distinct phases at a transition temperature of around 68°C [1]. Vanadium dioxide has a monoclinic structure below transition temperature and become tetragonal above transition temperature. It has narrow band gap of 0.7 eV below transition temperature. This phase transition is accompanied by greater changes in the VO_2 physical, electrical and optical properties [2, 3]. Due to changes of properties in the phase transition, vanadium dioxide has been proposed for the use in numerous applications ranging from anti-laser shields to smart windows, which selectively filter radiative heat during hot weather conditions. This application plays a major role in our society and community by providing windows that have been coated by vanadium dioxide thin film, which prevents heat from entering our households and there is less need for energy intensive cooling by air conditioning. Other applications include VO_2 used as a thermal regulator for space crafts, switching devices and modulators.

UNIVERSITY of the
WESTERN CAPE

The problem proposed to study in this work has two aspects: first from the technical perspective we need to deposit pure VO_2 nano-coatings by a homemade inverted cylindrical magnetron sputtering at iThemba LABS, and on the other hand optimize and understand the effective parameters that influence the semiconductor

to metal transition (SMT) of VO_2. The physics behind the SMT of VO_2 is still a subject of debate at this stage but certain parameters/factors; microstructure, stress, strain, morphology, and substrate temperature have been proposed to affect the SMT of VO_2.

Motivation and objectives

Scientifically point of view, it is very interesting to study nanostructured materials, either because their properties may be modified as a function of the particle size. These smart materials whose mechanisms are based on phase transitions, such as metal-semiconductor transformations, are particularly intriguing, since the associated property changes induced by external perturbations such thermal stimulus can be rapid, reversible, and may span several orders of magnitude. This is certainly true for the specific case of vanadium dioxide.

The main objective of this research has been to explore physical properties of thin solid films materials and to carry out fundamental research studies for describing the relationship between substrate growth temperature, structure / composition and physical properties of thermochromic VO_2.

UNIVERSITY of the
WESTERN CAPE

Aims

The aim of this work is to synthesize VO_2 nano-coatings deposited on glass substrates at various substrate temperatures by the inverted cylindrical magnetron sputtering (ICMS) technique for their application as cost effective intelligent coatings for smart windows. We are interested in investigating the effect of the substrate temperature on the crystalline, morphology and optical properties of VO_2 thin films.

Thesis outline

The whole work is structured as follows:

UNIVERSITY of the
WESTERN CAPE

Chapter 1 gives an introduction, motivation, aims, objectives and also the state of the art in VO_2 as well some latest findings of its phase transition. Its spectacular solid-solid phase transition or thermal induced metal-insulator phase transition remains a hot topic debated by the researchers for a half of century.

Chapter 2 gives an overview on the physical method of deposition used in this study. It explains different kind of sputtering techniques that has been used in the synthesis of VO_2 and introduces the off-axis sputtering technique, inverted cylindrical magnetron sputtering, used for the synthesis of VO_2 thin films in this

study. In addition the sputtering parameters and modes of thin films will be described in this chapter.

Chapter 3 is dedicated to describing and explaining the different techniques employed throughout this work to characterize their structure, morphology and optical properties.

Chapter 4 describes the experimental details, synthesis and characterization of the VO_2 thin films, also with the results and discussion of the successfully deposited VO_2 thin films by inverted cylindrical inverted magnetron sputtering.

UNIVERSITY of the
WESTERN CAPE

Chapter 5 lastly gives an overall conclusion and future work is given related to the results obtained from this study.

1.2 LITERATURE REVIEW ON VO_2

Materials that exhibit an ultrafast thermochromic effect caused by a phase transition (PT) or induced by laser excitation are of central interest at present in optoelectronics and nonlinear optics (NLO) due to their potential application in ultrafast optical switching and passive optical device systems. A number of oxides categorized as Mott insulators exhibit an insulator-to-metal transition upon heating at a specific temperature known as the metal-insulator transition (T_{tr}). Most

notably, vanadium oxides, such as V_2O_3 (T_{tr} = 150 K) and VO_2 (T_{tr} = 341 K), show an increase of conductivity by a factor greater than 10^4 across T_{tr}; and this results in a significant change in the optical properties. Vanadium dioxide is a rich and widely studied material. It is of technological interest as its transition point occurs at the readily accessible temperature of 68°C which can be easily reached by physical warming, heat deposition, or by laser excitation at a sufficient level [1, 2].

Vanadium dioxide (VO_2) has been perennial in theoretical and experimental condensed-matter and materials research for half a century [3]. Bulk VO_2 crystals exhibit a semiconductor to metal transition (SMT), also widely known as the metal-insulator transition (MIT), at a transition temperature of 68 °C, accompanied by a first-order structural phase transformation from a monoclinic (M_1-$P2_1/c$) for low-temperature semiconductor to a tetragonal (rutile-$P4_2/mnm$) structure for the high-temperature metal [4] characterized by a small lattice distortion along the c-axis.

UNIVERSITY of the
WESTERN CAPE

In the metallic high-temperature tetragonal rutile structure, each vanadium ion is situated in the centre of an oxygen octahedron with the parameters a = b = 4.55 Å, c = 2.88 Å [5, 6]. The semiconductor low-temperature form of VO_2 is a monoclinic distortion of the rutile that involves a pairing between two V^{4+} and an off-axis displacement of alternate vanadium ions along the rutile c-axis. The resultant distortion lowers the symmetry to a monoclinic structure with a = 5.75 Å, b = 5.42 Å and c = 5.38 Å [5, 7].

The two crystallographic structures are illustrated in Figure 1.1. In fact, it is the intricate interplay between electronic and structural degrees of freedom between carrier localization due to electron-electron repulsion (Mott-Hubbard correlation) [8,

9] and unit-cell doubling due to lattice instability (Peierls distortion) [8, 9] that has been at the heart of an enduring debate [10-, 13, 14-21] about the precise cause and effect linkage in the mechanism of the VO_2 transition.

As a transition-metal oxide with narrow d-electron bands, this strongly correlated electron system is extremely sensitive to small changes in extrinsic parameters such as temperature, pressure, or doping [15,22-25]. The first-order phase transition is accompanied by an abrupt change in resistivity of several orders of magnitude as illustrated in figure 1.2 , as well as its sharp change optical properties in the near-infrared region [26-28]. In bulk crystals, the change in resistivity is of the order of 10^3 - 10^5 with a hysteresis width of ~ 1°C [27]. In thin films, on the other hand, hysteresis widths may be of the order of 10-15 °C; [29] in nano-precipitate VO_2, the hysteresis widths may be even larger [30].

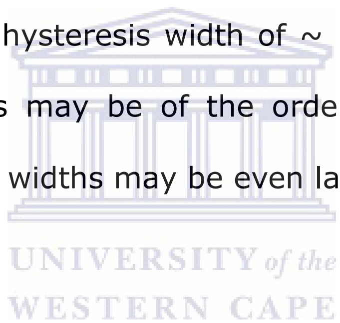
UNIVERSITY of the
WESTERN CAPE

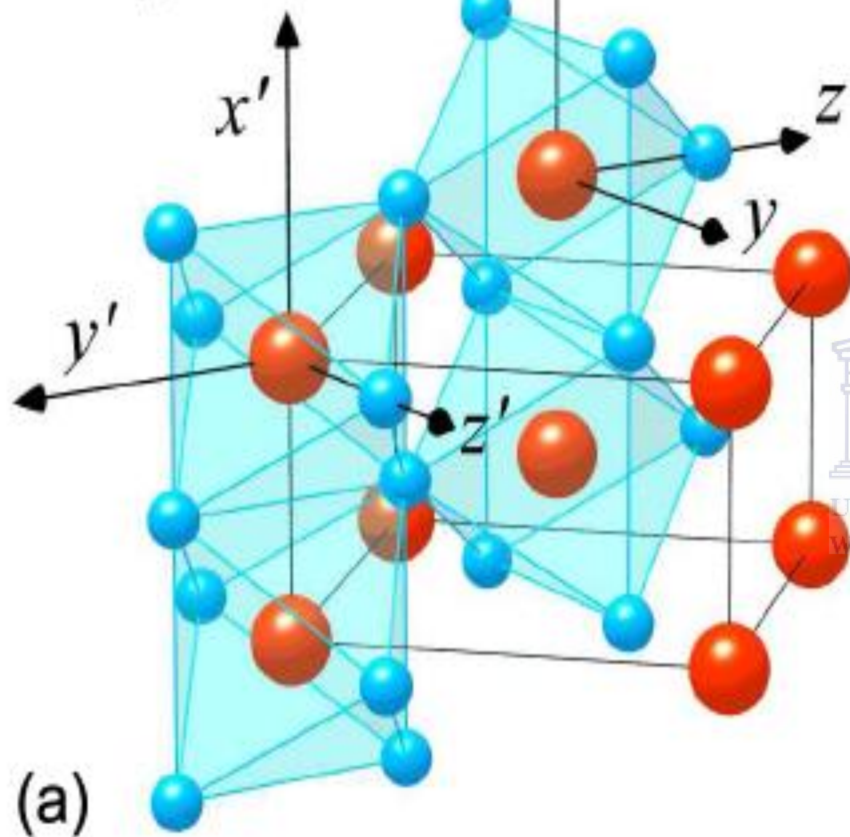

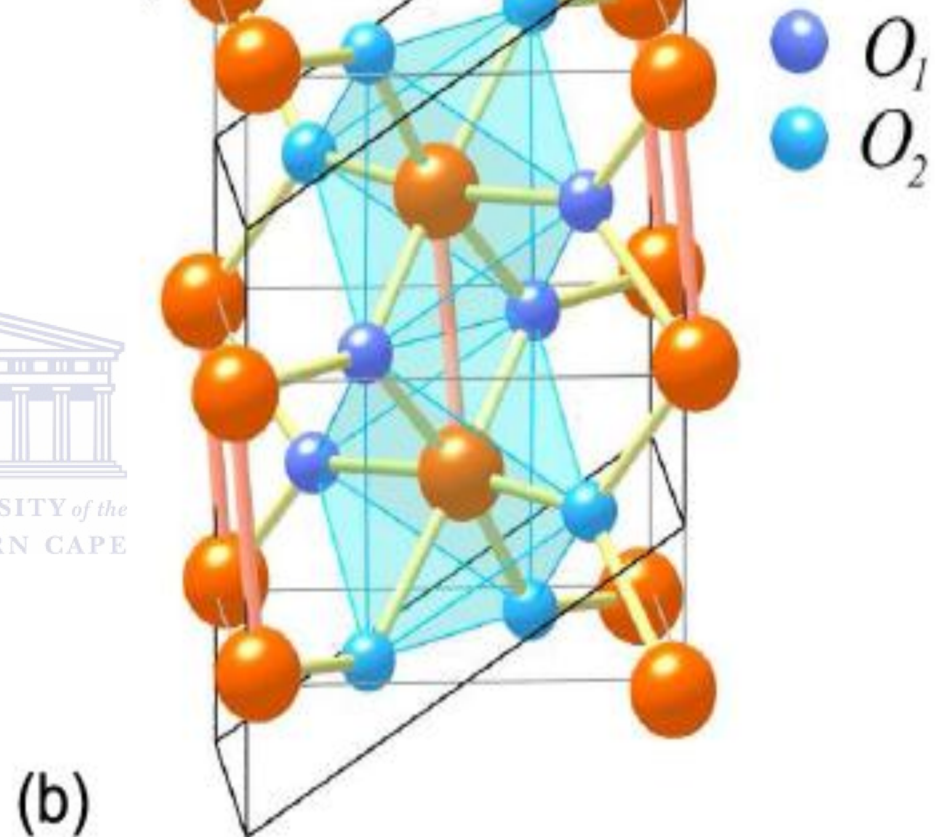

UNIVERSITY of the
WESTERN CAPE

Figure 1.1: Crystallographic structures of vanadium dioxide (VO_2) [25].

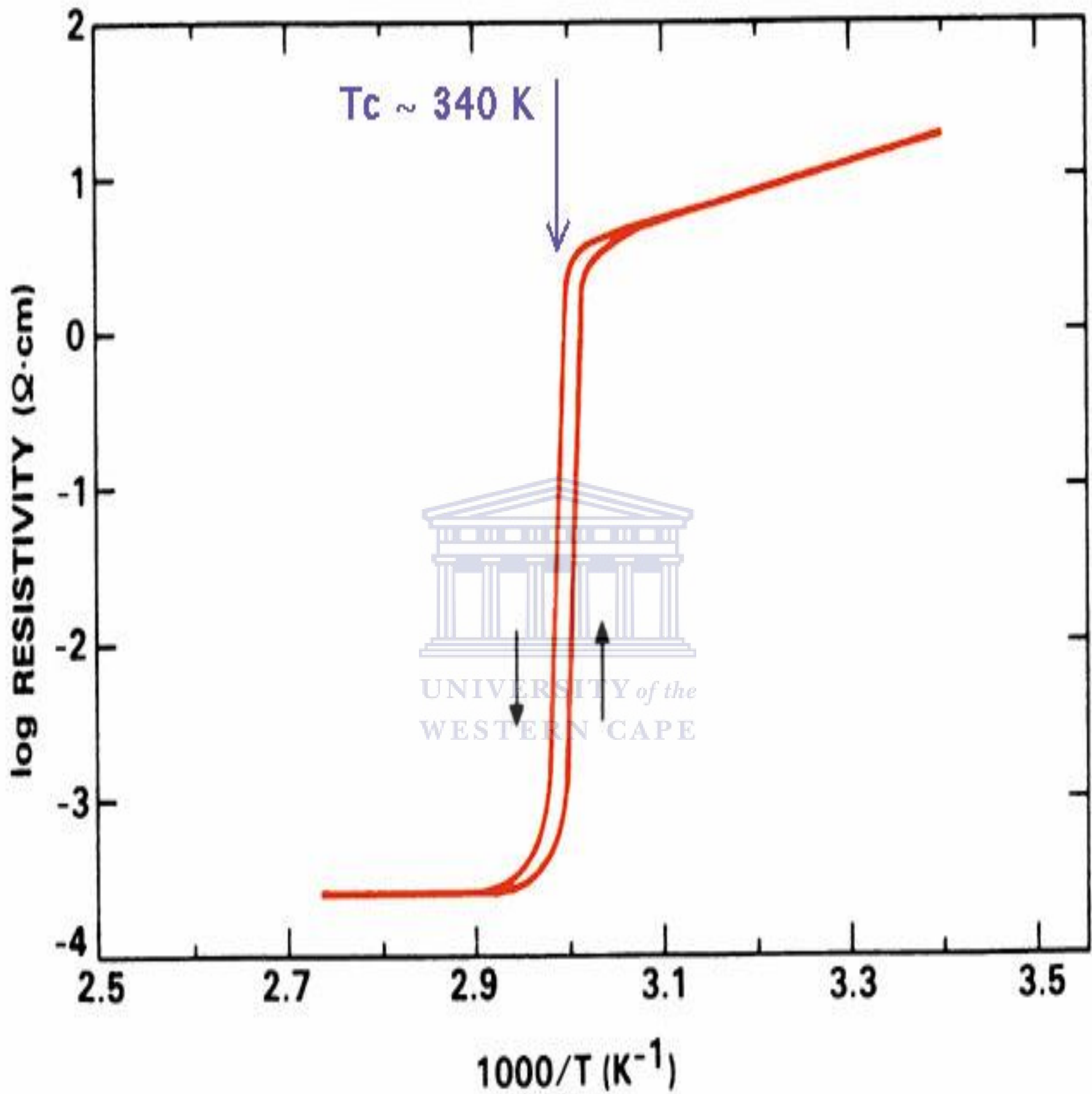

UNIVERSITY of the
WESTERN CAPE

Figure 1.2: Variation of VO_2 electrical resistivity with temperature.

The change in resistivity is of the order of 10^3 - 10^5 with a hysteresis width of ~ 1 °C After Reference [27].

1.2.1 ELECTRONIC and STRUCTURE OF VO_2

Vanadium is known to exist in different valence states and, consequently, to have many possible oxides. Oxides where all of the vanadium atoms have the same valence are well known: VO, VO_2, V_2O_3, and V_2O_5, but there also oxides where the vanadium atoms have different valences: between V_2O_3 and VO_2, the series of Magneli phases V_nO_{2n-1} (n> 1) and also V_4O_9, V_6O_{13} and V_3O_7 [31]. In addition to VO_2, many of these vanadium oxides also exhibit metal-insulator transitions at transition temperatures specific to their stoichiometric phases; as depicted in Figure 1.3 and others do not exhibit any metal-insulator transition such as V_2O_5, V_7O_{13}, V_5O_9, V_3O_5, V_6O_{11}. Among these numerous oxides, VO_2 is of special interest given the existence of a solid-solid phase transition at T_{tr} = 68 ^oC with sharp switching properties aforementioned.

UNIVERSITY of the
WESTERN CAPE

Above the transition temperature T_{tr}, the R-phase of VO_2 exhibits the characteristics of a metal and has a tetragonal body-centered unit cell of vanadium (V) atoms, each surrounded by an orthorhombically distorted octahedron of six oxygen (O) atoms. The octahedra stack by sharing edges that form chains along the c-axis, which are in turn coupled to each other by sharing corner O atoms. The closest V-V distance is 2.85 Å in chains along the c-direction (Figures 1.1, 1.4, and 1.5).

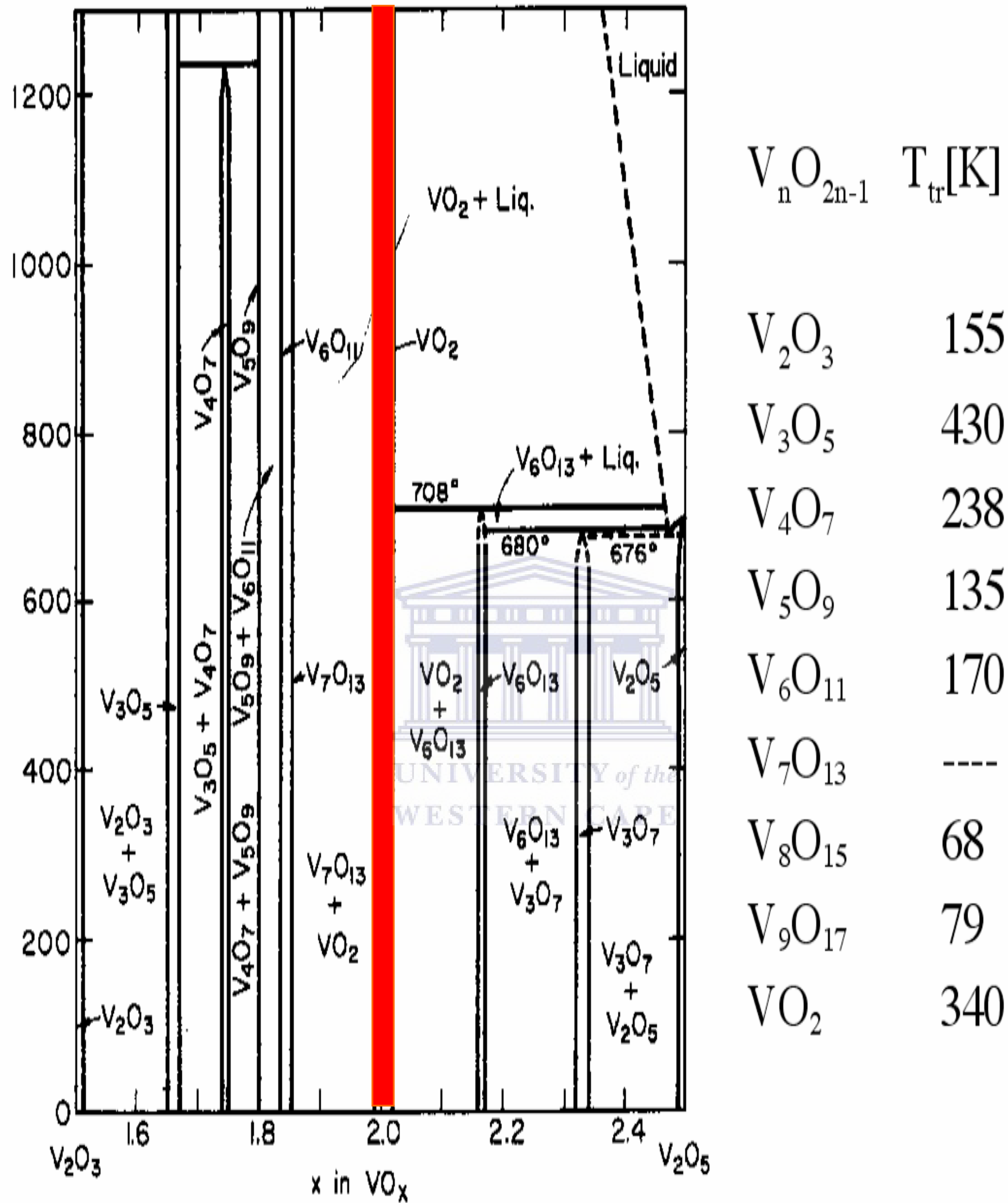

Figure 1.3: Phase diagram for the vanadium-oxygen system. It gives the corresponding phase transition temperatures of several vanadium oxides. After reference [32].

The metal atoms are located at the Wyckoff positions (2a): (0,0,0), (1/2,1/2,1/2) and the oxygen atoms are located at the positions (4f): ±(u,u,0), ±(1/2+u, 1/2-u,1/2). According to McWhan the lattice constants and the internal oxygen are: a = 4.5546 Å, c = 2.8514 Å [33]. According to Eyert [25], the lattice parameters are: for the tetragonal rutile phase, a_t = b_t = 4:5546Å, c_t = 2:8514Å, axial = 90 °. Below T_{tr}, the M_1-phase of VO_2 is a monoclinic semiconductor with a ~0.7-eV optical band gap [13, 28, 34, 35-36] and a distorted structure (Figures 1.1, 1.4, and 1.5): the V atoms pair/dimerize along the chain, resulting in unit-cell doubling, and also tilt transversely in a zigzag-like fashion; the V-V pairing and tilting also cause the O-octahedra to distort and twist slightly [25]. According to Eyert [25], the lattice parameters are: the M_1 phase, a_m = 5.7517 Å = 2ct, b_m = 4.5378 Å, c_m = 5:3825 Å, β_m = 122.646 °. Note again the doubling of the monoclinic cell along the rutile c-axis, i.e., a_m = $2c_t$. Metal-metal pairing and tilting in the M_1 phase result in two different V-V distances along the monoclinic a-axis: 2.619 Å and 3.164 Å [37]. Kana kana et al [38, 39] reported that according to Anderson the lattice constants on the monoclinic phase and angle are a = 5.743 Å, b = 4.517 Å, c = 5.375Å and is β = 122.61^0 respectively [40]. Longo and Kierkegaard reported that the lattice parameter and monoclinic phase and angle are a = 5.7517 Å, b = 4.5378 Å, c = 5.3825Å and b = 122.646 ° respectively [41]. The unit cell consists of four formula units. The metal atoms and the two kind different oxygen atoms occupy the general Wyckoff (4e): ±(x, y, z), ±(x, 1/2-y, 1/2 +z). Anderson et al [40], Longo et al [41] in Table 1 to 2 and 1 to 3 [40, 41] give the atomic positions. Wentzcovitch et al [42,43] determined the lattice parameters and monoclinic angle as a = 5.629 Å, b = 4.657 Å, c = 5.375 Å and b =122.646° respectively; and the crystal structure

UNIVERSITY of the
WESTERN CAPE

parameters which were derived from the variable cell shape molecular dynamics calculations are listed in Tables 1.1, 1.2 and 1.3. The monoclinic M_2 phase differs from monoclinic M_1 since VO_2 in this phase crystallizes in a centered monoclinic lattice space group C2/m [44]. In M_2 phase, the monoclinic angle distorts the basal plane of the original rutile cell hence the setup of the new primitive translations is different from that of the M_1 phase. There are two different types of metal atoms and three types of oxygen atoms and this occupy subsets on the general Wyckoff position: ±(x,y,z), ±(x,-y,z), 1/2,1/2,0)±(x,y,z), and (1/2,1/2,0)±(x,-y,z).The crystal structure is shown in (Figure 1-5, and this only happen when VO_2 is doped with small amount (few percent) of Al, Cr, Fe and Ga [44]. The essential structural and electronic details of both VO_2 phases, first proposed by Goodenough [13] are neatly summarized by Cavalleri et al. [45]. The $[Ar]4s^2 3d^5$ V atoms, each bound to two $1s^2 2s^2 2p^4$ O atoms, cede four electrons to $d_{||}$ the O 2p shells, leaving V^{4+} cations with a single valence electron near the Fermi level. The closed-shell O 2p electrons are now tightly bound and lie well below the Fermi level, not contributing significantly to the conductivity.

UNIVERSITY of the
WESTERN CAPE

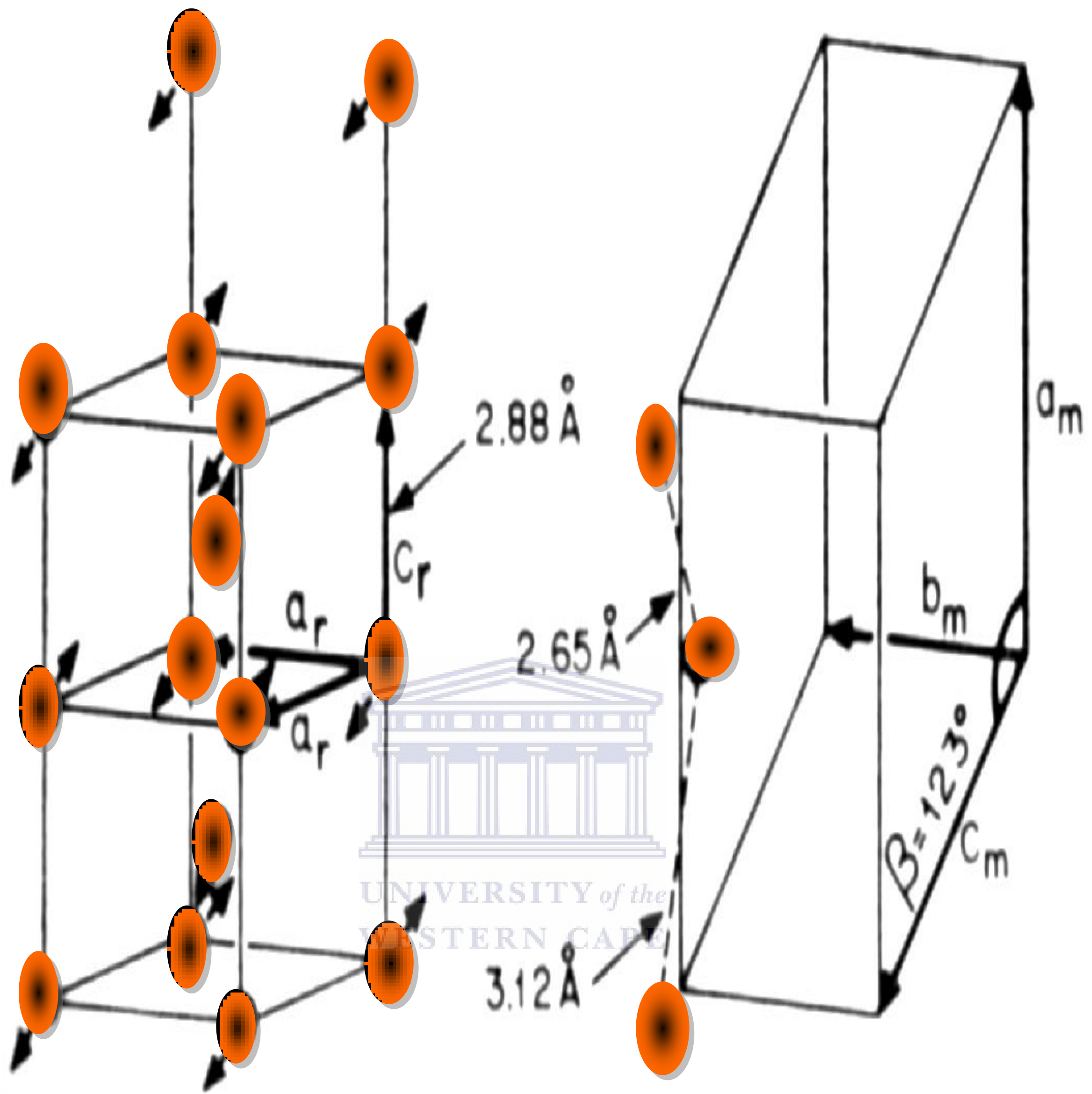

UNIVERSITY of the
WESTERN CAPE

Figure 1.4: VO_2 unit cells above and below the phase transition. After reference [28].

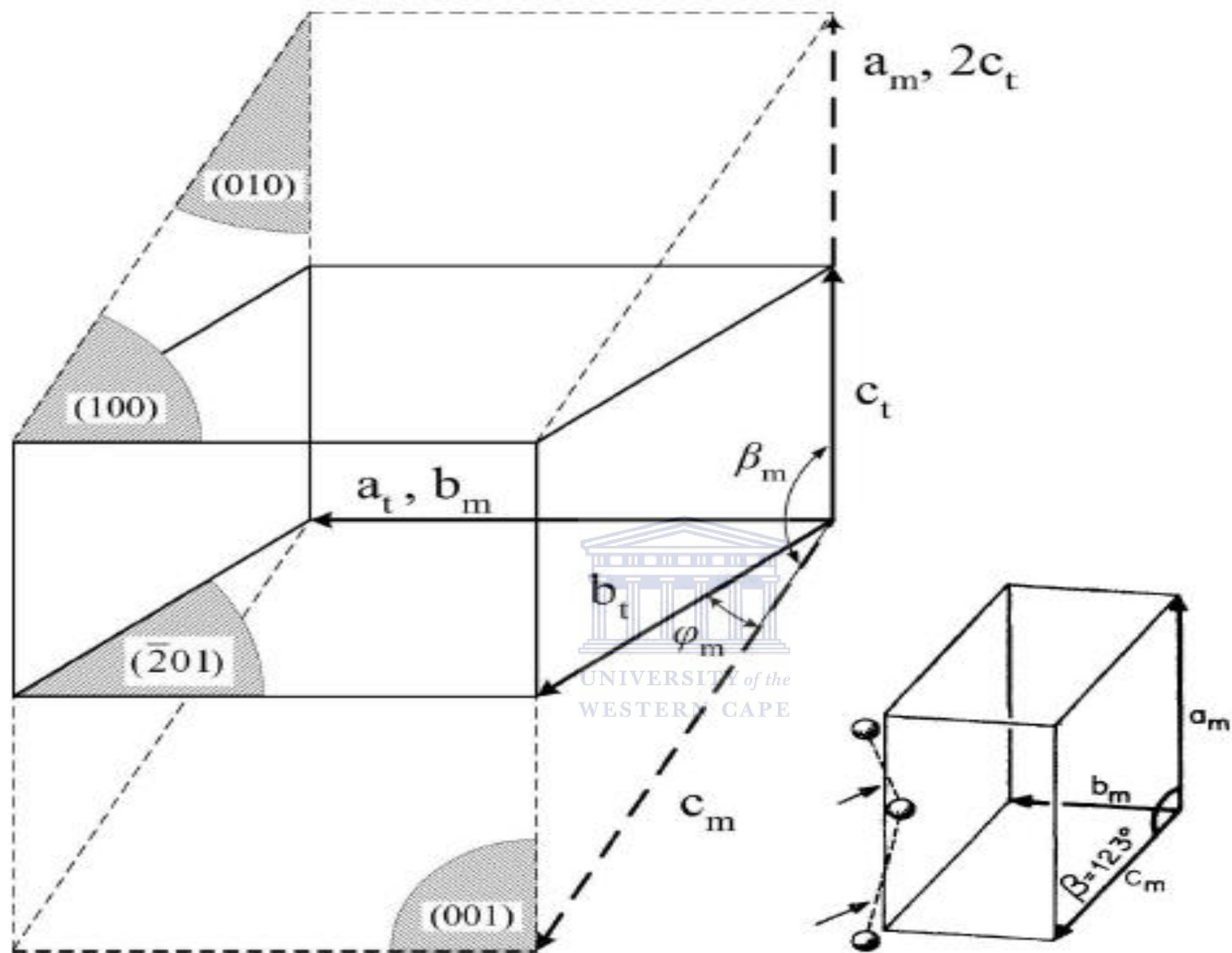

UNIVERSITY of the
WESTERN CAPE

Figure 1.5: Orientation and dimensions of tetragonal/rutile R (solid lines, "t" subscripts) and monoclinic M_1 (dashed lines, "m" subscripts) unit cells of VO_2

Atom	Wyckoff positions	Parameters		
		X	Y	Z
V	(4e)	0.242	0.975	0.025
O1	(4e)	0.1	0.21	0.2
O2	(4e)	0.39	0.69	0.29

Table 1.1 Anderson crystal structure parameters of M1-VO2 [40]

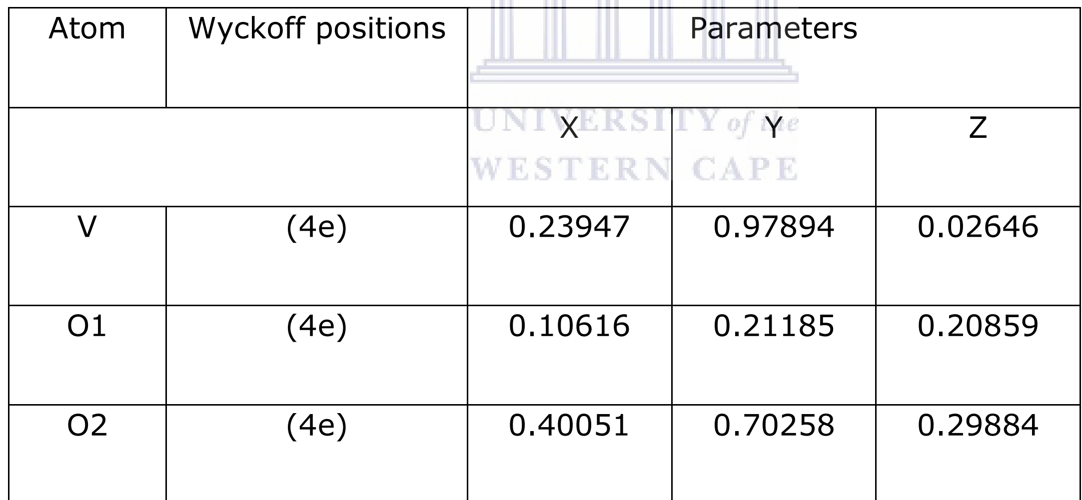

Atom	Wyckoff positions	Parameters		
		X	Y	Z
V	(4e)	0.23947	0.97894	0.02646
O1	(4e)	0.10616	0.21185	0.20859
O2	(4e)	0.40051	0.70258	0.29884

Table 1.2: Crystal structure parameters given by longo and Kierkegaard [41]

Atom	Wyckoff positions	Parameters		
		X	Y	Z
V	(4e)	0.233	0.976	0.021
O1	(4e)	0.118	0.212	0.228
O2	(4e)	0.399	0.685	0.293

Table 1.3: Crystal structure parameters of M_1 VO_2 given by wentzcovitch [42,43].

UNIVERSITY of the
WESTERN CAPE

The remaining one electron per V^{4+} cation occupies the lowest of the 3d levels, making VO_2 a $3d^1$ compound.

The bands in transition-metal compounds form under the strong influence of anisotropic crystal fields. The fivefold energy-degenerate 3d levels of the isolated V^{4+} cation are split in VO_2 by the cubic and orthorhombic components of the octahedral field of the six surrounding oxygens [14] resulting in a higher-energy two-level manifold (e_g) and a lower-energy three-level manifold (t_{2g}). The t_{2g} states, located near the Fermi energy, are split into a $3d_{//}$ state, which is directed along the rutile c-axis with good metal-metal bonding, and the remaining $3d_{\Pi}$ states. Thus, a single electron resides in the lowest vanadium d band, $3d_{//}$, which is the reason for R-phase VO_2 being metallic (see figure 1.6). In the monoclinic M_1 phase, V-V pairing within the chains parallel to the rutile c-axis causes splitting of the $3d_{//}$ band

into filled bonding and empty antibonding states. In addition, the $3d_{\Pi}$ bands move to higher energies due to increased overlap of these states with the O 2p states, caused by the zigzag-like tilting of the V-V dimmers. As a result, a band gap of ~0.7 eV opens between the bonding $3d_{//}$ band and the other t_{2g} bands (Figure 1.6); the $3d_{//}$ band splitting amounts to ~2.5 eV, while the $3d_{\Pi}$ band is raised by ~0.5 eV [35].

UNIVERSITY of the
WESTERN CAPE

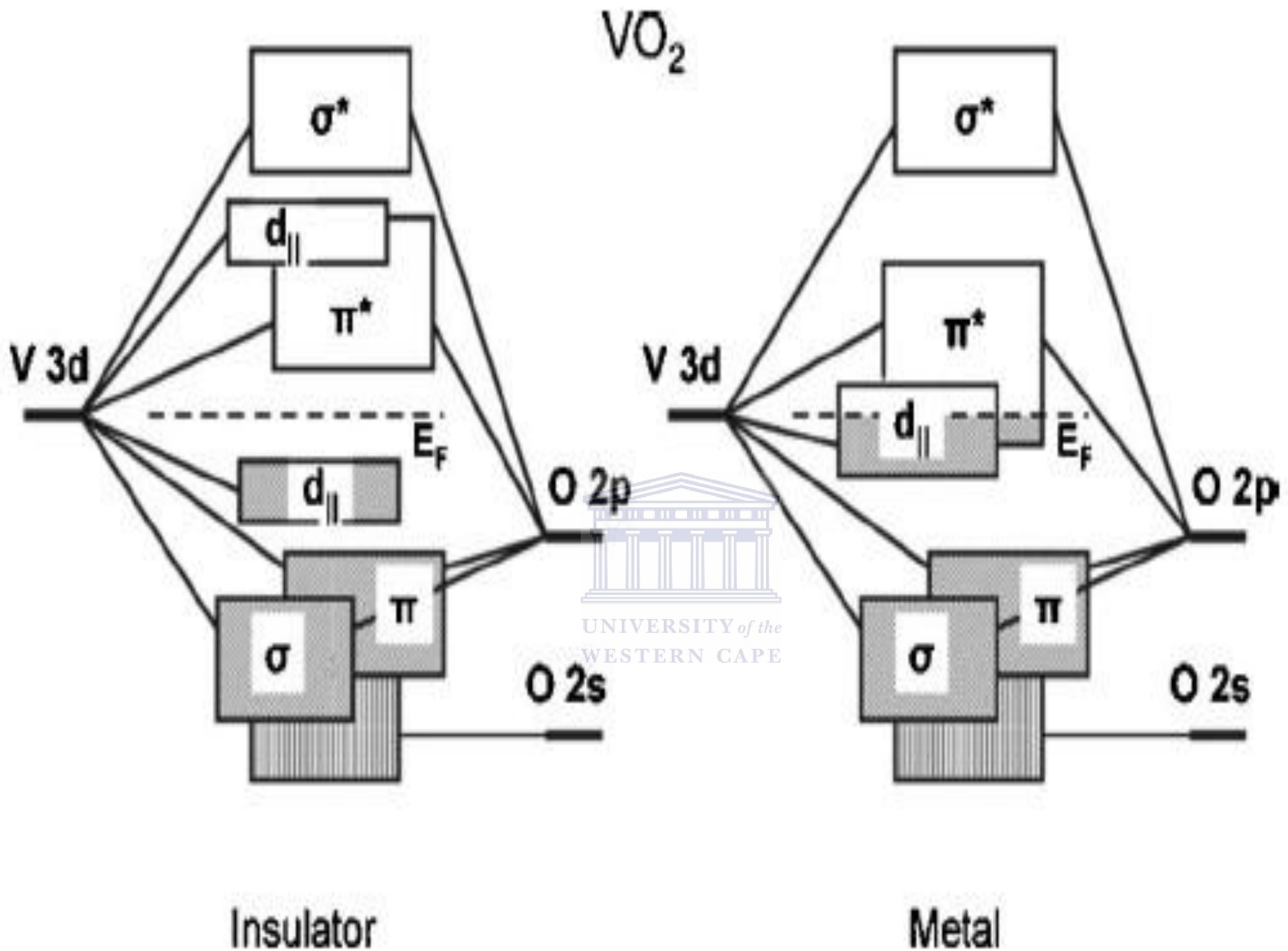

UNIVERSITY of the
WESTERN CAPE

Figure 1.6: Energy-level diagram of VO_2 [38].

1.2.2 OPTICAL PROPERTIES OF VO_2

Pure thermochromic VO_2 thin films transit noticeably between the semiconductor and metallic state at the transition T_{tr} of 68 ^{0}C. At temperatures below T_{tr} the material is transparent in both the infra red and visible part of the spectrum (see figure 1.7), thus allowing solar radiation to pass through the window maximizing the heating effect of sunlight and black body radiation within the building. Hence there is high optical transmission in the semiconducting state of VO_2 thin films. At elevated temperatures above T_{tr} the coating is transparent in the visible, more reflective in the infra red part of the spectrum (see figure 1.7). This prevents the thermal part of solar radiation from heating the building interior. This also allows for the greatest use of natural light which is highly desirable as internal lighting contributes towards the buildings energy use and maintenance costs [46]. At the transition temperature (68 ºC) vanadium (IV) oxide is too high to be effective in maintaining a comfortable temperature (18 – 25 ºC). The use of dopant has been shown to affect the transition temperature. This may increase or decrease depending on factors such as dopant size and dopant charge [47, 48] as well as the changes in electron carrier density [49]. Tungsten has been shown to be the most effective dopant to lower the T_{tr} of vanadium (IV) oxide [47] with a 2 atom% tungsten loading reducing T_{tr} to around 25 ºC in films prepared by physical vapor deposition and sol-gel coating [50,51].

UNIVERSITY of the
WESTERN CAPE

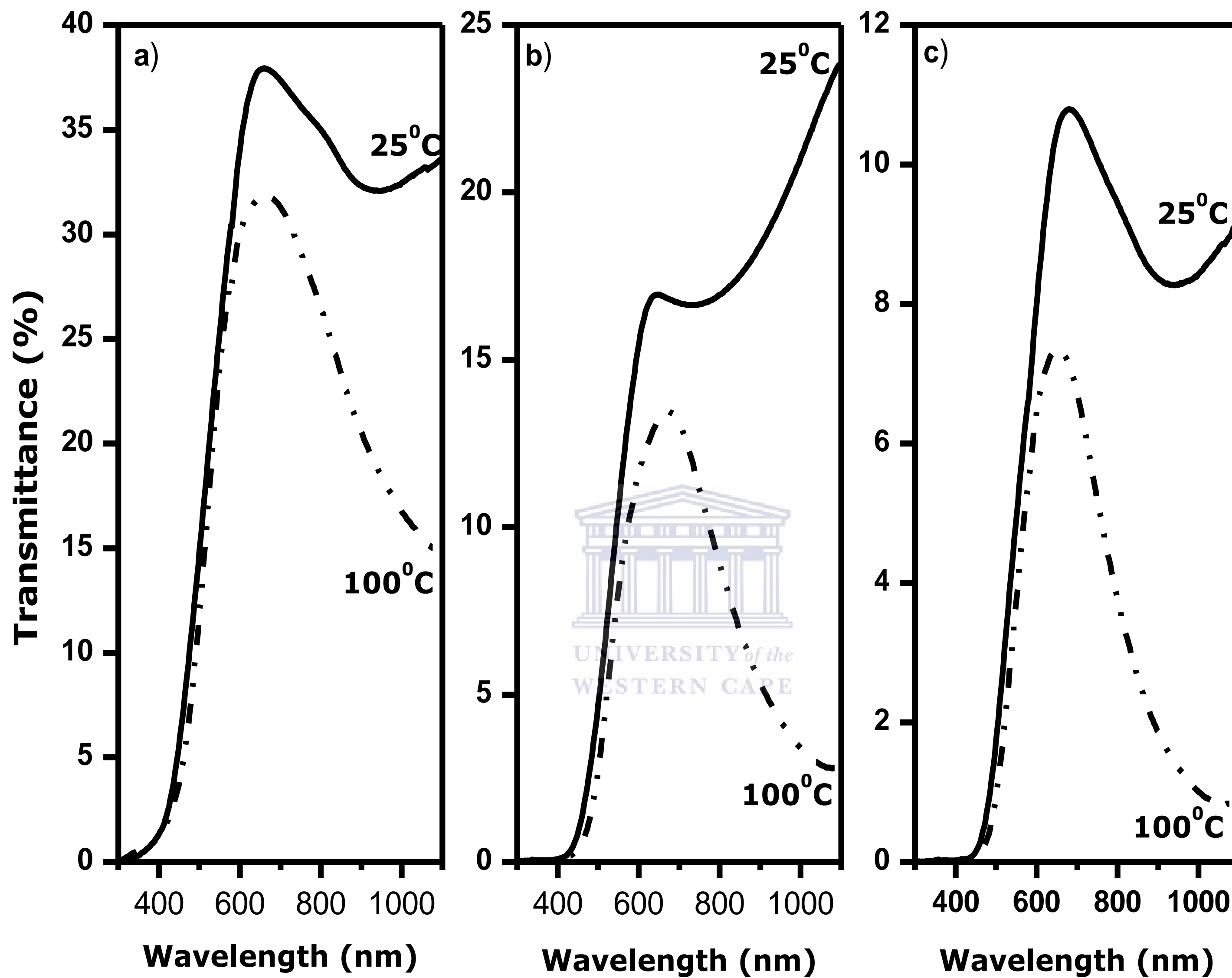

Figure 1.7: Optical switching mechanism of VO_2 thin films between semiconductor and metal state [79]

Fluorine has also been used to dope vanadium (IV) oxide. Fluorine doping [52] into VO_2 thin films by radio frequency sputtering usually forms films of VO_xF_y, resulting into improved transmittance properties and lead to a decrease in T_{tr}. Fluorine doping has however been reported to decrease the sharpness of thermochromic transition, potentially reducing their usefulness in glazing.

1.2.3 ELECTRICAL PROPERTIES OF VO_2

Semiconductor to metal transition of VO_2 thin films is accompanied by greater changes in the electrical and magnetic properties. As the temperature goes beyond the transition temperature the V-V bonds are broken and electrons are unlocked up, able to move, and therefore the band gap decreases making the material to conduct. Hence electrical conductivity, thermal conductivity and magnetic susceptibility increases in the metallic state. During the SMT resistivity decreases in magnitude of about 10^5 in the metallic state. This abrupt change in electrical properties has been associated to disorientation between grains, and grain size and other morphological faults [53].

UNIVERSITY of the
WESTERN CAPE

The variation of T_{tr} and switching in the SMT has been strongly reported to depend on the orientation of the grains, hysteresis loop and residual stress caused by the deposition process and interaction of film with the substrate. Types of stress that are involved in this case are the Extrinsic and intrinsic stress. Extrinsic stress is caused by the mismatch between thermal expansion coefficients of the thin film and substrate, whilst the intrinsic one is caused by the voids and grain boundaries

The effect of hydrostatic pressure on the electrical switching in VO_2 has been examined, and the results showed that T_{tr} increases linearly with pressure at a rate of 0.082K/bar. Also the effect of certain dopant such F, Fe, Co, Ni, Ti, Mo, Ta, and W have been reported to play a role in the behavior of electrical switching mechanism and also lowers T_{tr}, while Al, Cr and Ge increases T_{tr} noticeably [53].

1.2.4 VO_2: PHASE TRANSITION CHARACTERISTICS

The semiconductor-metal transition (SMT) of VO_2 is characterized by four main parameters: transition temperature, abruptness or sharpness, hysteresis width and amplitude of the SMT; these parameters can be evaluated quantitatively from the resistivity or transmittance variation curves. The SMT characteristics vary strongly according to the synthesis conditions of single crystals and thin films. It was reported that the VO_2 single crystals have stronger abruptness of electrical resistance and optical transmittance, narrower hysteresis width of 1-2 ^{o}C [27,54], while thin films tend to have smaller abruptness and wider hysteresis width of 10-15 ^{o}C [29]. The variations in the VO_2 switching properties can be affected by the deposition parameters such as substrate temperature, thickness, oxygen partial pressure, substrate bias, ion bombardment, internal or external stress which can induce the mismatch between lattice constants [32,55-60]. The effect of various dopants has been investigated extensively in the literature. T_{tr} is lowered by addition of dopant such as W, Ti, F, Mo, Nb, Cr, Li and Ta [61-65]. However, the doping of VO_2 is always followed by some alteration of the switching characteristics.

UNIVERSITY of the
WESTERN CAPE

Lowering T_{tr} of VO_2 without altering its semiconductor-metal transition characteristics remains a challenge.

1.2.5 VO_2 THIN FILMS: DEPOSITION TECHNIQUES

The fabrication of better quality VO_2 thin films by novel methods is still an active area of research. Numerous fabrication techniques have been used successfully to produce high stoichiometric VO_2 thin films. Stoichiometric VO_2 depositions have been accomplished using a variety of techniques such as reactive evaporation, metal-organic chemical vapor deposition (MOCVD), Sol-gel method, ion implantation, pulsed laser deposition (PLD) and several sputtering methods [66-74]. In this thesis, we will concentrate on the sputtering techniques most commonly used nowadays for the fabrication of VO_2 thin films. Sputtering in various forms is one of the most common physical vapor deposition processes [75] for growing VO_2 thin films. VO_2 thin films were first grown by reactive sputtering in 1967 by Fuhs, Hensler and Ross of the Bell Telephone Laboratories [65], who made the films by reactive ion-beam sputtering of vanadium target in an argon-oxygen atmosphere. The three most common methods used to facilitate the deposition process include direct current (DC), reactive frequency (RF), and magnetron sputtering. The comparative advantages of the sputtering process include film uniformity, scalability to larger substrates and efficiency of deposition. Following the first experiments in VO_2 deposition by reactive sputtering, and further analysis in those samples by Rozgonyi and Hensler both RF and DC reactive sputtering were studied by Duchene et al, [78]. Films with similar qualities were obtained in both cases, but

UNIVERSITY of the

since RF sputtering was more suitable for depositing high quality of VO_2 and had many advantages over DC sputtering.

Among the plethora of sputtering methods, we developed a novel physical vapor deposition; an uncommon sputtering technique called RF reactive inverted cylindrical magnetron sputtering (hollow cathode magnetron sputtering) for the synthesis of high quality of VO_2 thin films [79]. This coating technology offers advantages over others physical vapor deposition such as laser ablation and classical sputtering. It is a low-cost and has significant potentiality to coat wires, ribbons as well as all sides of three dimensional complex substrates. The complete description of this novel technique will be done in chapter 2.

1.3 REFERENCES

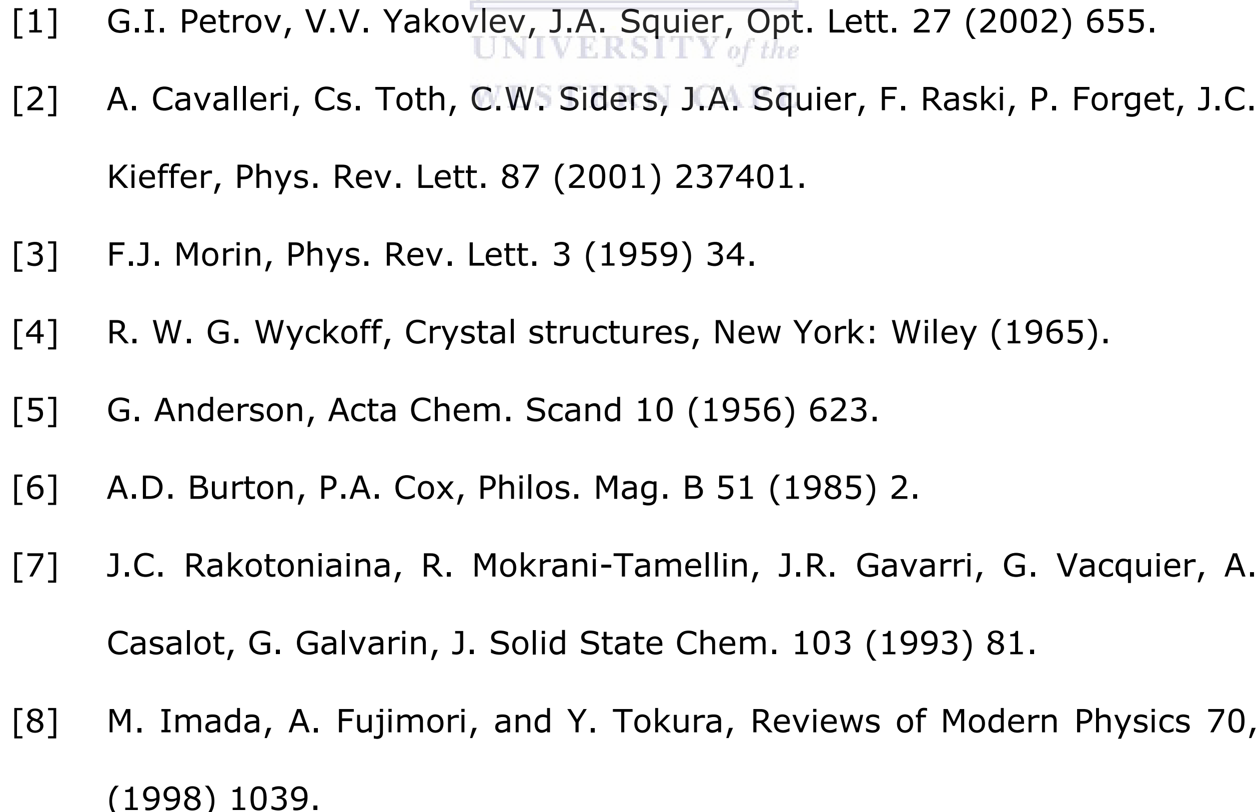

UNIVERSITY of the
WESTERN CAPE

[1] G.I. Petrov, V.V. Yakovlev, J.A. Squier, Opt. Lett. 27 (2002) 655.

[2] A. Cavalleri, Cs. Toth, C.W. Siders, J.A. Squier, F. Raski, P. Forget, J.C. Kieffer, Phys. Rev. Lett. 87 (2001) 237401.

[3] F.J. Morin, Phys. Rev. Lett. 3 (1959) 34.

[4] R. W. G. Wyckoff, Crystal structures, New York: Wiley (1965).

[5] G. Anderson, Acta Chem. Scand 10 (1956) 623.

[6] A.D. Burton, P.A. Cox, Philos. Mag. B 51 (1985) 2.

[7] J.C. Rakotoniaina, R. Mokrani-Tamellin, J.R. Gavarri, G. Vacquier, A. Casalot, G. Galvarin, J. Solid State Chem. 103 (1993) 81.

[8] M. Imada, A. Fujimori, and Y. Tokura, Reviews of Modern Physics 70, (1998) 1039.

[9] P. A. Cox, Transition metal oxides: An introduction to their electronic structure and properties, The International Series of Monographs on Chemistry, Clarendon Press; Oxford University Press, Oxford New York, (1992).

[10] C. Kübler, H. Ehrke, R. Huber, R. Lopez, A. Halabica, R. F. Haglund, and A. Leitenstorfer, Phy.review. Lett. 99. (2007) 116401.

[11] M. M. Qazilbash, M. Brehm, B. G. Chae, P. C. Ho, G. O. Andreev, B. J. Kim, S. J. Yun, A. V. Balatsky, M. B. Maple, F. Keilmann, H. T. Kim, and D. N. Basov, Science 318, (2007) 1750.

[12] P. Baum, D. S. Yang, and A. H. Zewail, Science 318, (2007) 788.

[13] J. B. Goodenough, J. Solid State Chem. 3, (1971) 490 .

[14] A. Zylbersztejn and N. F. Mott, Physical Review B 11, (1975) 4383.

[15] D. Paquet and P. L. Hugon, Physical Review B 22, (1980) 5284.

[16] R. M. Wentzcovitch, W. W. Schulz, and P. B. Allen, Phys. Rev. Lett. 73, (1994) 3043 .

[17] T. M. Rice, H. Launois, and J. P. Pouget, Phys. Rev. Lett. 73, (1994) 3042.

[18] R. M. Wentzcovitch, W. W. Schulz, and P. B. Allen, Phys. Rev. Lett.72, (1994) 3389.

[19] S. Biermann, A. Poteryaev, A. I. Lichtenstein, and A. Georges, Phys. Rev. Lett. 94, (2005) 026404.

UNIVERSITY of the
WESTERN CAPE

[20] A. Cavalleri, T. Dekorsy, H. H. W. Chong, J. C. Kieffer, and R. W. Schoenlein, Phys. Rev. B 70, (2004) 161102.

[21] H. T. Kim, Y. W. Lee, B. J. Kim, B. G. Chae, S. J. Yun, K. Y. Kang, K. J. Han, K. J. Yee, and Y. S. Lim, Phys. Rev. Lett. 97, (2006) 266401.

[22] G. Kotliar and D. Vollhardt, Phys. Today 57 (2004) 53.

[23] D. Adler, Rev. Mod. Phys. 40 (1968) 714.

[24] C.N. Berglund and H.J. Guddenheim, Phys. Rev. 1 (1969) 1022.

[25] V. Eyert, Ann. Phys. Lpz 11, (2002) 650.

[26] A.S. Barker, H.W. Verleur and H.J. Guggenheim, Phys. Rev. Lett. 17 1286 (1966) 1286.

[27] J.F. DeNatale, P.J. Hood and A.B. Harker, J. Appl. Phys. (1989) 66.

[28] H.W. Verleur, A.S. Barker and C.N. Berglund, Phys. Rev. 172, 788 (1968) 5844.

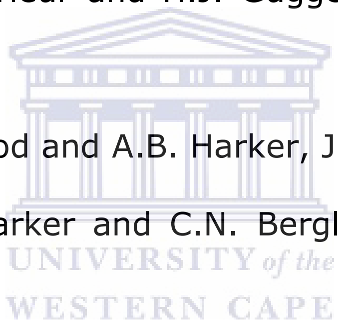
UNIVERSITY of the
WESTERN CAPE

[29] D. Brassard, S. Fourmaux, M. Jean-Jacques, J. C. Kieffer, and M. A. El Khakani, Appl. Phys. Lett. 87, (2005) 051910.

[30] R. Lopez, L. A. Boatner, T. E. Haynes, R. F. Haglund, and L. C. Feldman, Appl. Phys. Lett. 79, (2001) 3161 .

[31] G. Nihoul, C. Leroux, V. Madigou, and J. Durak, Solid State Ionics 117, (1999) 105.

[32] C.H. Griffith and H.K. Eastwood, J. Appl. Phys. 45 (1974) 2201.

[33] D.B Mcwhan, J. P. Remeika, and P.D Dernier, Phys. Rev. 172 (1968) 788-798.

[34] A. Cavalleri, M. Rini, and R. W. Schoenlein, Jpn. J. Phys. Soc. 75, (2006) 011004.

[35] S. Shin, S. Suga, M. Taniguchi, M. Fujisawa, H. Kanzaki, A. Fujimori, H. Daimon, Y. Ueda, K. Kosuge, and S. Kachi, Phys. Rev. B 41, (1990) 4993.

[36] M. M. Qazilbash, A. A. Schafgans, K. S. Burch, S. J. Yun, B. G. Chae, B. J. Kim, H. T. Kim, and D. N. Basov, Phys. Rev. B 77, (2008) 115121.

[37] S. Lysenko, V. Vikhnin, F. Fernandez, A. Rua, and H. Liu, Physical Review B 75, (2007) 075109.

[38] J. B. Kana kana. PHD. University of yaounde. Reversible Tunability in novel ultrafast nanoplasmonics: synthesis and characterization of Au-VO_2 nanophotonics (2008).

[39] J. B. Kana kana. PHD. University of The Western cape. Towards stimuli- responsive functional nano composite: smart tunable plasmonic nanostructures Au-VO_2 (2010).

[40] G. Anderson, Acta Chem.Scand 15 (1956) 623.

[41] M. Longo and P.Kierkegaardt, Acta Chim.Scand. 24 (1970) 420.

[42] R. M. Wentozcovitch, W W Schulz, and P b Allen, phy.Rev. Lett.72(1994)3389.

[43] R. M. Wentzcovitch, W.W Schulz, and P B Allen, Phys. Rev.Lett.73 (1994) 3389.

UNIVERSITY of the
WESTERN CAPE

[44] M. Marezio, D.B Mcwhan, J.P Remeika and P D dernier phy.rev. B5 (1974)490.

[45] A. Cavalleri, M Rini, and R W Schoenlein, J. Phys. Society of Japan 75, (2006) 011004.

[46] I. P. Parkin, R Binions, C Piccirillo, C S Blackman, T D Manning, journal of nano research Vol. 2 (2008) pp1-2.

[47] J. B. MacChesney. H. J. J. Guggenheim, Phys. Chem. Solids 30. (1969) 225-234.

[48] T. E. Phillips, R. A. Murray, T. O. Poehler, Mater. Res. Bull 22. (1987) 1113-1123.

[49] J. W. Pierce. J. B. Goodenough. Phys. Rev. B 5, (1972), 4104-4111.

[50] W. Burkhardt, T Christmann, B K Meyer, W Niessner, D Schalch, A Scharmann. Thin Solid Films, 345 (1999) 229-235.

[51] J. Livage. Coord. Chem. Rev. 190-192 (1999) 391-403

[52] C. G. Granqvist. Thin Solid Films, 193/194 (1990), , 730-741

[53] H.B Cele. M.Sc Desertation. University of Zululand. Nano structured VO_2 for IR modulation, (2009)

[54] L. A. Ladd. W. Paul, Solid State Commun. 7 (1969) 425.

[55] E.E. Chain J. Vac. Sci. Technol. A 4 (1986) 432.

[56] G. Xu, P. Jin, M. Tazawa, K. Yoshimura Appl.Surf. Sci. 244 (2005) 449.

UNIVERSITY of the
WESTERN CAPE

[57] K. Nagashima, T. Yanagida, H. Tanaka and T. Kawai, J. Appl. Phys. 100 (2006) 063714.

[58] H. Miyazaki and I. Yasui J. Phys. D: Appl. Phys. 39 (2006) 2220.

[59] F. C. Case, J. Vac. Sci. Technol. A 2, (1984) 1509.

[60] Y. Muraoka and Z. Hiroi, Appl. Phys. Lett. 80, (2002) 583.

[61] C. B. Greenberg Thin Solid Films, 251 (1994) 81.

[62] C. G. Granqvist, Crit. Rev. Solid State Mater. Sci. 16 (1990) 291.

[63] W. Burkhardt, T, Christmann, S. Franke, W. Kriegseis, D. Meister, B.K. Meyer, W. Niessner, D. Schalch and A. Scharmann, Thin Solid Films 402 (2002) 226.

[64] M. Soltani, M. Chaker, E. Haddad, R.V. Kruzelecky and D. Nikanpour, J. Vac. Sci. Technol. A 22, (2004) 859.

[65] H. Futaki and M. Aoki, Jpn. J. Appl. Phys. 8 (1969) 1008.

[66] T. D. Manning and I. P. Parkin, J. Mater. Chem. 14, (2004) 2554.

[67] T.D. Manning, I.P. Parkin, C. Blackman and U. Qureshi, J. Mater. Chem. 15, (2005) 4560 .

[68] G. Guzman, F. Beteille, R. Morineau and J. Livage, Mater. Res. Bull. 29 (1994) 509.

[69] D.P. Partlow, S.R. Gurkovitch, K.C. Radford and L.J. Denes, J. Appl. Phys. 70 (1991) 443 .

[70] F. Beteille, and J. Livage, J. Sol-Gel Sci. Technol. 13 (1998) 915.

[71] D.H Kim and H.S. Kwok, Appl. Phys. Lett. 65 (1994) 3188.

UNIVERSITY of the WESTERN CAPE

[72] M. Maaza, K. Bouziane, J. Maritz, D.S. McLachlan, R. Swanepoel, J.M. Frigerio and M. Every, Opt. Mater. 15 (2000) 41.

[73] E. E. Chain, J. Vac. Sci. Technol. A 5 (1987) 1836.

[74] K. Okimura and N. Kubo, Thin Solid Films, 515 (2007) 4992.

[75] J. A. Thornton, Thin Solid Films 107 (1983) 3.

[76] E. N. Fuhs, D.H. Hensler and A.R. Ross, Appl. Phys. Lett. 10 (1967) 199.

[77] G. A. Rozgonyi, and D.H. Hensler J. Vac. Sci. Technol. 5 (1968) 194 .

[78] J. Duchene, M. Terraill and M. Pailly, Thin Solid Films 12 (1972) 231 .

[79] J. B. Kana Kana, J.M. Ndjaka, P. Owono Ateba, B.D. Ngom, N. Manyala, O. Nemraoui, A.C. Beye and M. Maaza, Appl. Surf. Sci. 254 (2008) 3959.

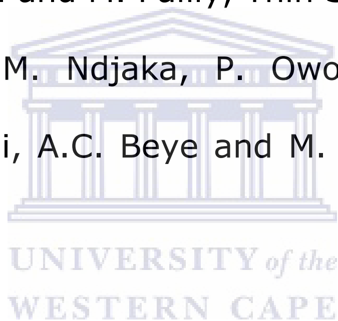
UNIVERSITY of the
WESTERN CAPE

CHAPTER 2

2. OVERVIEW ON SPUTTERING

2.1 Introduction and principles of sputtering.

2.1.1 Introduction

Sputtering was first observed in a direct current (DC) gas discharge tube by Grove in 1852 [1]. He discovered the cathode surface of the discharge tube was sputtered by energetic ions, and cathode materials were deposited on the inner wall of the discharge. Sputtering is a physical vapor deposition process widely used for deposition of thin films, cleaning surface, depth profiling and a number of applications which requires careful, microscopic erosion of a surface. Sputtering is a process whereby gas ions are accelerated out of plasma towards a target material to be deposited. Accelerated ions remove atoms from the target material which are afterwards deposited on a substrate. The process takes place in a close recipient, which is pumped down to a vacuum base pressure before the deposition starts. Figure 2.1 shows the basic sputter deposition system. Sputtering process takes place in a vacuum, where-in the argon gas is introduced, ionized into the chamber. Argon is introduced into the chamber to facilitate the ignition of the plasma. The target material is positioned at a negative potential relative to the positively charged argon atoms. The

UNIVERSITY of the
WESTERN CAPE

positive ion accelerates towards the negative charge, striking the target with sufficient force to remove the material. The argon atoms do not become embedded in the target material, they slam into the target like a steel ball into the wall and tears off some of the target material. The impact of an atom or ion on surface results in ejection of atoms from the surface as a result of collisions and momentum transfer from the incoming particles. This process is known as sputtering, no chemical reaction happens between the sputter gas and the target atoms [1-2].

2.1.2 Principles of sputtering

The process of sputtering takes place in a vacuum chamber, typically the substrate is placed opposite to the target material. The chamber is evacuated and backfilled with a sputtering gas (argon). The electric field inside the sputtering chamber accelerates electrons which collide with Ar atoms producing Ar^+ ions and more electrons and a characteristic purple plasma. The resulting positive ions are strongly attracted to the target, which carries a negative charge. The effect is a physical process similar to the interaction of atomic billiards in a confined space. As the relatively large argon ions impact the target, atoms/molecules of the target material are physically removed from the target. Due to its close proximity, the majority of sputtered atoms land on the substrate. The intent is for this material to arrive at the substrate with enough energy to form a thin, strongly attached

UNIVERSITY of the
WESTERN CAPE

film, one monolayer at a time, as reported in details by Sigmound and Mattox [3,4]

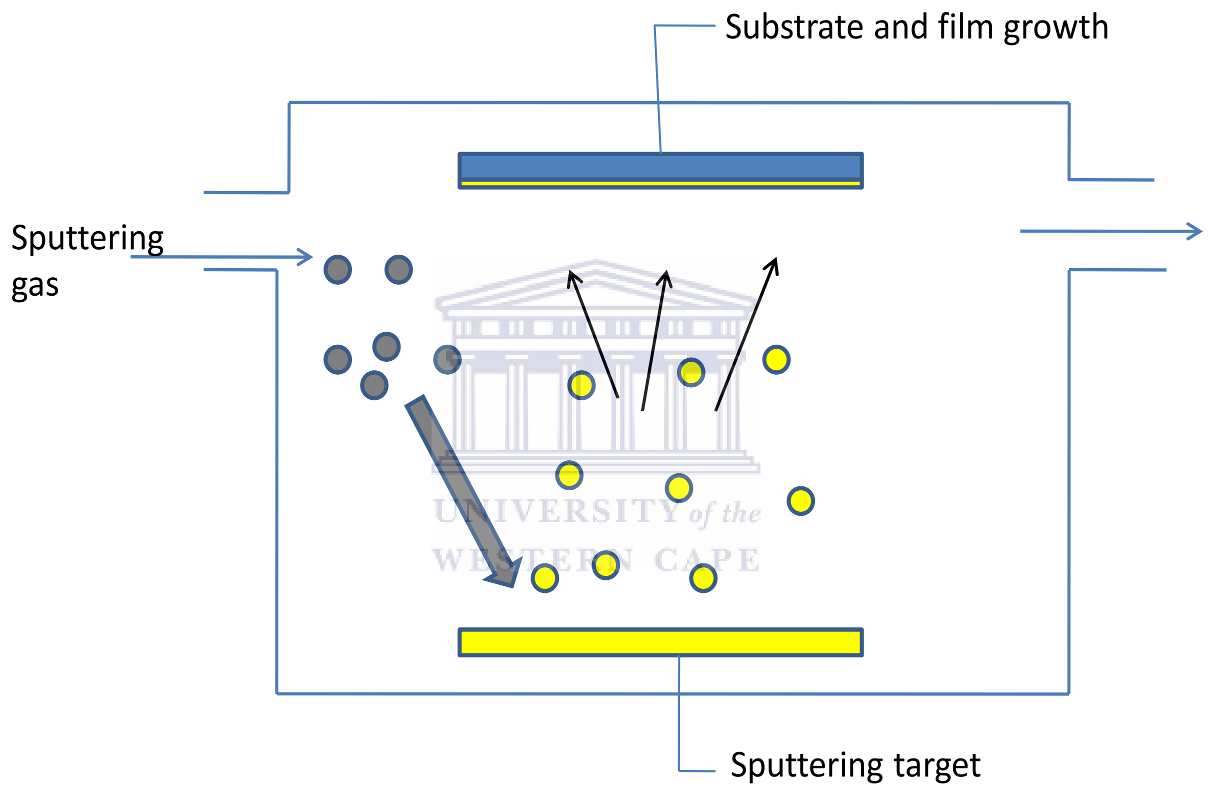

Figure 2.1 Sputter deposition systems

2.1.3 Sputtering parameters

During sputtering deposition of thin films, the resulting film properties can be controlled by adjusting the following sputter parameters:

The **sputter current I_{sp}** determines mainly the rate of the deposition process and hence the time which remains for the arriving particles during the growth process for either surface diffusion and agglomeration on existing growth centers or nucleation with other adatoms. The **applied voltage** determines the maximum energy, with which sputtered particles can escape from the target (reduced by the Binding energy). Energies of the sputtered particles show a broad distribution with a maximum of the distribution between 1 eV and 10 eV. The applied voltage determines also the sputter yield, which is the number of sputtered particles per incoming ion. The **pressure p** in the sputter chamber determines the mean free path (λ) for the sputtered material, which is proportional to 1/p. Together with the target substrate distance (T-S) the pressure controls, how many collisions occur for the particles on their way from the target to the substrate. This can influence the porosity of the films, also the crystallinity and texture can be affected [6]. Via the gas mixture one can control the stoichiometry of films, which are sputtered from a metallic target. The **oxygen flow $P(O_2)$** is the parameter varied, whereas the desired total pressure is kept constant by regulation of the Argon-flow P(Ar). The **substrate temperture** can have a strong impact on the growth behavior with respect to crystallinity or density

UNIVERSITY of the
WESTERN CAPE

of the samples. It can be adjusted between room temperature and 600^0 C. But even during sputtering without external heating the substrate temperature may rise considerably, especially during long sputtering times for the deposition of thick films. In principle a **bias-voltage** can be applied to the substrate up to 100V, which has the effect of accelerating electrons or ions towards the substrate or keeping them away. Both may have an influence on the layer growth as reported in the literature [8]. Usually substrate and target surface are parallel to each other. A variation of the deposition angle (also: sputtering under oblique incidence) can be achieved by tilting the substrate. Thereby a new preferential direction for the film growth and potentially anisotropic films can be produced.

2.2 Different methods of sputtering.

WESTERN CAPE

2.2.1 Reactive sputtering

In reactive sputtering, the deposited film is formed by chemical reaction between the target material and a gas which is introduced into the vacuum chamber. Oxide and nitride films are often fabricated using reactive sputtering. The target material is sputtered in the presence of a reactive gas, usually oxygen for the deposition of oxides material. In reactive sputtering, the coating rate and film stoichiometry are sensitive functions of the reactive gas partial pressure and control of this pressure is key to producing good quality coatings with reasonable deposition rates. The

applications of reactive have expanded significantly in the last decade for optical coating and optical waveguides, decorative coatings, hard coatings, magnetic films and etc. The advantages of reactive sputtering are: compounds can be formed using relatively easy–to-fabricate metallic targets, insulating compounds can be deposited using DC power supplies and films with graded compositions can be formed. The difficulty in the reactive sputtering process is the complexity which accompanies its versatility [5-6].

Several studies have been reported on the preparation of VO_2 thin films by reactive sputtering. Fuls [9] reported on the thin films of vanadium dioxide formed by reactive sputtering of vanadium in an argon atmosphere doped with a partial pressure of oxygen. The films were deposited on sapphire substrates held at 400°C and exhibit a highly oriented polycrystalline monoclinic structure at room temperature. The semiconductor to metal transition was observed at 345°K with a slight hysteresis with temperature reversal. Rozgoni [10] reported on the structural and electrical properties vanadium dioxide thin films by reactive sputtering. Richardson et al [11] reported on the infrared optical modulators for missile testing. This paper described the fabrication of infrared optical modulators for use in high dynamic range and high frame rate scene generation. Modulation is produced by the heating of a variable reflectivity coating. This was achieved

UNIVERSITY of the
WESTERN CAPE

by coating a suitable substrate with a thin film of vanadium dioxide (VO_2) by reactive sputtering process.

2.2.2 Direct current (DC) sputtering

Direct Current (DC) Sputtering is the simplest sputtering process. It cannot be used to deposit dielectric or inorganic materials like oxides, but it can be used to deposit almost any metallic material. Most of the part covered so far about sputtering has dealt with DC sputtering also known as the Diode sputtering. The diode sputtering is composed of a pair of planar electrodes, one of the electrodes is a cold cathode and the other is an anode. The top plasma-facing surface of the cathode is covered with a target material and the reverse is water cooled. The substrates are positioned at the anodes. The ion in plasma will be accelerated toward cathode, hit the target and transfer the energy sputtering the target to substrate surface. However it is important to note how the relative film deposition-rate depends on sputtering pressure and current. At low pressures, the cathode sheath is wide, ions are produced far from the target, and therefore their chances of being lost to the walls are great. The mean free electron path between collisions is large, and electrons collected by the anode are not replenished by ion impact-induced secondary-electron emission at the cathode. Therefore, ionization efficiencies are low and self sustained discharges cannot be maintained below about 10mtorr. As the pressure is increased at

UNIVERSITY of the WESTERN CAPE

a fixed voltage, the electron mean free path is decreased, more ions are generated, and larger currents flow. But if the pressure is too high, the sputtered atoms undergo increased collusion scattering and are not efficiently deposited.

During the DC sputtering the atoms that leave the target with typical energies of 5eV undergo gas scattering events in passing through the plasma gas; this is so even at low operating pressures. As a result of repeated energy-reducing collisions they eventually thermalize or reach the kinetic energy of the surrounding gas [12]. Several studies have been reported on the preparation of VO2 thin films by DC sputtering. Batista et al [13] reported on the DC Sputtered W-Doped VO_2 thermochromic thin Films for Smart Windows with Active Solar Control. Ufert [14] reported on the stress induced switching in VO_2 thin films by reactive DC sputtering.

UNIVERSITY of the
WESTERN CAPE

2.2.3 Magnetron sputtering

The magnetron sputtering has been long used in large area coating applications. It is used to improve the efficiency of sputtering process. Magnetron sputtering differs from other sputtering methods due to the application of magnetic field around the target in order to energize argon atoms for bombarding the target. Using magnetic field leads to trapping electrons in the magnetic field created around the target which enhances

plasma. This results in higher ionization of Argon atoms and bombarding rate that finally increases the rate of deposition. Magnetron sputtering is the most widely used variant of DC sputtering. Important implications of this are higher deposition rates or alternatively, lower voltage operation than for simple DC sputtering. Another important advantage is reduced operating pressures. At typical magnetron sputtering pressures of a few millitorr, sputtered atoms fly off in ballistic fashion to impinge on substrates. Gan et al [15] reported on the optical and electrical properties of sputtered vanadium dioxide thin films. Thin films of VO_2 with thickness 0.1 to 0.2 μm were deposited on Si_3N_4/Si substrate by rf magnetron sputtering. Lee et al [16] reported on the fiber optic application for thermal switching in vanadium dioxide thin films prepared by DC magnetron sputtering. Kusano [17] reported on the deposition of vanadium dioxide films by direct current magnetron sputtering.

UNIVERSITY of the
WESTERN CAPE

2.2.4 Radio frequency (RF) sputtering.

The RF sputtering can be used to sputter electrically insulating materials although the sputtering rate is very low. A major disadvantage in rf sputtering of dielectric materials, is that most electrically insulating materials have poor thermal conductivity and high coefficients of thermal expansion and are usually brittle materials. Since most of the bombarding energy

produces heat, a large thermal gradients can be generated that result in fracturing the target if high power levels are used. Radio Frequency (RF) sputtering will allow the sputtering of targets that are electrical insulators (SiO_2, etc). The target attracts Argon ions during one half of the cycle and electrons during the other half cycle. The electrons are more mobile and build up a negative charge called self bias that aids in attracting the Argon ions which does the sputtering. Christmann et al [18] reported on the thermochromic VO_2 thin films studied studied by photo electron spectroscopy. Thermochromic VO2 thin films were deposited by reactive rf-sputtering. The films were grown on quartz polycrystalline and unidirectional. Photoelectron spectroscopy was applied to study the density of states distribution in the valence band regime below and above the phase transition temperature. Miyazaki et al [19] reported on the substrate bias effect on the fabrication of thermochromic VO_2 reactive RF sputtering. Vanadium oxide VO_x films were deposited by reactive RF magnetron sputtering by applying a substrate bias, in which the Ar ions in plasma impacted the growing film surface. The vanadium valence of the VO_x film decreased when the substrate negative bias voltage was increased. The VO_2 film was successfully deposited at a substrate temperature of 400 °C and with a bias voltage of −50 to −80 V. The transition temperatures of the VO_2 films with a substrate bias of −50 and −80 V were about 56 °C and 44 °C.

UNIVERSITY of the
WESTERN CAPE

2.3 Choice of deposition methods

The choice of deposition methods of thin films depends on several factors;

- The nature of the material to deposit.
- Nature of the substrate to be used.
- The stoichiometry desired.
- Rate of deposition.
- Adhesion of the film on the substrate.
- Cost effective of the technique.

UNIVERSITY of the
WESTERN CAPE

A home-made radio frequency inverted cylindrical magnetron sputtering (ICMS), at iThemba LABS was used in this work for the deposition of VO_2 thin films on glass substrates. Inverted cylindrical magnetron sputtering also known as the hallow cathode is used to sputter from the inner surface of the cylindrical targets and highly conformal coatings [20]. ICMS has an enclosed geometry, it produces intense and very uniform plasma next to the target surface which results in high deposition rates of thin films [21]. ICMS also lead to excellent target erosion because the sputtered atoms that are not deposited on the substrate get re-deposited on the cathode. It has low target cost and produce large area uniform films [22, 23].

2.4 Radiofrequency inverted cylindrical magnetron sputtering

Cylindrical magnetrons were invented earlier in the mid- 1970s by Penfold and Thornton [24,25]. ICMS sputter off of the inside surfaces of cylindrical targets. ICMS is a promising candidate to prepare new nano-composite films with uniform coating on complex shapes which are required for a variety of applications, ranging from X-ray telescope mirrors to biomedical implants. Figure 2.2 shows the schematic representation of the ICMS sputter gun. The ICM gun is mounted in a double cross-piece vacuum chamber on a standard DN 100 CF flange with a mounting depth of 120 mm. The rings magnets and cylindrical target assembly are attached to a water cooled backing plate that limits heat buildup in the target and magnets. The substrate holder is situated 2cm from the sputtering head. The temperature of the substrate heater is controlled by a thermocouple k-type thermocouple with an Omega CN 370 temperature controller capable to reach 700°C.

UNIVERSITY of the
WESTERN CAPE

The vacuum chamber is evacuated by a diffusion pump backed by a rotary pump. The vacuum system is separated from the deposition section by a pneumatic gate valve which is bypassed by a constricted diameter bellows tube with an adjustable flow control valve. This allows for differential pumping on the upper and lower chambers thus enabling the use of high gas pressures needed during the sputtering without causing damage to the diffusion pump.

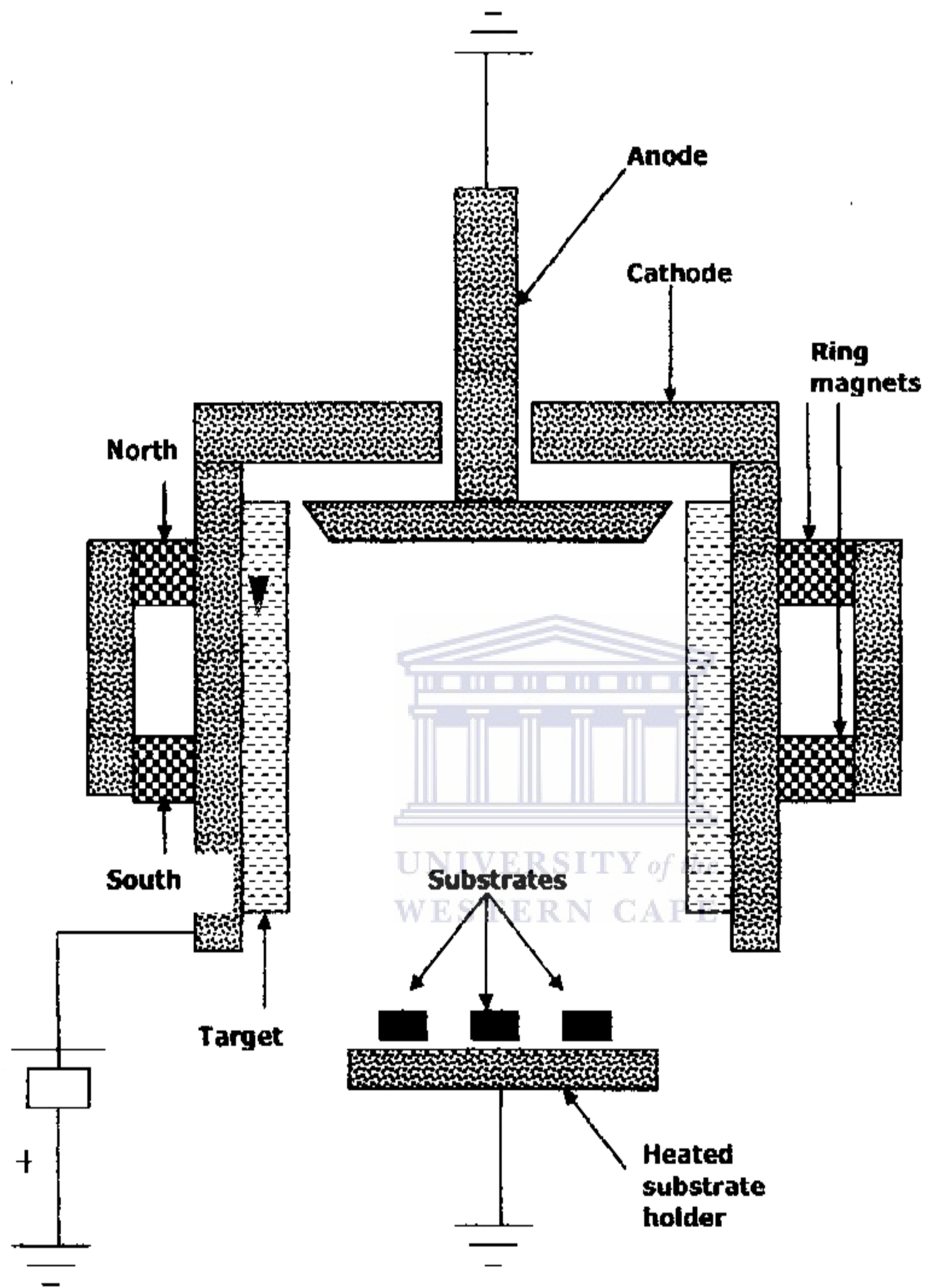

UNIVERSITY of the
WESTERN CAPE

Figure 2.2: Schematic representation of the inverted cylindrical magnetron sputter gun [28].

The gate valve is opened during the pump–down stage for fast evacuation of the chamber and kept semi-closed during the deposition. High purity Argon and mixture Oxygen (10%) and Argon gases are fed into the gun positioning and the vacuum components.

A Cesar Dressler, high-frequency generator is used as the power supply for the ICMS gun, generating electromagnetic power in the Megahertz-region, usually 13.56 MHz. The output voltage and current capabilities of these generators are limited. The plasma impedance is normally different from this, so a matching network is connected to the cathode to transform the cathode impedance to power needed by the generator. When the alternating signal is applied to the cathode, generating plasma, then the plasma acts as a rectifier that generates an average negative voltage at the smaller of both electrodes, which is in general the target. This negative voltage is called the self-bias or V_{DC} voltage of a radiofrequency cathode [24]. There have been excellent reports on the synthesis VO_2 thin films by home-made ICMS at ithemba labs. Kana kana et al [26] reported on the thermally tunable optical constants of vanadium dioxide thin films measured by spectroscopic ellipsometry. VO_2 thin films were prepared by ICMS and demonstrated the thermal controllable reversible of optical constants of VO_2 thin films. Optical/dielectric constants showed an abrupt thermal hysteresis which confirmed clearly the electronic structural change. He also reported on the thermochromic VO_2 thin films synthesized by ICMS. The paper reported on

UNIVERSITY of the
WESTERN CAPE

the first synthesis and feasibility of reliably reproduced stoichiometric pure textured VO2 nano-structures by the ICMS [27]. They also reported on the thermochromic nanocrystalline Au-VO_2 composite thin films deposited on glass substrates by ICMS. The plasmonic properties and thermochromic behavior of the synthesized composite of Au-VO_2 by ICMS were reported to be comparable to those Au-VO_2 thin films prepared by laser ablation, classical sputtering or other coating techniques [28]. Msomi et al [29] reported on the influence of deposition temperature on vanadium dioxide thin films microstructure and physical properties prepared by ICMS. VO_2 thin films were successfully synthesized on soda lime glass substrates. An increase in deposition temperature was reported to give rise to an increase in grain size and causes deterioration of the orientation (texture) of the grain size.

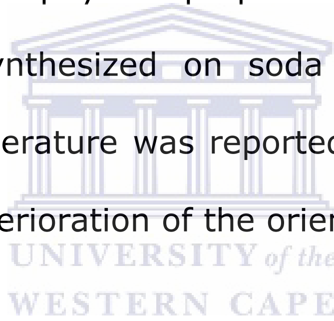
UNIVERSITY of the
WESTERN CAPE

2.5 Modes of thin films

During the Physical vapor deposition coating processes, such as magnetron sputtering and arc evaporation the film material is usually deposited atom by atom on a substrate by condensation from the vapour phase to the solid phase. This condensation step is not a random impingement of atoms that stick on the surface at the point of impact, due to the development of inter-atomic attractive forces, thermal mobility considerations and surface defects.

Generally a four stage dynamic process occurs. At first the nucleation of single atoms on the surface occurs. If the time of atom migration (determined by the atom's energy) on the surface is great enough to meet another atom before being evaporated these atoms join together to form an island. As the energy required to evaporate one of the atoms from this pair is considerably higher than that needed for a separate atom stable islands (nuclei) start to form on the surface. The islands coalesce and finally the continuous growth of the film takes place. During the island coalescence, three common mechanisms can occur namely:

Volmer- Weber growth

In Volmer-Weber (VW) growth, adatom-adatom interactions are stronger than those of the adatom with the surface leading to the formation of three-dimensional adatom clusters or islands Growth of these clusters, along with coarsening, will cause rough multi-layer films to grow on the substrate surface.

UNIVERSITY of the
WESTERN CAPE

Frank-van der Merwe growth

During this growth adatoms attach preferentially to surface sites resulting in atomically smooth, fully formed layers. This layer-by-layer growth is two dimensional, indicating that complete films form prior to growth of subsequent layers.

Stranski-Krastanov growth

Stranski-Krastanov growth is an intermediary process characterized by both 2D layer and 3D island growth. Transition from the layer-by-layer to island-based growth occurs at a critical layer thickness which is highly dependent on the chemical and physical properties, such as surface energies and lattice parameters, of the substrate and film. Figure 2.7 - 2.9 below shows a schematic representation of the three main growth modes for various surface coverage [30,31].

UNIVERSITY of the
WESTERN CAPE

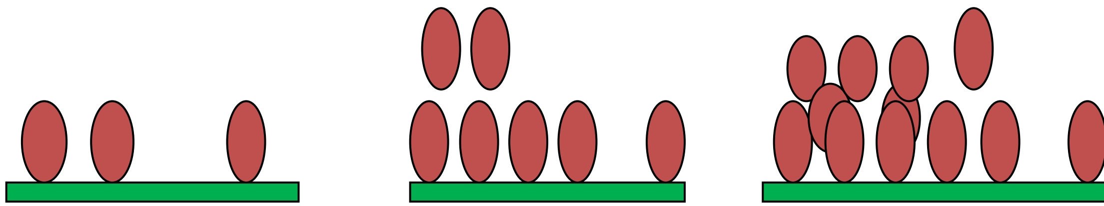

Figure 2.7 island growth (volmer-weber)

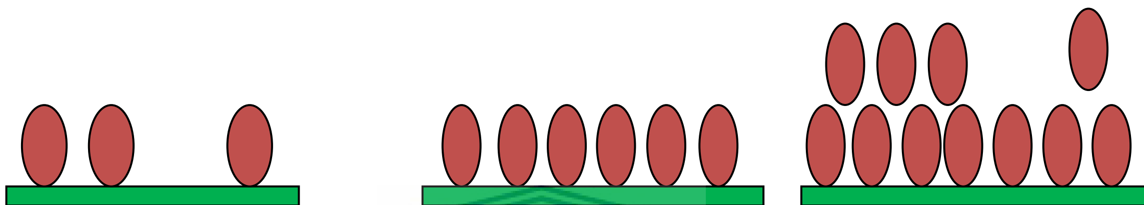

UNIVERSITY of the
WESTERN CAPE

Figure 2.8 layer by layer growth

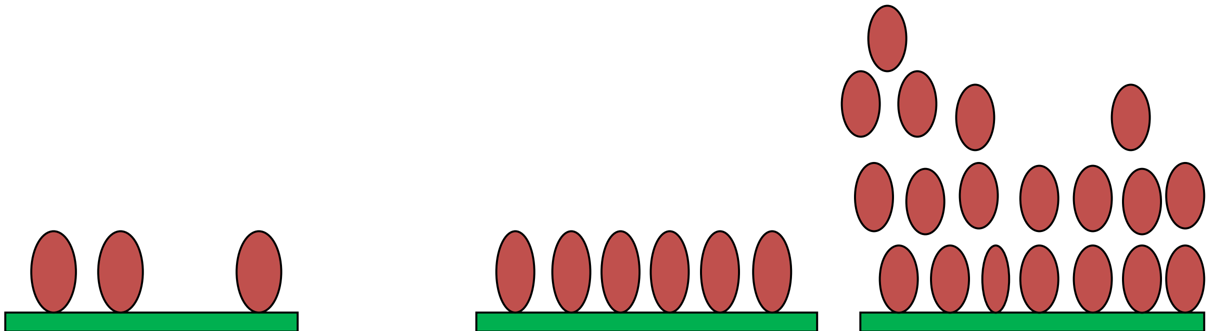

Figure 2.3 layer plus island formation

2.6 References

[1] K. Wasa, S. Hayakuwa, S. Rossnagel. Handbook of sputter deposition technology: Principle, technology and application. (1992)

[2] K. seshan, S. Rossnagel. Handbook of thin film deposition process and technique: sputtering and sputter deposition. (2012)

[3] P. Sigmound, sputtering by particle bombardment, springer-verlag, New-york, (1981).

[4] D. M. Mattox, Handbook of physical vapor deposition;film formation. (1998).

[5] F. C. Powell, H. Joseph, Oxley, and J. M. Blocher, Jr; Vapor deposition, John Wiley (1966)

[6] D. L. Smith, Thin film deposition: Thin film Deposition: principle and practice, McGraw-Hill, Inc. (1995)

[7] K. S. Sreeharsha, Principle of physical vapor deposition. Technology and engeneering- Elsevier. (2006)

[8] R. Wendt and K. Ellmer. Surf. Coating Technol; 93 (1997) 27.

[9] E. N. Fuls. Appl. Phys. Let. 10 (1967) 7

[10] G. A. Rozgoni. J.Vac.Sci.Tech. 5 (1968) 6

[11] M. A. Richardson, A. J. Coath. Opt. laser. Tech. 30 (1998)2

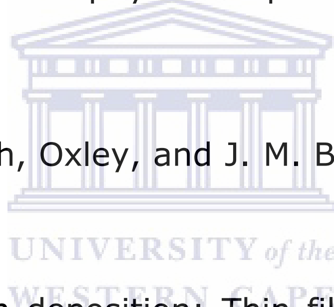
UNIVERSITY of the
WESTERN CAPE

[12] R. M. Oksuzoglu. O. Gonenc. N. C. Aslandere. Thin film process and characterization laboratory I and II. Script for theoretical and experimental preparation. Anadolu University.

[13] C. Batista, R. Ribeiro. J. Carneiro. V. Teixeira. J. Nano.Sci. Nano.tech. 9 (2009) 7

[14] K. D. Ufert. Physica status solid. 34 (2006) 1 K83-K86

[15] F. Y. Gan. P. Laou. J. Vav. Sci. A22 (2004) 3

[16] C. E. Lee, R. A. Atkins. W. N. Gibler. H. F. Taylor. Appl. Optics. 28 (1989) 21. 4511-4512

[17] E. Kusano. J. Vac.Sci. tech. 6 (1988) 3 1663-1667

[18] T. Christmann. B. Felde. W. Niessner. D. Schalch. A. Scharmann. Thin solid films. 287(1996) 134-138

[19] H. Miyazaki. I. yasui. J. phys. D: Appl. Phys. 39(2006) 220

[20] J. A. Thornton. A. S. Penfold. Cylindrical magnetron sputtering in: Thin films processes, edited by J.L Vossen and W. Kern. (1978) 75

[21] D. A. Glocker, proceedings of the annual SCV conference (1995) 298

[22] D. E. Siegfried, D. Cook, Ion tech inc. 39th annual technical conference proceedings of the society of the vacuum coaters 505/ 856 (1996) 97

[23] J. A. Thornton. V. Hedgcoth. J.Vac.Sci. tech. 12 (1975) 93

[24] A.S. Penfold, J.A.Thornton, U.S. Patents #3,884, (1975)793.

UNIVERSITY of the WESTERN CAPE

[25] A. Thornton, A. S. Penfold. inc: J. L. Vossen, W. Kern(Eds),Thin Films Processes, Academic Press, New York, (1978), 76

[26] J. B. Kana Kana. J. M. Ndjaka. G. Vignaud. A. Gibaud. M. Maaza. Optics. Communications. 284 (2011) 807-812.

[27] J. B. Kana Kana. B. D. Ngom. J. M. Ndjaka. P. Owono Ateba. O. Nemraoui. N. Manyala. A.C. Beye. M. Maaza Appl. Surf. Sci. 254(2008) 13. 3959-3963.

[28] J. B. Kana Kana. B. D. Ngom. J. M. Ndjaka. P. Owono Ateba. O. Nemraoui. N. Manyala. A. Y. Fesasi. R. Nemutudi. A. Gibaud. D. Knoesen. M. Maaza. Thin. Solid. Films. 518(2010)6. 1641-1647

[29] V. Msomi, O. Nemraoui, S.Afr. J. Sci. 106 (2010) 1-4

[30] P. Klapetek, Ph.D. Thesis, MASARYK UNIVERSITY BRNO, (2003).

[31] R. Palisaitis, Vasiliauskas, Linköping University, Epitaxial growth of thin films, Physics of advanced materials winter school, (2008).

UNIVERSITY of the
WESTERN CAPE

CHAPTER 3

3 CHARACTERIZATION TECHNIQUES.

This chapter is dedicated on explaining the different techniques of characterization used in this work. Atomic force microscopy, X-ray diffraction, Rutherford backscattering spectrometry, Elastic recoil detection and the Ultraviolet-visible spectrophotometer were used to characterize VO_2 thin films synthesized by Inverted cylindrical magnetron sputtering. All the experimental work was done iThemba LABS, a general description of the afore-mentioned techniques is given below.

UNIVERSITY of the
WESTERN CAPE

3.1 Atomic force microscopy (AFM)

3.1.1 Principles of AFM

The atomic force microscope (AFM) was invented by Binning et al, in 1986 [1]. AFM is a high-resolution type of scanning probe microscopy, with demonstrated resolution on the order of fractions of a nanometer, more than 1000 times better than the optical diffraction limit. AFM consist of a cantilever with a sharp probe at its end which is used to scan the specimen surface. The cantilever is typically silicon or silicon nitride with a tip radius of curvature on the order of nanometers. The amount of force between the probe and sample is dependent on the spring constant (stiffness) of the cantilever and the distance between the probe and the sample surface. This force can be described using Hooke's Law. Depending on the situation,

forces that are measured in AFM include mechanical contact force, van der waal's forces, capillary forces, chemical bonding, electrostatic forces, magnetic forces, Casimir forces and solvation forces. Along with force, additional quantities may simultaneously be measured through the use of specialized types of probes. Typically, the deflection is measured using a laser spot reflected from the top surface of the cantilever into an array of photodiodes. Other methods that are used include optical interferometry, capacitive sensing or piezoresistive AFM cantilevers. These cantilevers are fabricated with piezoresistive elements that act as a strain gauge. Using a wheatstone bridge, strain in the AFM cantilever due to deflection can be measured, but this method is not as sensitive as laser deflection or interferometry.

UNIVERSITY of the
WESTERN CAPE

If the tip was scanned at a constant height, a risk would exist that the tip collides with the surface, causing damage. Hence, in most cases a feedback mechanism is employed to adjust the tip-to-sample distance to maintain a constant force between the tip and the sample. Traditionally, the sample is mounted on a piezoelectric tube that can move the sample in the *z* direction for maintaining a constant force, and the x and y directions for scanning the sample. Alternatively a 'tripod' configuration of three piezo-crystals may be employed, with each responsible for scanning in the x, y and z directions. This eliminates some of the distortion effects seen with a tube scanner. In newer designs, the tip is mounted on a vertical piezo scanner while the sample is being scanned in X and Y using another piezo block. The resulting map of the area $z = f(x,y)$ represents the topography of the sample [2-4].

3.1.2 Modes of operation

The AFM can be operated in a number of modes, depending on the application. In general, possible imaging modes are divided into: static (also called contact) modes and a variety of dynamic (or non-contact) modes where the cantilever is vibrated.

In the contact-AFM mode, the tip makes soft “physical contact” with the surface of the sample. The deflection of the cantilever Δx is proportional to the force acting on the tip, via Hook’s law;

(1)

Where k is the spring constant of the cantilever. In contact-mode the tip either scans at a constant small height above the surface or under the conditions of a constant force. In the constant height mode the height of the tip is fixed, whereas in the constant-force mode the deflection of the cantilever is fixed and the motion of the scanner in z-direction is recorded. By using contact-mode AFM, even “atomic resolution” images are obtained

UNIVERSITY of the
WESTERN CAPE

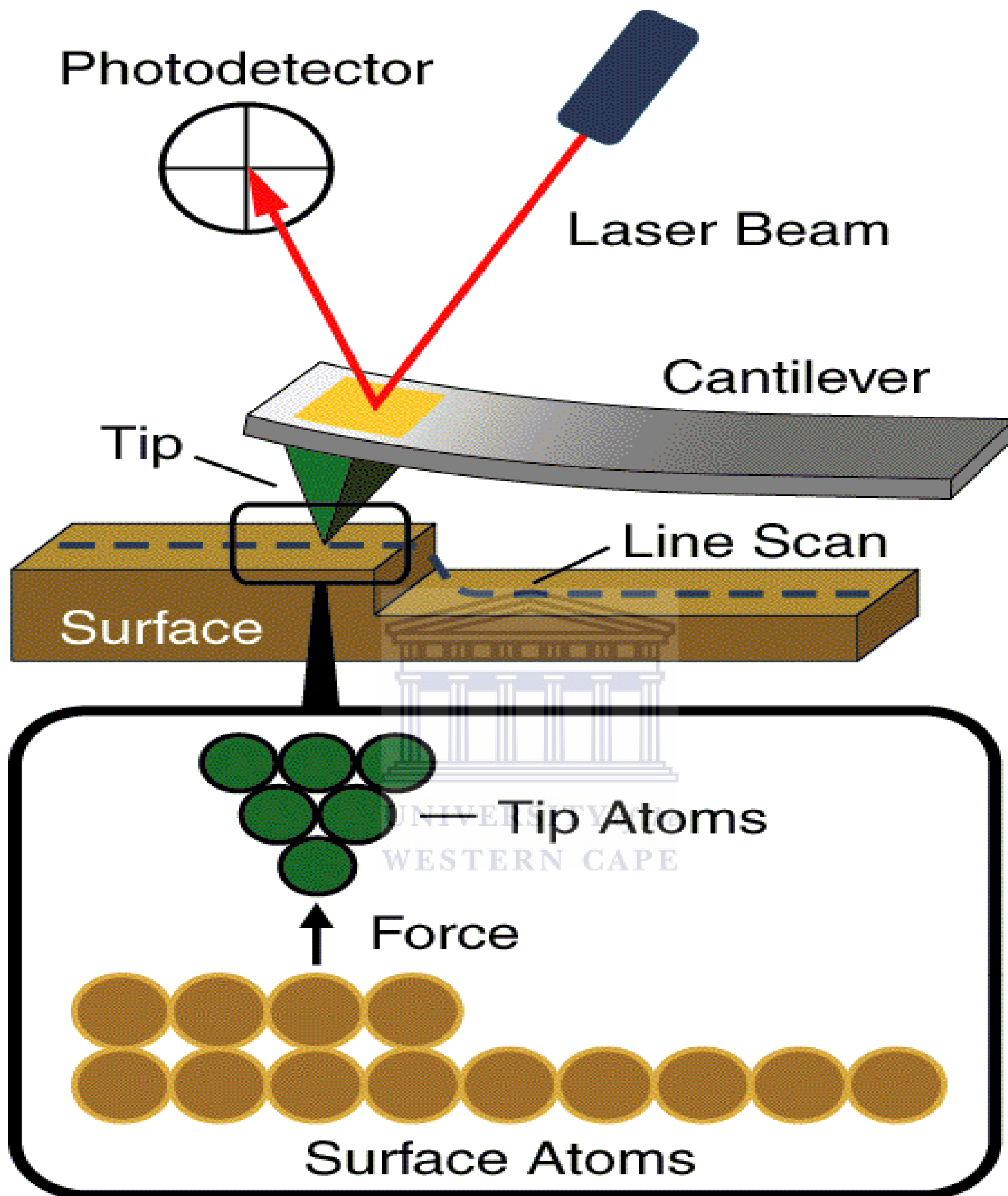

WESTERN CAPE

Figure 3.1: Principles of atomic force microscopy [2]

In non Contact modes mode, the tip of the cantilever does not contact the sample surface. The use of non-contact mode allowed scanning without influencing the shape of the sample by the tip-sample forces. In most cases, the cantilever of choice for this mode is the one having high spring constant of 20-100 N/m so that it does not stick to the sample surface at small amplitudes. The tips mainly used for this mode are silicon probes

In tapping modes, the force measured by AFM can be classified into long-range forces and short range forces. The first class dominates when we scan at large distances from the surface and they can be Van der Waals force, capillary forces (due to the water layer often present in an ambient environment). When the scanning is in contact with the surface the short range forces are very important, in particular the quantum mechanical forces (Pauli Exclusion Principle forces). In tapping mode-AFM the cantilever is oscillating close to its resonance frequency. An electronic feedback loop ensures that the oscillation amplitude remains constant, such that a constant tip-sample interaction is maintained during scanning. Forces that act between the sample and the tip will not only cause a change in the oscillation amplitude, but also change in the resonant frequency and phase of the cantilever. The amplitude is used for the feedback and the vertical adjustments of the piezo-scanner are recorded as a height image. Simultaneously, the phase changes are presented in the phase image (topography). The advantages of the tapping mode are the elimination of a large part of permanent shearing forces and the causing of less damage to the sample surface, even with stiffer probes. Different components of the sample which exhibit difference adhesive and

UNIVERSITY of the
WESTERN CAPE

mechanical properties will show a phase contrast and therefore even allow a compositional analysis. For a good phase contrast, larger tip forces are of advantage, while minimization of this force reduces the contact area and facilitates high-resolution imaging. So in applications it is necessary to choose the right values matching the objectives. Silicon probes are used primarily [4,5].

AFM provides a 3D profile of the surface on a nano-scale, by measuring forces between a sharp probe (less than 10 nm) and surface at a very short distance (0.2-10 nm probe-sample separation). Figure 3.2 shows an example of a 3D AFM image of VO_2 thin film grown on glass substrate. In this work the Atomic Force microscopy of the various thin films of VO_2 were carried out in continuous mode with a Veeco type AFM-MFM unit on a surface of 10x10mm. An AFM using nanoscope IIIa, digital instruments operated in tapping mode was used to capture the images of surface morphology of the thin films; parameters such as roughness were also investigated

UNIVERSITY of the
WESTERN CAPE

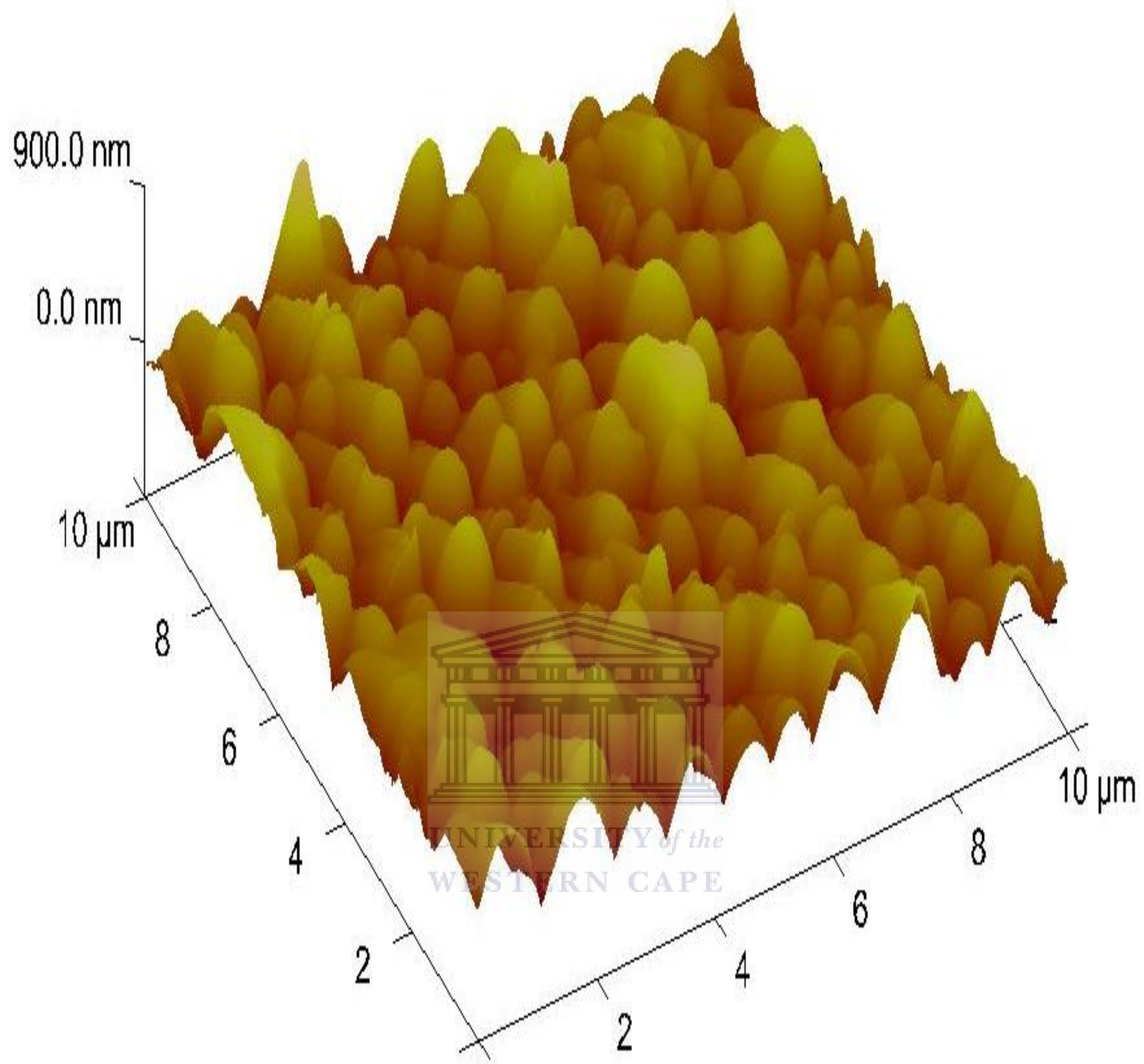

UNIVERSITY of the
WESTERN CAPE

Figure 3.2: Morphology of a 3D image of a VO_2 thin film grown on glass substrate [7]

3.2 X-ray diffraction technique (XRD)

X-ray diffraction (XRD) is a versatile, non-destructive technique that reveals detailed information about the chemical composition and crystallographic structure of natural and manufactured materials.

3.2.1 Fundamental Principles

X-ray diffraction is based on constructive interference of monochromatic X-rays and a crystalline sample. These X-rays are generated by a cathode ray tube, filtered to produce monochromatic radiation, collimated to concentrate, and directed toward the sample. The interaction of the incident rays with the sample produces constructive interference (and a diffracted ray) when conditions satisfy Bragg's law;

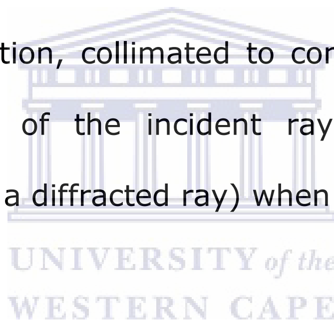
UNIVERSITY of the
WESTERN CAPE

(2)

This law relates the X-rays wavelength to the diffraction angle and the lattice spacing in a crystalline sample. These diffracted X-rays are then detected, processed and counted. By scanning the sample through a range of 2θ angles, all possible diffraction directions of the lattice should be attained due to the random orientation of the powdered material. Conversion of the diffraction peaks to d-spacing allows identification of the phases because each material has a set of

unique d-spacing. Typically, this is achieved by comparison of d-spacing with standard reference patterns.

Phase identification using x-ray diffraction depends on the positions of the peaks in a diffraction profile as well as the relative intensities of these peaks to some extent.

Another aspect of the diffraction from material is the importance to consider how diffraction peaks are changed by the presence of various types of defects such as small number of dislocations in crystals with dimensions of millimeters. Small size of grain size can be considered as another kind of defect and can change diffraction peak widths. Very small crystals cause peak broading.

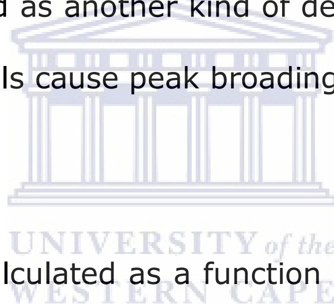
UNIVERSITY of the
WESTERN CAPE

The crystallite size is easily calculated as a function of peak width (specified as the full-width at half maximum peak intensity (FWHM)), peak position and wavelength using the well known Scherrer's formula.

$$D = \frac{0.9\lambda}{\Delta(2\theta)Cos\theta} \quad (3)$$

It is used to estimate the size of crystals from measured width of their diffraction curves. Note that whether a value of 0.9 or 1 is used depends on shapes of the crystallites assumed to be sample.

3.2.2 Principle of operation

X-ray diffractometers consist of three basic elements: an X-ray tube, a sample holder, and an X-ray detector. X-rays are generated in a cathode ray tube by heating a filament to produce electrons, accelerating the electrons toward a target by applying a voltage, and bombarding the target material with electrons.

When electrons have sufficient energy to dislodge inner shell electrons of the target material, characteristic X-ray spectra are produced. These spectra consist of several components, the most common being K_α and K_β. K consists, in part, of K_1 and K_2. K_1 has a slightly shorter wavelength and twice the intensity as K_2. The specific wavelengths are characteristic of the target material (Cu, Fe, Mo, Cr).

UNIVERSITY of the
WESTERN CAPE

Filtering, by foils or crystal monochrometers, is required to produce monochromatic X-rays needed for diffraction. K_1 and K_2 are sufficiently close in wavelength such that a weighted average of the two is used. Copper is the most common target material for single-crystal diffraction, with CuK radiation = 1.5418Å. These X-rays are collimated and directed onto the sample.

As the sample and detector are rotated, the intensity of the reflected X-rays is recorded. When the geometry of the incident X-rays impinging the sample satisfies the Bragg Equation, constructive interference occurs and a peak in intensity occurs.

A detector records and processes this X-ray signal and converts the signal to a count rate which is then output to a device such as a printer or computer monitor. The geometry of an X-ray diffractometer is such that the sample rotates in the path of the collimated X-ray beam at an angle θ while the X-ray detector is mounted on an arm to collect the diffracted X-rays and rotates at an angle of 2θ.

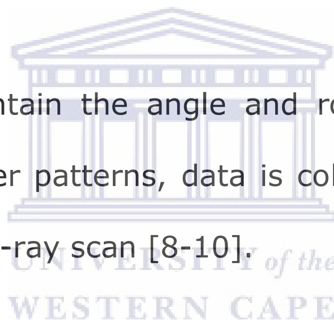
UNIVERSITY of the
WESTERN CAPE

The instrument used to maintain the angle and rotate the sample is termed a goniometer. For typical powder patterns, data is collected at 2θ from ~5° to 70°, angles that are preset in the X-ray scan [8-10].

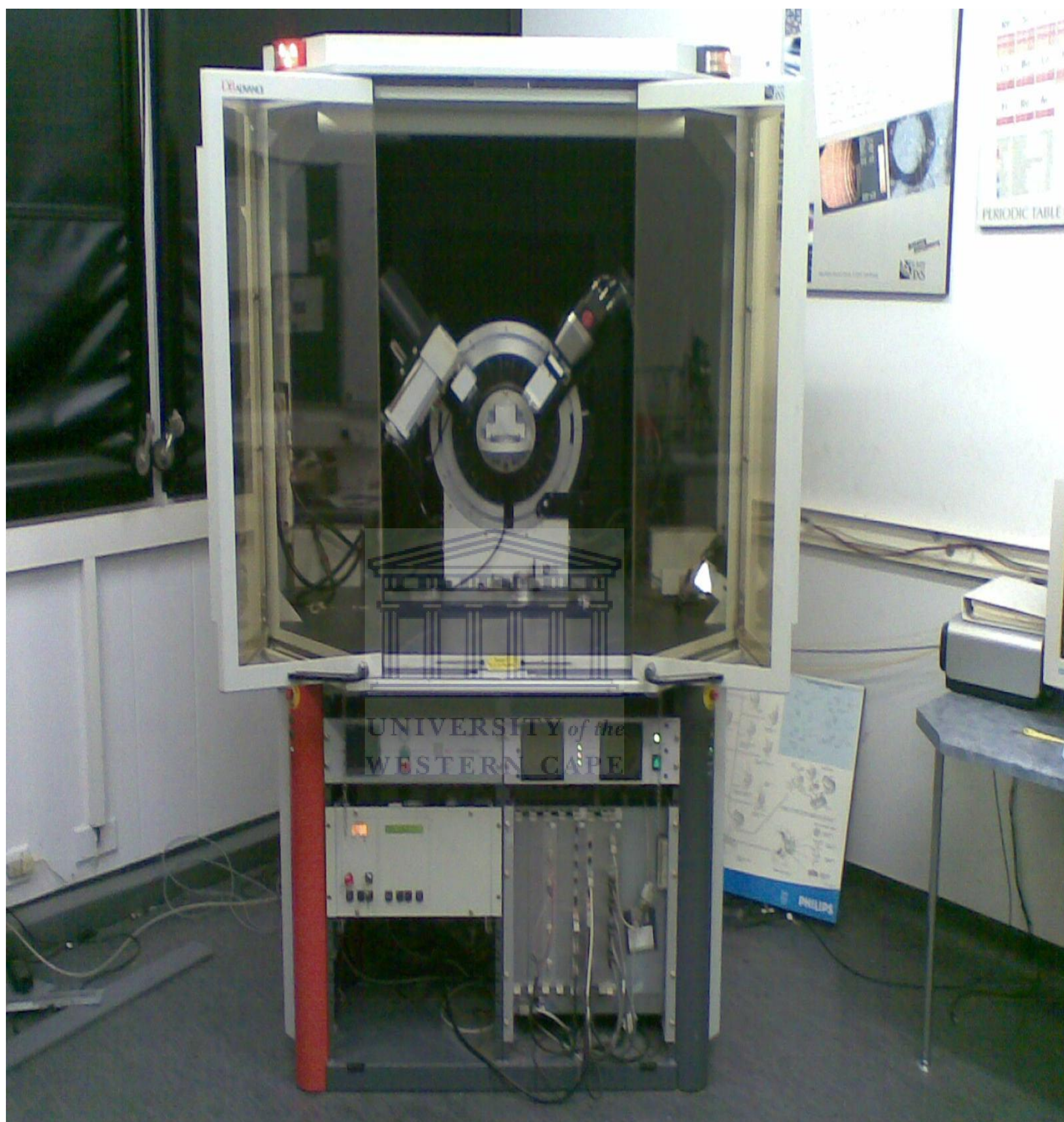

UNIVERSITY of the
WESTERN CAPE

Figure 3.3: Bruker's X-ray Diffraction D8-Discover instrument at iThemba LABS.

3.3 Rutherford backscattering spectrometry (RBS)

RBS is an analytical technique used in material science. This is a non-destructive technique since the erosion and the radiation degradation of the sample material by the particle impact is negligible. Sometimes referred to as high-energy ion scattering (HEIS) spectrometry, RBS is used to determine the structure and composition of materials by measuring the backscattering of a beam of high energy ions impinging on a sample.

In RBS, ions of a high kinetic energy (0.5-4MeV) are directed at the sample. The incident ions are elastically scattered from the atoms in the sample. The number of scattered ions and their energy is measured. The data obtained from the spectrum gives the information on the composition of the sample, the distribution of the components and the thickness of the sample. The incident ions from a Van der Graaf are positively charged He+ atoms or protons. In order for the signal from the detector to be processed, common nuclear electronics and the particle energy spectra are stored in a computer based multi channel analyzer. The data evaluation is accomplished using standard procedures and computer codes. The advantage of the RBS analysis depends in the quantitative analysis of major and minor constituents lying in the first 0.5 to 2.0 micrometers of a material. The detection limits vary from 10^{11} to 10^{15} at.cm^{-2} for heavy and light elements depending on the sample structure and composition respectively. The best

UNIVERSITY of the
WESTERN CAPE

solution for improving the detection limits of some light elements is to use resonant scattering. The depth distribution of constituents can be reconstructed with a depth resolution approximately 10-20 nm.

3.3.1 Kinematic factor

The interaction between the projectile ion and the target atom can be properly described by a simple elastic collision of two isolated particles when the conditions below are fulfilled.

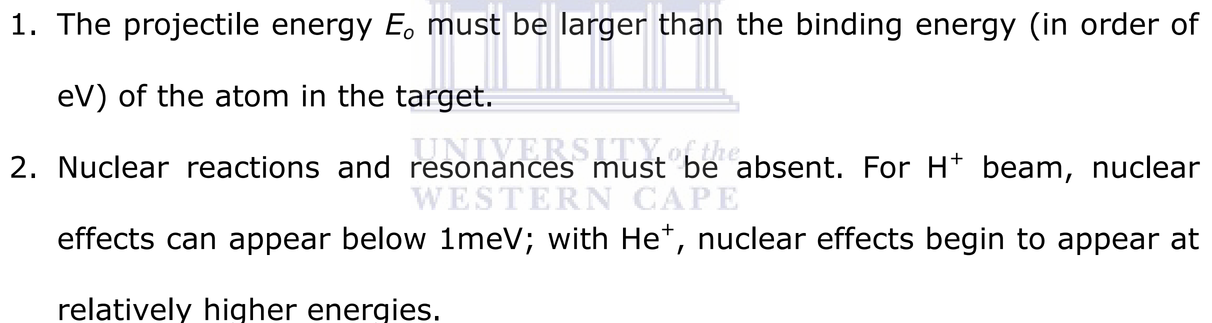

UNIVERSITY of the WESTERN CAPE

1. The projectile energy E_o must be larger than the binding energy (in order of eV) of the atom in the target.
2. Nuclear reactions and resonances must be absent. For H^+ beam, nuclear effects can appear below 1meV; with He^+, nuclear effects begin to appear at relatively higher energies.

From the assumptions, we consider the collision between two particles. The projectile of mass M_1 has an incident energy E_o and the target of mass M_2 is initially at rest. After the elastic collision, a part of projectile energy transfers to the target.

The kinematics of the simple elastic collision can be fully solved by applying the principles of conservation of energy and momentum. The ratio K of the scattering energy to the incident energy can be defined as:

$$K = \frac{E_1}{E_0} = \left[\frac{(M_2{}^2 - M_1{}^2 \sin^2 \theta)^{0.5} + M_1 \cos\theta}{M_1 + M_2} \right]^2 \quad (3)$$

The ratio K is also called *kinematic factor.* The scattered angle θ, which is defined as the angle between the projectile incident direction and the scattered angle is shown in Figure. Using kinematic factor formula, M_2 can be determined from the known incident particle mass M_1, the initial energy E_o, scattering angle θ and scattering energy E_1.

The small mass difference ΔM_2 produces a small energy change ΔE_1 in the measured energy ΔE_1 of the projectile after the collision. The relation between ΔM_2 and ΔE_1 is given by:

UNIVERSITY of the
WESTERN CAPE

$$\Delta E_1 \approx E_0 \left(\frac{dK}{dM_2} \right) \cdot \Delta M_2 \quad (4)$$

Therefore, the mass resolution can be estimated from the overall resolution δE of RBS as:

$$\delta M_2 = \frac{\delta E}{E_0} \left(\frac{dK}{dM_2} \right)^{-1} \quad (5)$$

If the mass difference of two elements in the target falls below the limit mentioned above, the distinction between two elements is lost.

3.3.2. Scattering cross section

Scattering cross section σ is the likelihood of occurrence of a two-body collision. This leads to the capability of quantitative analysis of analysis of atomic composition. The differential scattering cross section dσ/dΩ can be used to estimate how frequently a collision actually occurs and ultimately the scattering yield at a certain angle θ.

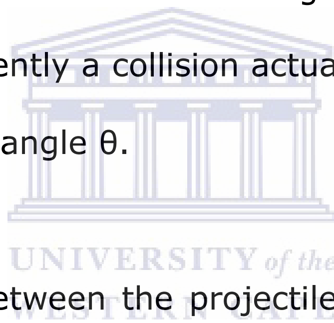
UNIVERSITY of the
WESTERN CAPE

In most cases, the force between the projectile ion and the target atom is very small described by Coulomb repulsion of the two nuclei as long as the distance of closest approach is large compared with nuclear dimensions, but small compared with the Bohr radius $a_B=\hbar/m_e.e=0.53Å$. The assumptions made came out with the differential scattering cross section given by Rutherford formula:

$$\left(d\sigma/d\Omega\right)_c=\left(\frac{Z_1Z_2e^2}{4E_0}\right)^2\times 4\frac{\left[\sqrt{\left(M_2{}^2-M_1{}^2\sin^2\theta\right)}+M_2\cos\theta\right]^2}{M_2\sin^4\theta\left(M_2{}^2-M_1{}^2\sin^2\theta\right)^{0.5}} \qquad (6)$$

where Z_1 and Z_2 represent nuclear charge of the incident particle and target atom, respectively. For a target of a thin film with thickness *D,* the scattering yield *Y(θ),* detected by a finite acceptance solid angle $\Delta\Omega$ at particular scattering angle *θ,* which can be given by:

$$Y(\theta) = N.D \times \frac{d\sigma}{d\Omega} \times \frac{\Delta\Omega.Q}{\cos\alpha} \qquad (7)$$

Where *Q* represents the number of incident ions impinging into the target, *N* is the atomic density of the target and is the incident angle.

UNIVERSITY of the
WESTERN CAPE

3.3.2 Stopping power

According to physics theory, an energetic particle that impinges upon a target will penetrate into it. If the particle pushes its way through the target, its kinetic energy decreases as the speed decreases. There are two mechanisms responsible for the energy loss of the projectile;

1. Nuclear stopping which originates from a multitude of small angle collisions of projectile with the atomic nuclei of the target, and
2. The electronic stopping comes from the frictional resistance that the projectile encounters on its pass through the electron clouds surrounding each target.

The energy loss per unit length *dE/dx* (in eV/Å) is called ***stopping power***. The stopping section *S* [eV/ (atoms/cm^2)] is related to stopping power and the atomic density *N* and is therefore more specific for a certain atomic species:

$$S = \frac{1}{N}\frac{dE}{dx} \qquad (8)$$

According to the investigation, the numerical predictions of stopping cross-section from the theory are difficult, because of large number of possible interactions that can conceivably take place.

3.4 Elastic recoil detection analysis (ERDA)

3.4.1 Introduction.

UNIVERSITY of the
WESTERN CAPE

Elastic recoil detection analysis (ERDA) is a nuclear technique in materials science to obtain elemental concentration depth profiles in thin films. ERDA was first demonstrated by Ecuyer et al. [12] in 1978 and by Doyle and Peercy [13] in 1979. It is the most frequently used method for depth profiling and content measurement in thin films and surfaces [14-16]. ERDA determines the yield and energy of particles ejected out of the surface region of samples under MeV ion bombardment, which is an ion beam analysis technique for quantitative analysis of light elements in solids. The sample which has to be analyzed is irradiated with ion beam energy (e.g. O, He, Li, Ag, Au) of several meV. Light elements from the sample are scattered in forward directions and can be detected with a solid state detector. ERDA makes use of the fact that the information about the target is carried by the

target nuclei themselves and not by the backscattered primaries as in RBS which enables to identify the particles under investigation. Detection in ERDA especially occurs in forward geometry, and therefore, both scattered and recoiled particles will move in the direction of detector [17].

3.4.2 Principles of ERDA

In an elastic collision of the incident particle of mass m_p (in atomic mass units) and energy E_p, with the atom of mass m_r (in atomic mass units) present in the sample, the atom in the sample which is at rest, recoils in forward direction after the collision. The energy E_r of the recoiling atom can be derived from the basic principle of conservation of energy and momentum which for atom with mass m_r at an angle ϕ with respect to the beam direction is given by;

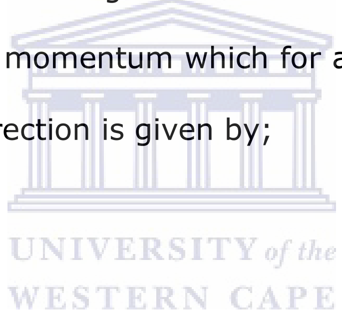
UNIVERSITY of the
WESTERN CAPE

(9)

Where K is the constant kinematic factor given by

$$\overline{} \qquad (10)$$

The projectile mass, its energy and recoil angle remains fixed under a given experimental condition, therefore atoms of different masses in the sample come out with different recoil energies as governed by equation (9). If m_p is greater than m_r,

projectiles can only be scattered in a limited angular range with a maximum angle ϕ defined by;

(11)

3.4.3 Depth profiling

The energy of recoils as detected by the detector depends on kinematics as per equation (9), energy loss of the incoming ion in the sample up to a certain depth *d*, energy loss of the recoil in the sample from depth *d,* where it originates, and energy loss of the recoil atom in the stopper foil. If the recoil originates from the surface, the energy of the recoil atom is determined only by the kinematics according to equation (9). This is the maximum energy of recoil of particular mass originating from the sample's surface. The energy of a recoil ion generated at depth *d* is given by;

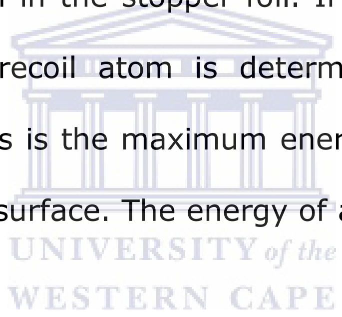
UNIVERSITY of the
WESTERN CAPE

(12)

Where $(dE/dx)_{in}$ is the energy loss of incoming ion in the sample material.

The energy of recoil E_{ds}, originating at depth *d*, coming out at the surface is given by;

(13)

Where $(dE/dx)_{out}$ is the energy loss of recoil in the sample. The recoil energy as detected by the detector is given by;

(14)

Where ΔE_{foil} is the energy loss of recoil in the foil, which is dependent on energy. The recoil energy is converted to depth scale using the equations. (12) to (14) shown above.

3.4.4 Depth resolution

Depth resolution depends on the energy resolution dE, which is governed by various factors such as, incident ion beam energy spread, straggling in the stopper foil and the detector system, in homogeneities in the stopper foil and the entrance window of the detector, detection system resolution, which is composed of the electronics noise and the detector resolution, kinematic broadening and angular and lateral spread due to multiple scattering, which adds to the kinematic broadening. Incident beam resolution is typically 50 keV. Detection system resolution is typically 1% and is therefore about 200 keV for 20 MeV heavy ion recoils. The experimental parameters are optimized in such a way that the recoil energy spread due to various factors is minimized.

3.5 UV-Visible Spectrophotometer (UV-vis)

The UV-visible (UV-Vis) spectrophotometer is a useful characterization technique for the absorption, transmission, and reflectivity of various technological important materials such as pigments, coatings, windows and filters. These applications are more important for the characterization of the optical or electronic properties of the materials.

3.5.1 Basic principles of the UV-Vi

The Ultraviolet (UV) and visible radiation constitute but a small part of the electromagnetic spectrum, most of the radiation that surrounds us cannot be seen, but can be detected by dedicated sensing devices. The electromagnetic spectrum ranges from very short wavelengths (including gamma and x-rays) to very long wavelengths (including microwaves and broadcast radio waves). Figure 3.4 displays many of the important regions of this spectrum. The energy associated with the electromagnetic radiation is given by;

UNIVERSITY of the
WESTERN CAPE

(15)

Where is the energy (in joules), is the planck's constant given by 6.62×10^{-34} Js and is the frequency in seconds.

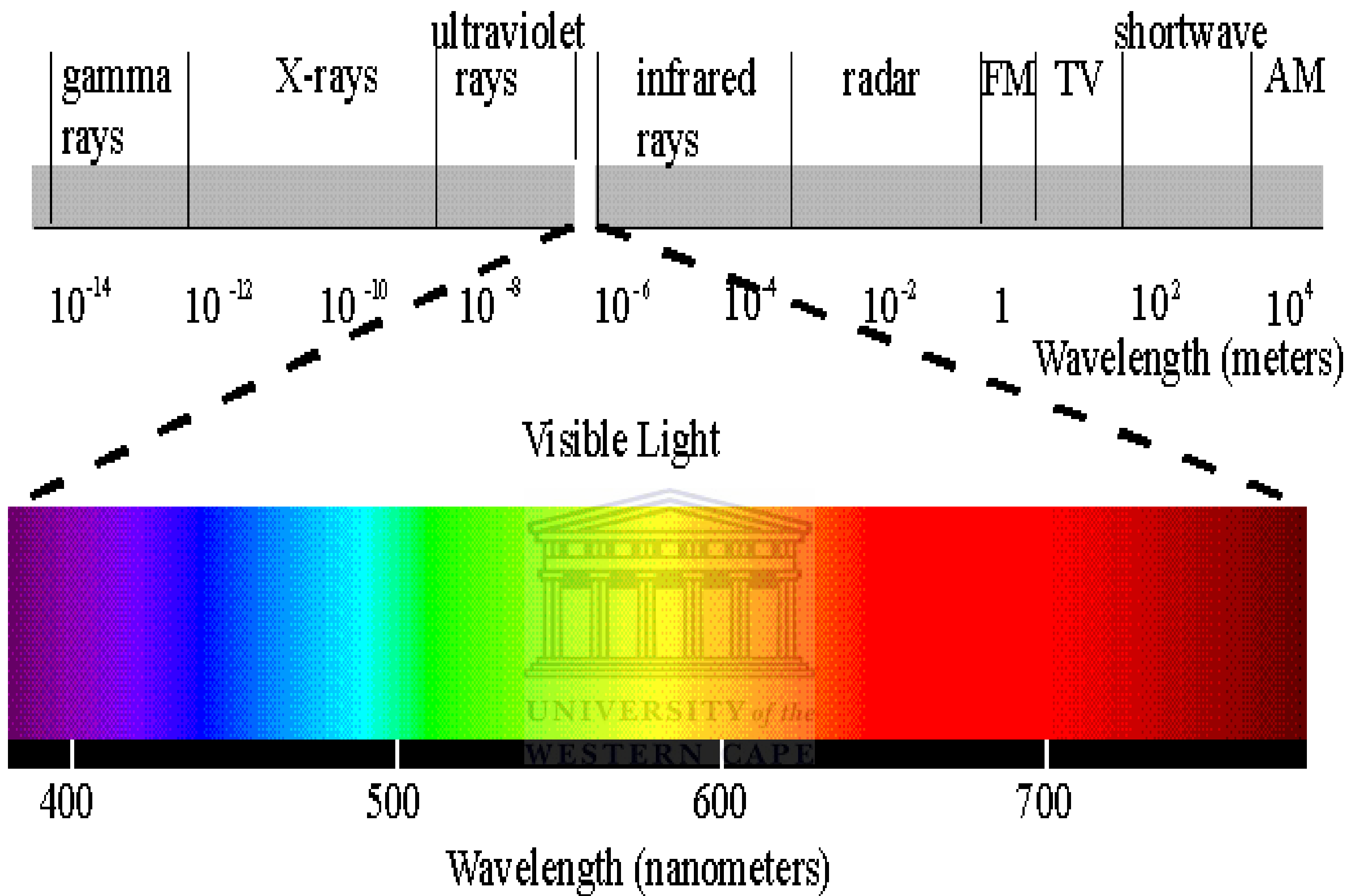

UNIVERSITY of the
WESTERN CAPE

Figure 3.4: Illustration of the electromagnetic spectrum.

Electromagnetic radiation can be considered as the combination of alternating electric and magnetic fieldz that travel through space with a wave motion. Radiation acts as a wave, it can be classified interms of either wavelength or frequency related to the following equation;

(16)

It follows from the above equation that the radiation of a shorter wavelength has high energy. In UV-visible spectroscopy, the low-wavelength UV light has the highest energy. When radiation interacts with matter, a number of processes can occur, when light passes through or is reflected from a sample, the amount of light absorbed is the difference between the incident radiation (I_o) and the transmitted radiation (I). The amount of light absorbed is expressed as either transmittance or absorbance. Transmittance usually is given in terms of a fraction of 1 or as a percentage and is defined as follows;

UNIVERSITY of the
WESTERN CAPE

(17)

The UV-vis equipment used in this study was a Cecil 200 spectrometer consisting of a light source, a sample holder with a heating stage and a data acquisition computer. The sample holder located between the light source

and the detector. The light source, detector, and sample holder are designed into a dark box which has a cover preventing unwanted light to interfere with the laser beam during the experiment. The optical transmission of VO_2 coatings were conducted from room (25°C) to high temperature (100°C) in the spectral range of 200- 1100 nm. The cycling process between the heating and cooling branches was also done at a step of 5 ^{0}C in between each transmission from 25-100 ^{0}C in the same spectral range. The UV-Vis measurements were used to investigate the optical switching properties of VO_2 thin films deposited on glass.

UNIVERSITY of the
WESTERN CAPE

3.6 References:

[1] G. Binning, C. F. Quate, Ch. Gerber. Atomic force microscope. Phys. Rev. Lett. 56 (9), (1986) 930.

[2] V. Clemente, K. Gloystein, Principles of atomic force microscopy, Physics of advanced materials winter school, (2008).

[3] Park Scientific Instruments. A practical guide to scanning probe microscopy. (1997).

[4] N. Yao, Z. L. Wang. Handbook of Microscopy for Nanotechnology. (2005).

[5] Veeco. Scanning Probe Microscopy Training Notebook. Version 3.0. (2000).

[6] G. Bolanos, C. Quinayas, H. Coy, M, F. Cordoba, and W. Lopera. VO_2 thin film.doc. Electrical and optica properties of VO2 thin films.

[7] H. B Cele. M.Sc desertation. University of Zululand. Nano structured thermochromic VO_2 for IR modulation application, (2009)

[8] B. D. Cullity, Elemets of X-ray Difraction, 2nd edn, Addison Wesley, Reading, MA. 1978.

[9] B. L. Dutrow. Louisana State University. M. C. Clark. Eastern Michigan University. X-ray powder difraction

[10] R. Jenkins, X-ray techniques:overview, Encyclopedia of analytical chemistry, R. A. Meyers (Ed.) (2000) 13269–13288

[11] J. A. Leavit, J. L. C McIntre, and M. R. Weller, Handbook of modern ion beam material Analysis, MRS, Pittsburgh (1995).

[12] J. L'Ecuyer, C. Brassard, C. Cardinal and B. Terreault, Nucl. Instr & Methods in Physics Research B, 149 (1978), 271.

[13] B. Doyle, L. Doyle and P. S. Peercey, Appl. Phys. Lett., (1979), 34, 812.

[14] L. S. Weilunski, R. E. Beneson, W. A. Lanford, Nucl Instr & Meth (1983) 218-120.

[15] A. Turos. O. Meyer. Nucl Intsr and Meth B (1984) 4:92.

[16] J. E. E. Kellock. A. J. Deline. V. R. Crockett MA, Shih AH. Nucl Intsr and Meth B (1992) 64-469

UNIVERSITY of the
WESTERN CAPE

[17] I. P. Jain, A. Jain, P. Jain. ERDA: Technique for Hydrogen Content and Depth Profile in Thin Film Metal Hydride.

CHAPTER 4

4- RESULTS AND DISCUSSIONS

4.1 Synthesis And Experimental Details

4.1.1 Synthesizing of thin films

A home-made Inverted cylindrical magnetron sputtering (ICMS) system at iThemba LABS, material science department was used to deposit the thin VO_2 films. Vanadium metal of 99.8% purity was used as the target, with diameter of 5cm mounted on the inverted cylindrical magnetron gun. The substrates (conical glass) were situated on a holder facing the cathode of the sputter gun. Substrates were heated, biased positively and the distance from the substrate holder to the sputtering head was approximate 2.0cm, this account for maximizing the rate of deposition and also minimizing the re-sputtering effect.

The base pressure of the vacuum chamber was pumped to 10^{-6} mbar by oil diffusion pump complimented by the rotary pump prior to deposition. A mixture of 10% O_2 (99.999% purity) and Ar (99.99%) were introduced separately into the chamber, with oxygen filled to $8x10^{-3}$ followed by argon filled to 10^{-2} mbar measured by the penning and pirani vacuum gauges mounted on the walls of the ICMS. During the deposition, the substrates were heated at different temperatures from 350 to 600°C at an interval of 50°C to make different set of samples while the others deposition parameters are kept constant. A Dressler Cesar RF power generator was used as the power supply to the cathode gun, using an RF power of 60 W. Immediately after the plasma was created in the vacuum, the deposition time was kept constant at 1hour for all the thin films at different substrate temperatures.

UNIVERSITY of the
WESTERN CAPE

4.1.2 Thin films analysis

The structure of the VO_2 thin films was characterized and confirmed by X-ray diffraction technique using the D8 advance Bruker diffractometer, with CuK_α radiation of wavelength 1.54 Å and a position sensitive Lynx-Eye, Si-strip detector with 196 channels. The intensity of the direct beam was scanned using a variable tube voltage of 40kV and current of 40mA. Measurements were taken using 2θ range of 20 to 80°, increment of 0.03 deg/step and measurement time of 3 sec/point.

The optical properties of the VO_2 thin films were analyzed by the UV-Vis measured in a wavelength between 200 to 1100 nm using the CECIL 200 spectrophotometer incorporated with the peltier thermoelectric heating and cooling system.

The morphology and roughness of the films was measured by the atomic force microscopy (AFM) using the nanoscope III a, digital instruments incorporated within the tapping mode.

The depth profiles of the films were observed by the HI-ERDA technique by the 6mV tandem accelerator using a 25.85 meV $^{63}Cu^{7+}$ beam at a grazing incidence angle of 14° to the sample surface.

UNIVERSITY of the
WESTERN CAPE

The stoichiometry and chemical composition of the films was confirmed using the Rutherford backscattering spectroscopy (RBS) using a 2 MeV H_e^{+} ion beam. The evaluation by the above characterization technique was done at iThemba laboratory in Cape Town and iThemba laboratory Gauteng for the HI-ERDA technique.

4.2 Results and Discussions

4.2.1 XRD-Structure Analysis

XRD was the first technique used to characterize the different thin films samples of VO_2 after deposition. The crystal structure and crystallite size evolution of the thin films were evaluated by the XRD technique. Figure 4.1 shows the XRD spectra scanned between 20 to 80° for the films at different substrate temperatures ranging from 350°C to 600°C.

All films exhibit a series of Bragg peaks for which the dominant (011) peak at around 27.7^{o}C was observed in all thin films. Other than the dominant (011) reflection, small peaks arising (020), (210), (021), (022), (300), (031) and (202) were observed noticeably when the films were deposited at high temperatures, identified more visible for the films at 550 and 600°C.

UNIVERSITY of the
WESTERN CAPE

All the aforementioned Bragg peaks correspond to pure VO_2 phase according to the JCPDS 0431051, Monoclinic with an average lattice parameters of about: a = 7.51Å b= 4.537Å c=5.382Å. There were no other peaks corresponding to vanadium oxide phases detected by XRD.

Figure 4.2a shows the growth evolution of the (011) plane of VO_2 thin films at different substrate temperatures, which was used to estimate the average crstallite size evolution along the (011) orientation by the Debye scherrer approximation (ref: Chapter 3 equation (3));

The full width at half maximum (FWHM) increases with the decrease in substrate temperature. Sharper is the peak smaller is the FHWM of the (011) peak and consequently bigger are the crystalline size along the (011) reflection.

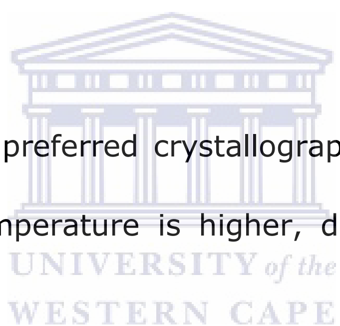
UNIVERSITY of the
WESTERN CAPE

In general the degree of the preferred crystallographic orientation in thin films is greater when the growth temperature is higher, due to the greater mobility of growth species.

The average grains growth evolution in the thin film increases when the deposition temperature is increased [1]. This trend is in line with the increase in average crystalline grain size with the substrate temperature along the (011) orientation as shown in figure 4.2b.

An increase in deposition temperature gives rise to an increase in average crystallite size and causes deterioration of the preferential orientation

(texture) of the films. The emerging small peaks are a clear indication of the deterioration of the preferential orientation growth of the VO_2 grains when the temperature increases [1, 2].

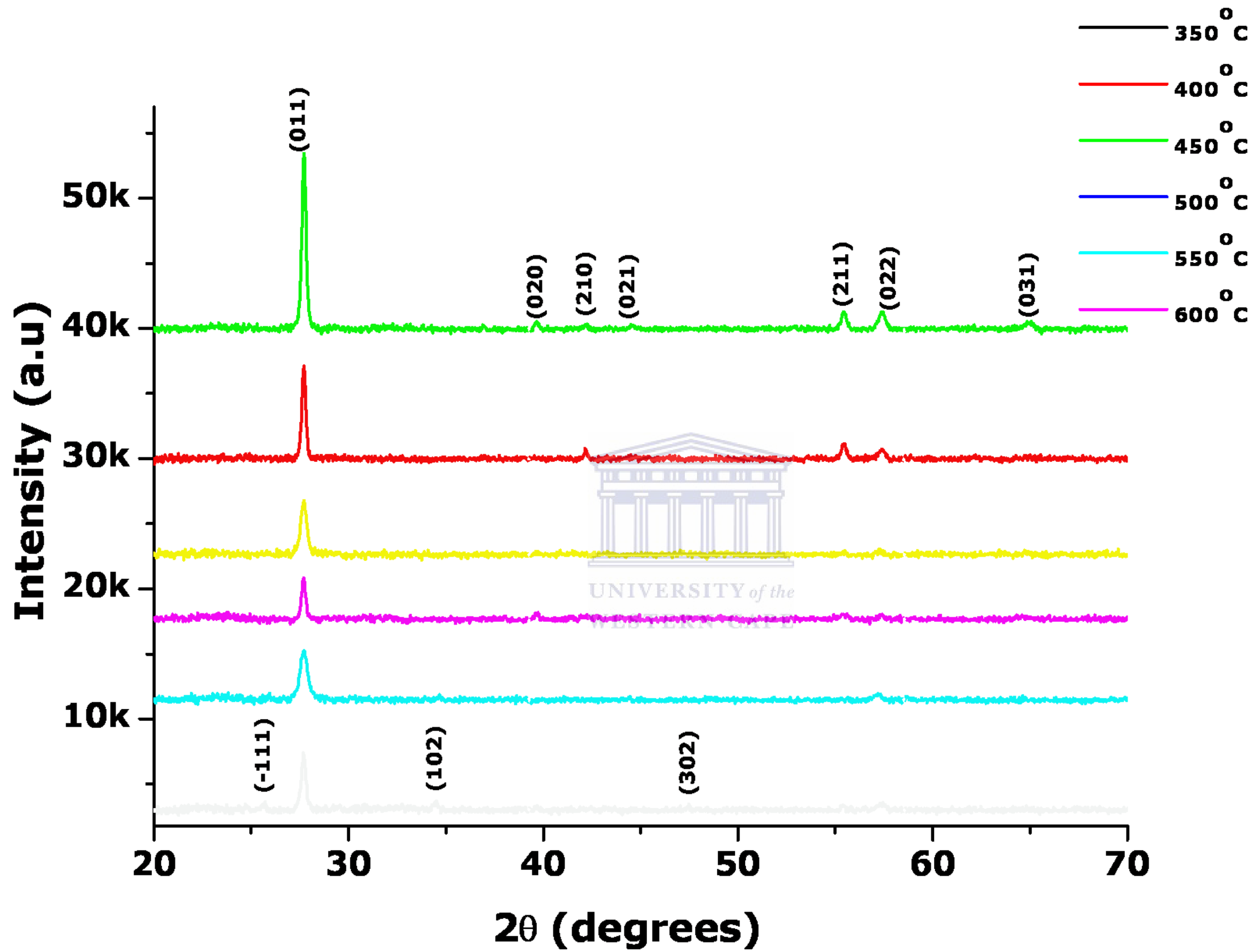

UNIVERSITY of the
WESTERN CAPE

Figure 4.1 XRD spectra of VO2 thin films

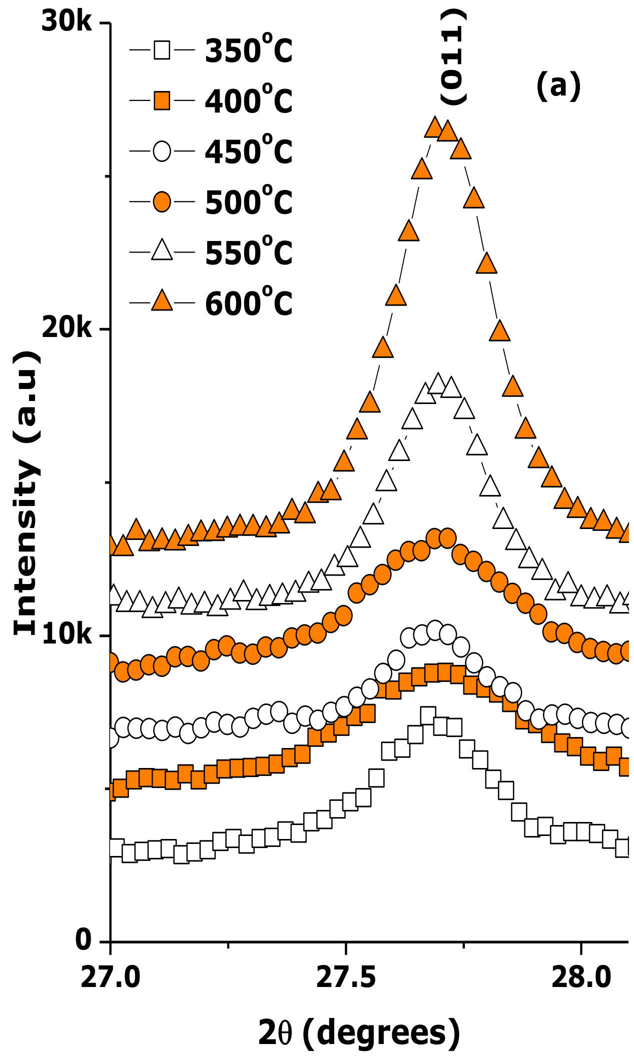

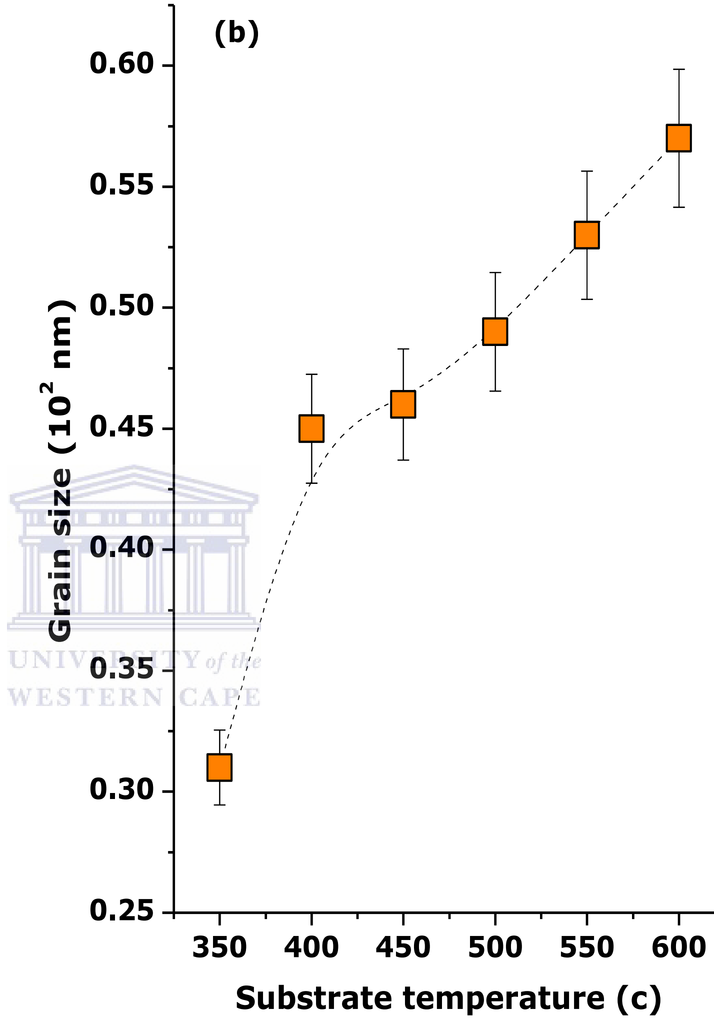

UNIVERSITY of the
WESTERN CAPE

Figure 4.2 (a) Evolution of the (011) plan of VO_2 thin films at different substrate temperature. (b): dependence of crystalline grain size on substrate temperature of VO_2 thin films along (011) plan.

4.2.2 Surface morphology

The Atomic Force microscopy of the various thin films was carried out in continuous mode with a Veeco type AFM-MFM unit on a surface of 10x10mm. Figure 4.3 to 4.6 shows a 3D AFM image sputtered at different substrate temperatures. The surface roughness (R_a) of all the films was calculated using the Nanoscope software.

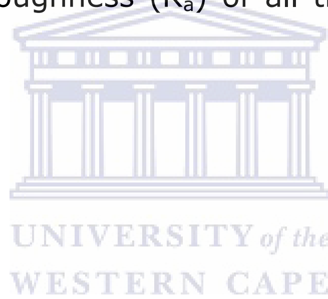
UNIVERSITY of the
WESTERN CAPE

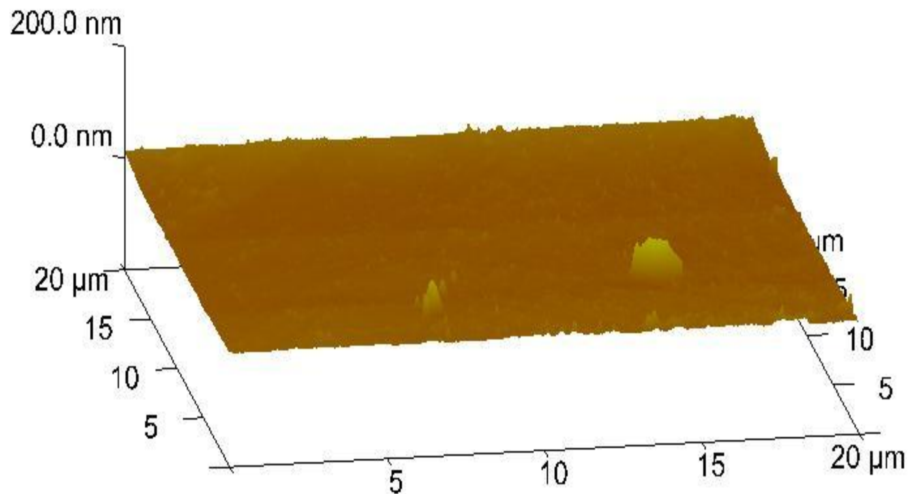

Figure 4.3: 3D AFM image of VO_2 at 350°c

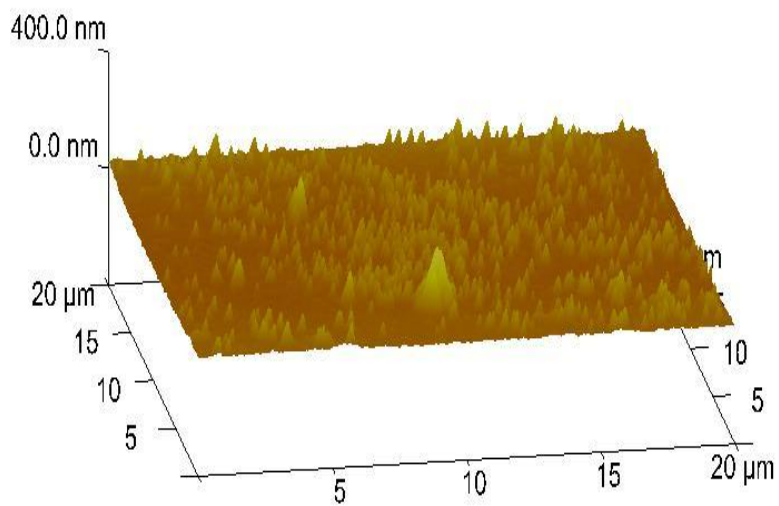

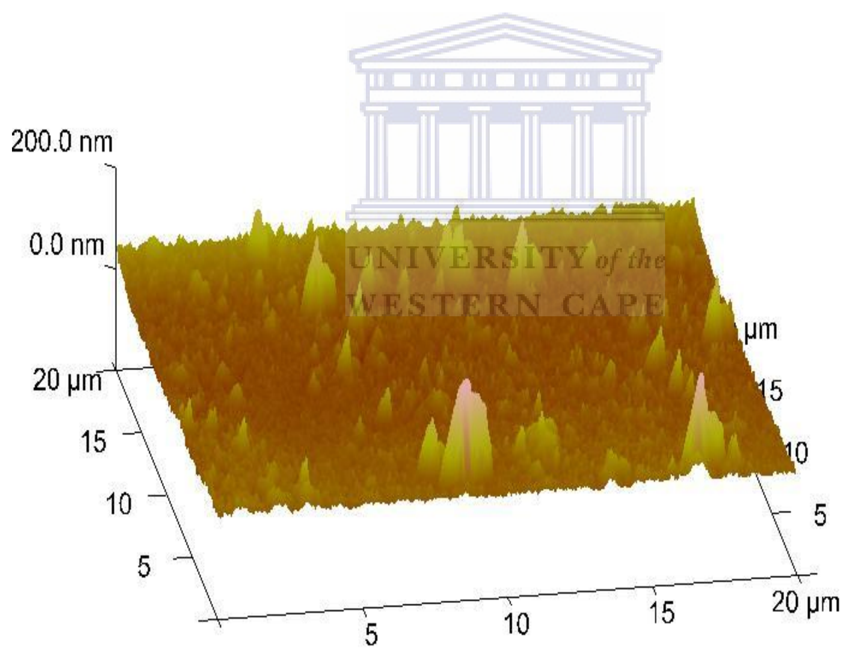

UNIVERSITY of the
WESTERN CAPE

Figure 4.4: 3D AFM image of VO2 at 400°C (top) and 450°c (bottom)

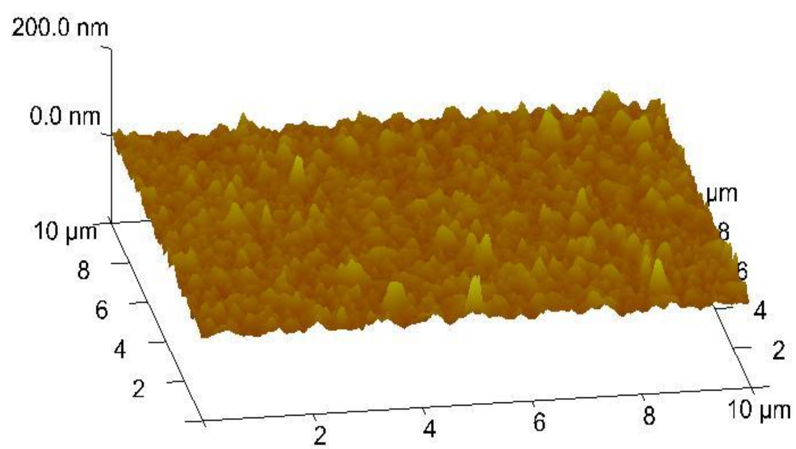

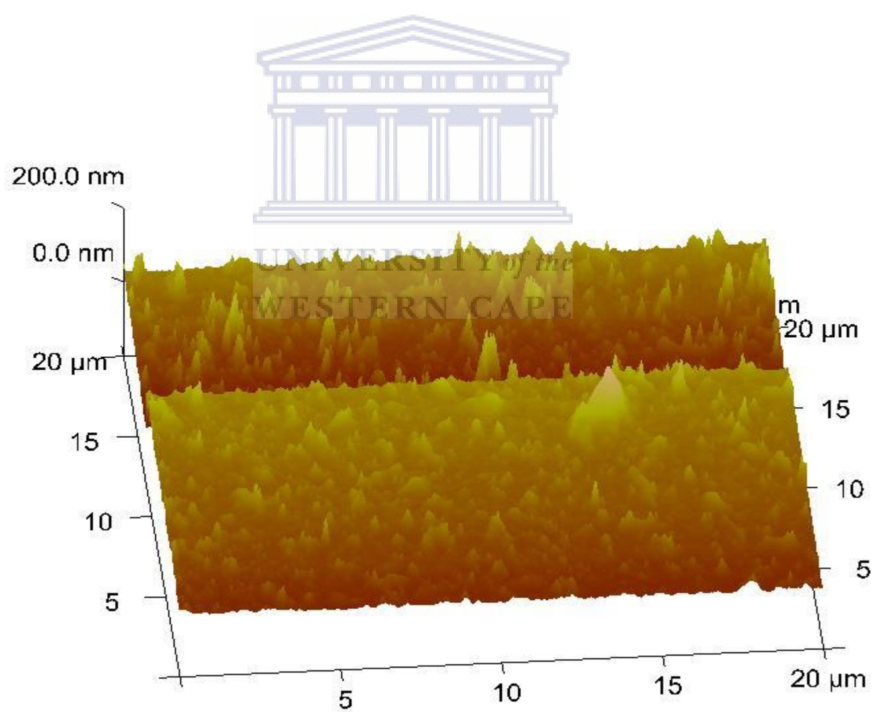

UNIVERSITY of the
WESTERN CAPE

Figure 4.5: 3D AFM image of VO_2 at 500°C (top) and 550°c (bottom)

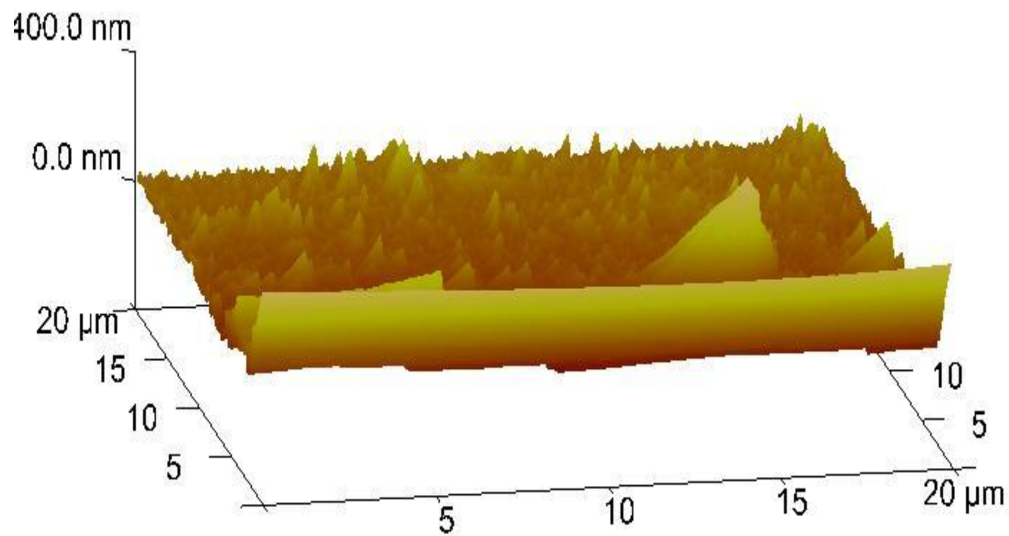

UNIVERSITY of the
WESTERN CAPE

Figure 4.6: 3D AFM image of VO2 thin film at 600°C.

The trend of the surface roughness of VO_2 thin films with respect to the substrate temperatures is shown below in figure 4.7. It is observed that the films are smooth at low temperature (≤550°C) and become rough at higher values (≥550°C). More precisely, the average surface roughness s_{rms} increases by approximately an order of magnitude.

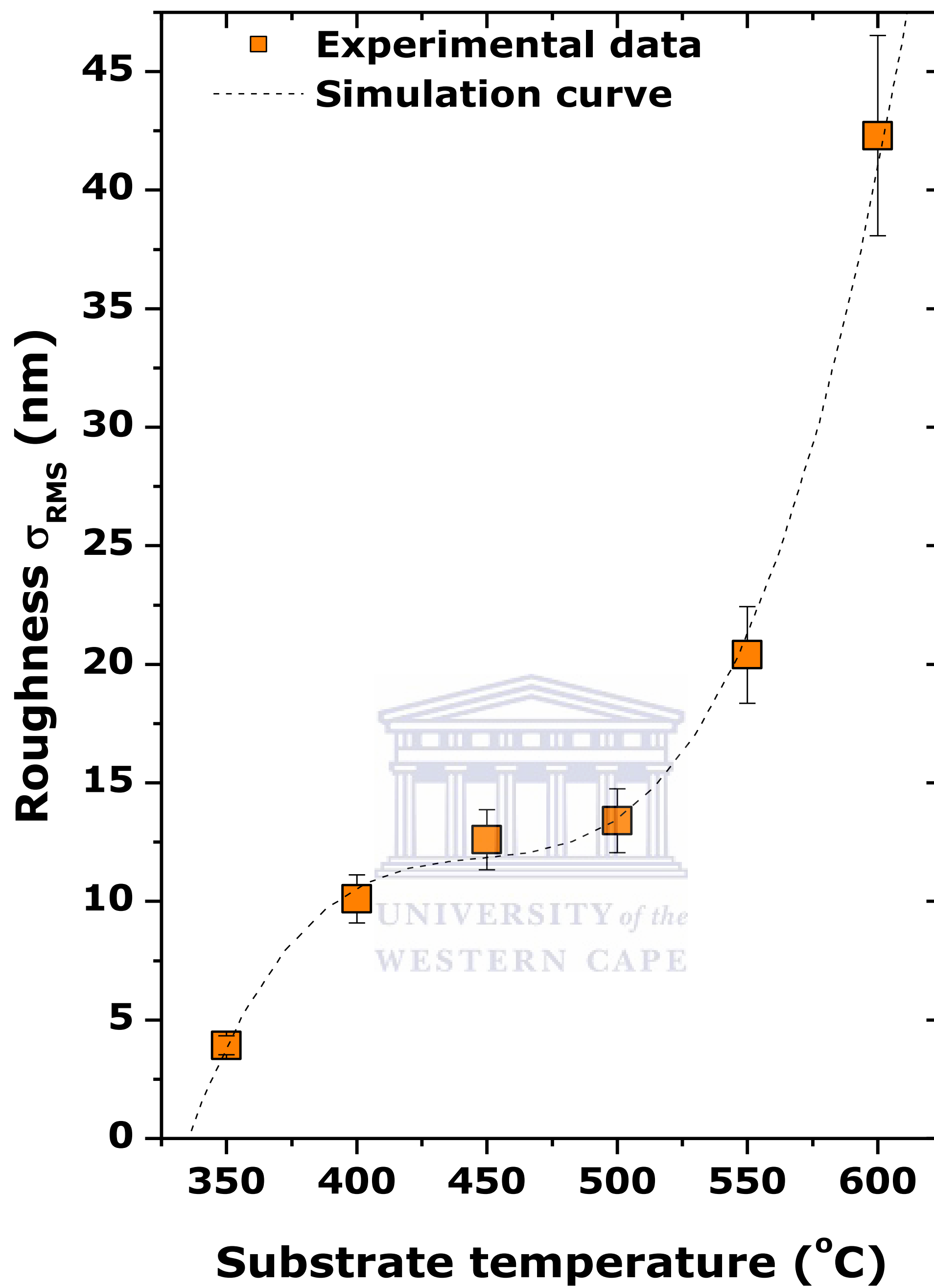

UNIVERSITY of the
WESTERN CAPE

Figure 4.7: Dependence of roughness on substrate temperature of VO_2 thin films.

The 3D AFM images of VO_2 revealed strong correlation between the surface morphology and average crystallite size formation with the substrate temperature. The surface roughness of the VO_2 thin films increases with the substrate temperature due to the nucleation of the glass substrate and coalescence of island formation followed by the polycrystalline island formation [3, 4]. Roughness of polycrystalline thin films increases most noticeably at a glass substrate temperature higher than 570°C as reported reported by Ngom et al [5], this fit well with the trend of roughness at substrate temperatures observed at temperatures above 550°C as shown in figure 4.7.

4.2.3 Stoichiometry and composition of the films.

UNIVERSITY of the
WESTERN CAPE

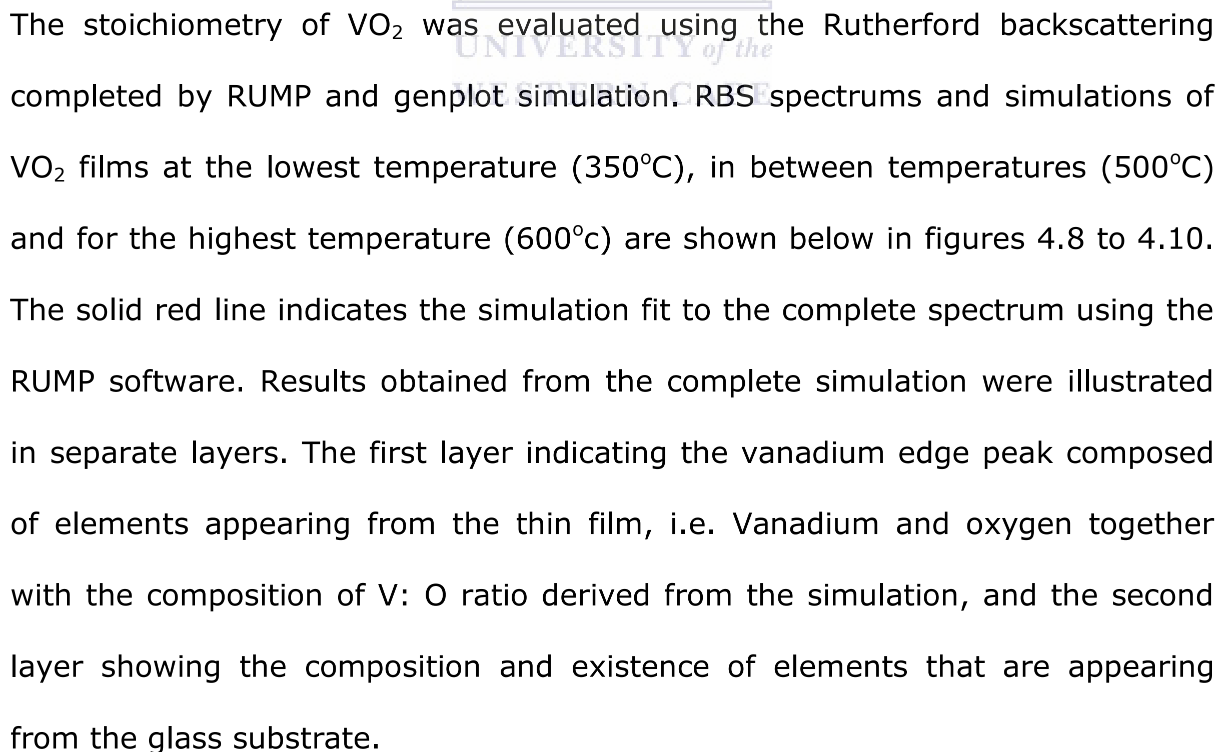

The stoichiometry of VO_2 was evaluated using the Rutherford backscattering completed by RUMP and genplot simulation. RBS spectrums and simulations of VO_2 films at the lowest temperature (350°C), in between temperatures (500°C) and for the highest temperature (600°c) are shown below in figures 4.8 to 4.10. The solid red line indicates the simulation fit to the complete spectrum using the RUMP software. Results obtained from the complete simulation were illustrated in separate layers. The first layer indicating the vanadium edge peak composed of elements appearing from the thin film, i.e. Vanadium and oxygen together with the composition of V: O ratio derived from the simulation, and the second layer showing the composition and existence of elements that are appearing from the glass substrate.

Table 4.1 shows the thickness and compositions from the vanadium edge layer at various substrate temperatures from the RBS simulations, normalized to the composition of oxygen.

The stoichiometry of the thin films slightly deviates from the VO_2 matrix. However considering the challenges that arises with doing simulations on glass substrates and that no oxygen resonance measurements were done, ERDA measurements may give a better insight on the elemental analysis and composition of the thin films.

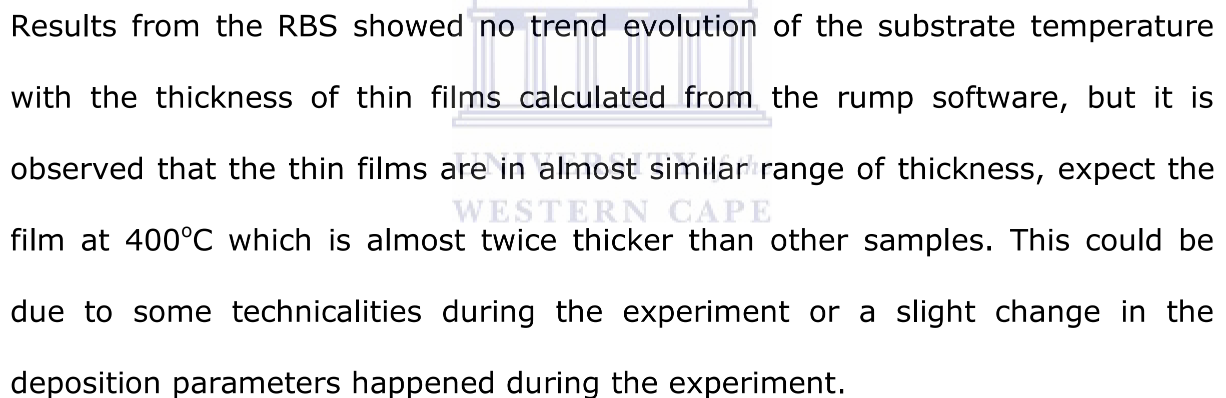

UNIVERSITY of the
WESTERN CAPE

Results from the RBS showed no trend evolution of the substrate temperature with the thickness of thin films calculated from the rump software, but it is observed that the thin films are in almost similar range of thickness, expect the film at 400°C which is almost twice thicker than other samples. This could be due to some technicalities during the experiment or a slight change in the deposition parameters happened during the experiment.

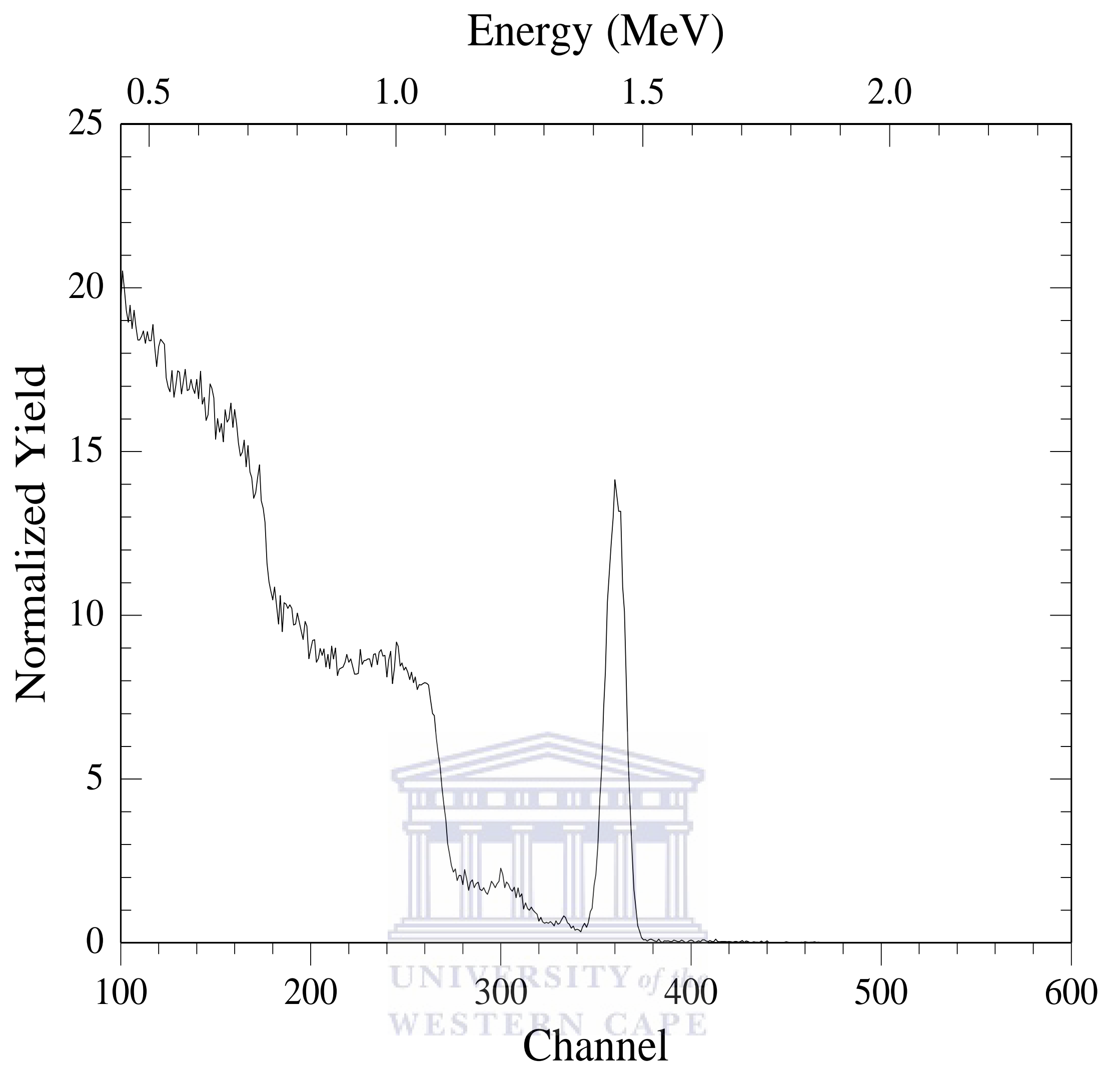

UNIVERSITY of the
WESTERN CAPE

Figure 4.8: RBS spectrum of VO_2 at 350°C

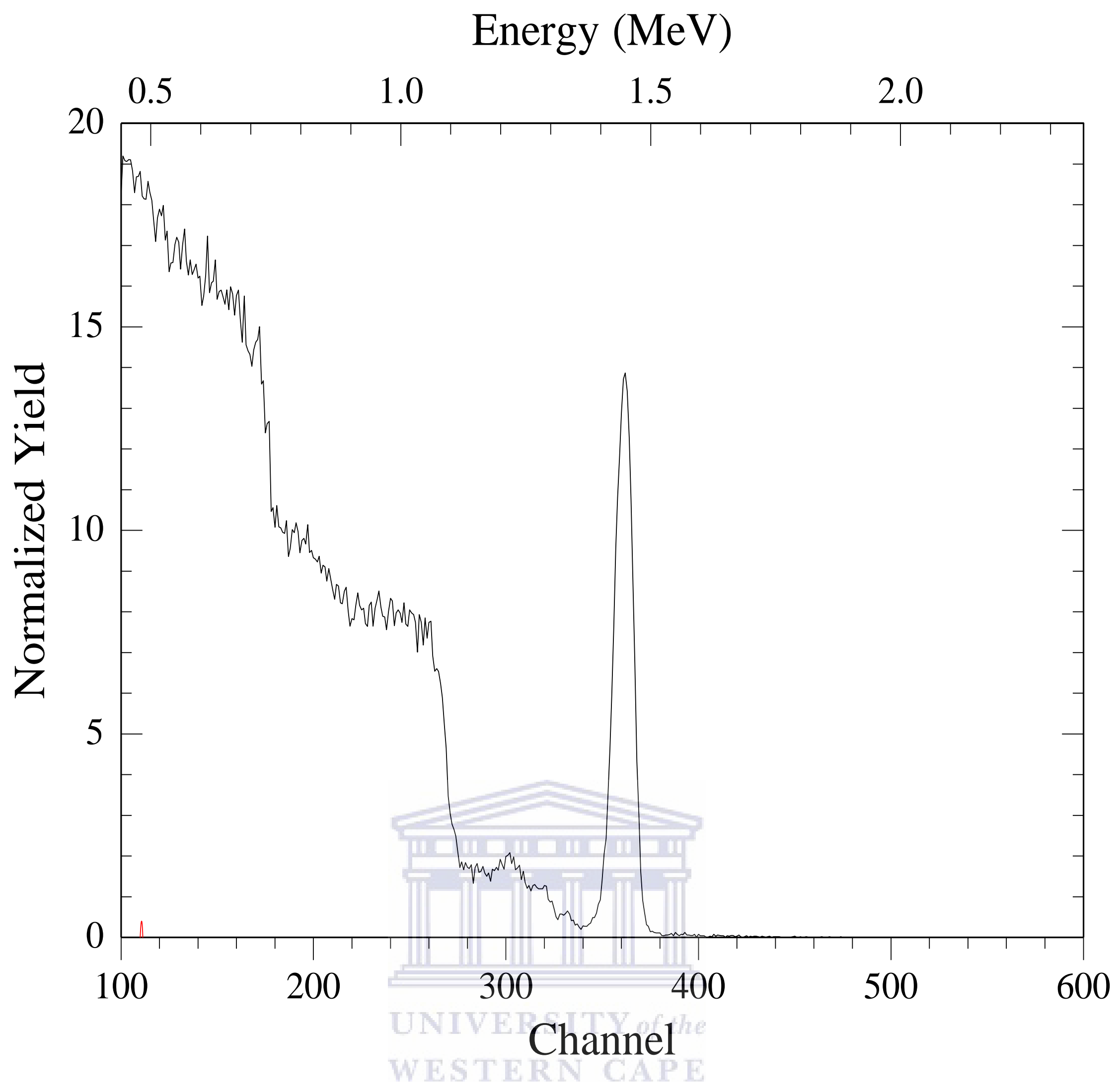

UNIVERSITY of the
WESTERN CAPE

Figure 4.9: RBS spectrum of VO_2 at 500°C

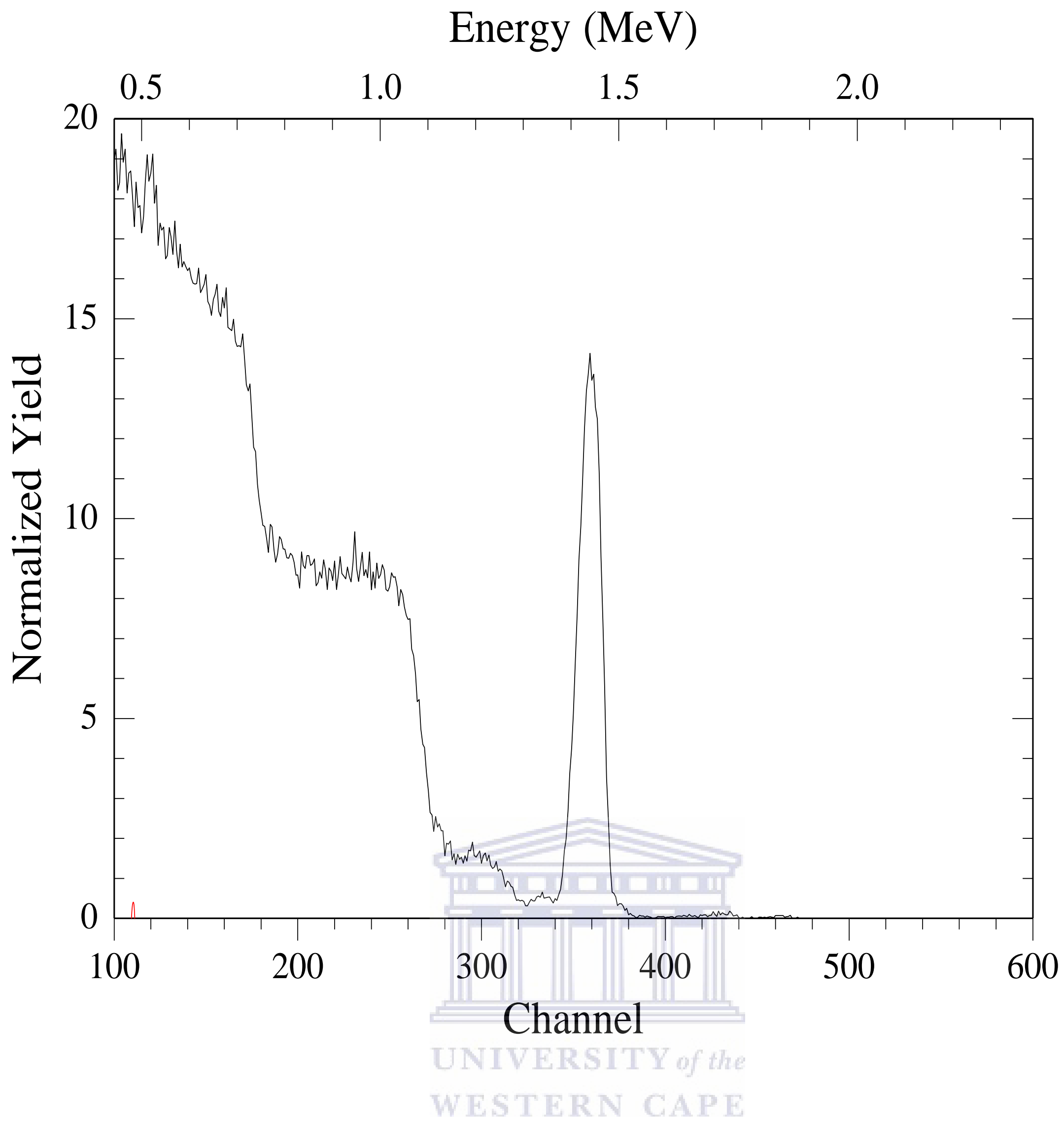

UNIVERSITY of the
WESTERN CAPE

Figure 4.10: RBS spectrum of VO2 at 600°C

Substrate temp (^oC)	Thickness (nm)	Composition
350	53.2	V: 0.77, O: 2.0
400	111.1	V: 0.9, O: 2.0
500	53.7	V: 0.76, O: 2.0
550	45.2	V: 0.9, O: 2.0
600	66.3	V: 0.76, O: 2.0

UNIVERSITY of the
WESTERN CAPE

Table 4.1: Thickness and composition of VO_2 thin films at different substrate temperatures obtained from the RBS simulations.

4.2.4 Elemental Analysis and depth profiling of thin films.

The samples were analyzed at the iThemba LABS (Gauteng) 6mV tandem accelerator using a 25.85 MeV $^{63}Cu^{7+}$ beam at a grazing incidence angle of 14° to the sample surface. The energy of the scattered recoils was measured using a mass-dispersive Time of Flight (ToF) spectrometer mounted at an angle of 30° to the beam axis. A direct energy-depth conversion algorithm was used to calculate elemental depth profiles from the measured energy spectra.

Figures 4.11 – 4.13 show the calculated depth profiles. The oxygen depth profile continues into the substrate since the latter contains mostly silica. The thickness of the as-deposited films was then estimated by a sigmoidal curve edge fit to the vanadium profile.

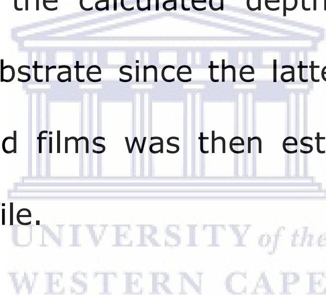
UNIVERSITY of the
WESTERN CAPE

AFM measurements showed that the samples were generally rough and the roughness increased substantially as the deposition temperature increased; from 3.9 nm at 350°C to 41 nm at 600°C. Roughness is known to be one of the main causes of low energy tailing in energy spectra; and this tailing can in turn lead to false broadening of depth profiles at interfaces [6, 7].

The broad edges observed in the (vanadium) profiles below are most likely due to sample roughness as no annealing was done to cause any intermixing between substrate and deposited film.

For all the VO_2 thin films at different substrate temperatures, it was observed that the vanadium ions deeply penetrate into the substrate [8], probable diffusion of vanadium onto the layer of SiO_2 native and the silicon ions diffuse into VO_2 layer however this statement need more details and study to conclude in regard to it.

A large interface region/layer is formed; observed at 400 x 10^{15} at/cm^2 for the film at 350°C, 300 x 10^{15} at/cm^2 for the film at 500°C and 450 x 10^{15} at/cm^2 for the film at 600°C.

UNIVERSITY of the
WESTERN CAPE

Table 4.2 shows the thickness estimated from the ERDA depth profiling comparing them with the ones estimated from the RBS. Thickness obtained from the ERDA analysis does correlate with RBS.

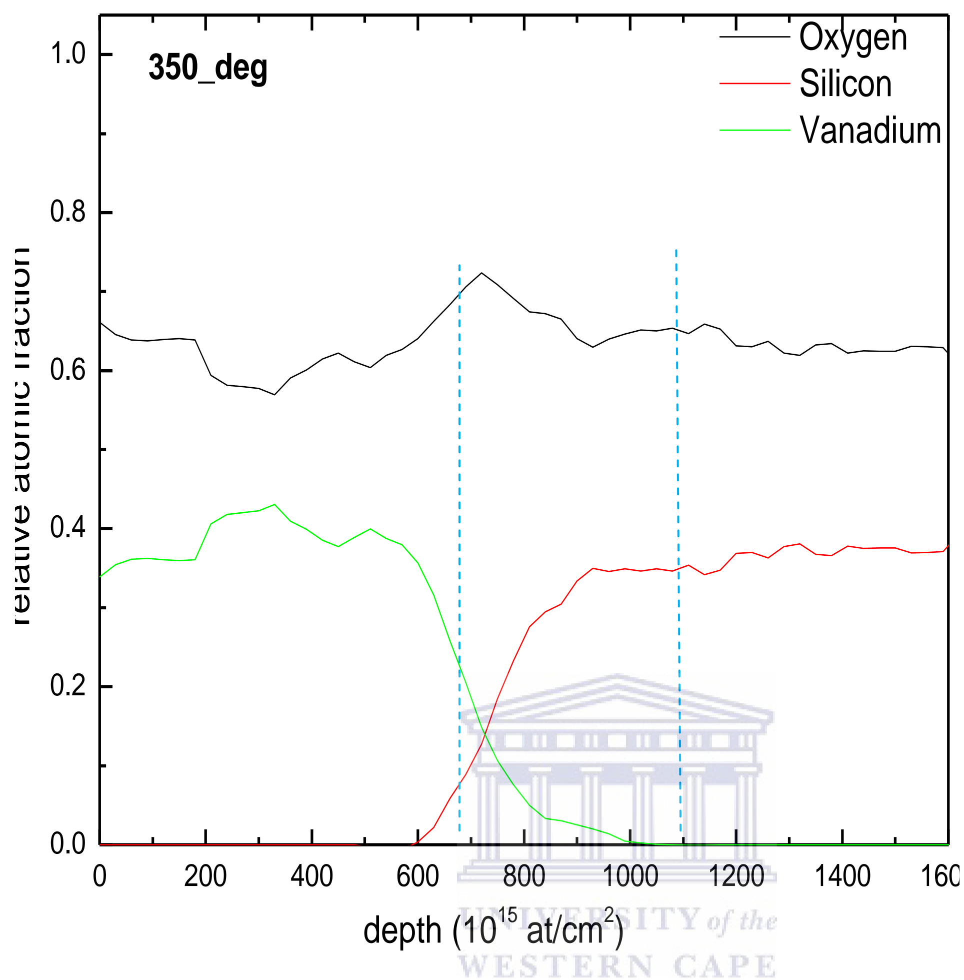

UNIVERSITY of the
WESTERN CAPE

Figure 4.11: Vanadium edge fit (701±110) x 10^{15} at/cm^2 of VO_2 film at 350^0C.

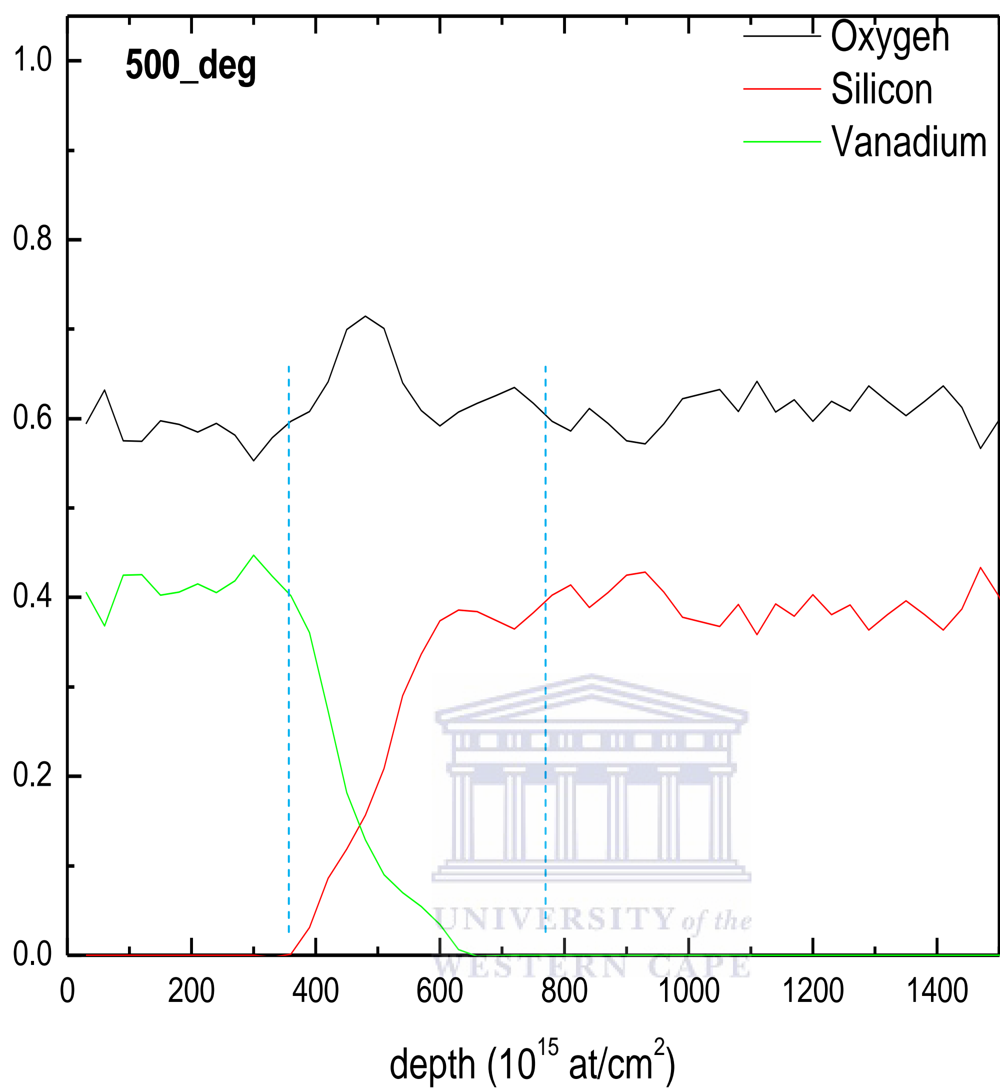

UNIVERSITY of the
WESTERN CAPE

Figure 4.12: Vanadium edge fit (450±90) x 10^{15} at/cm^2 of VO_2 film at 500^0C.

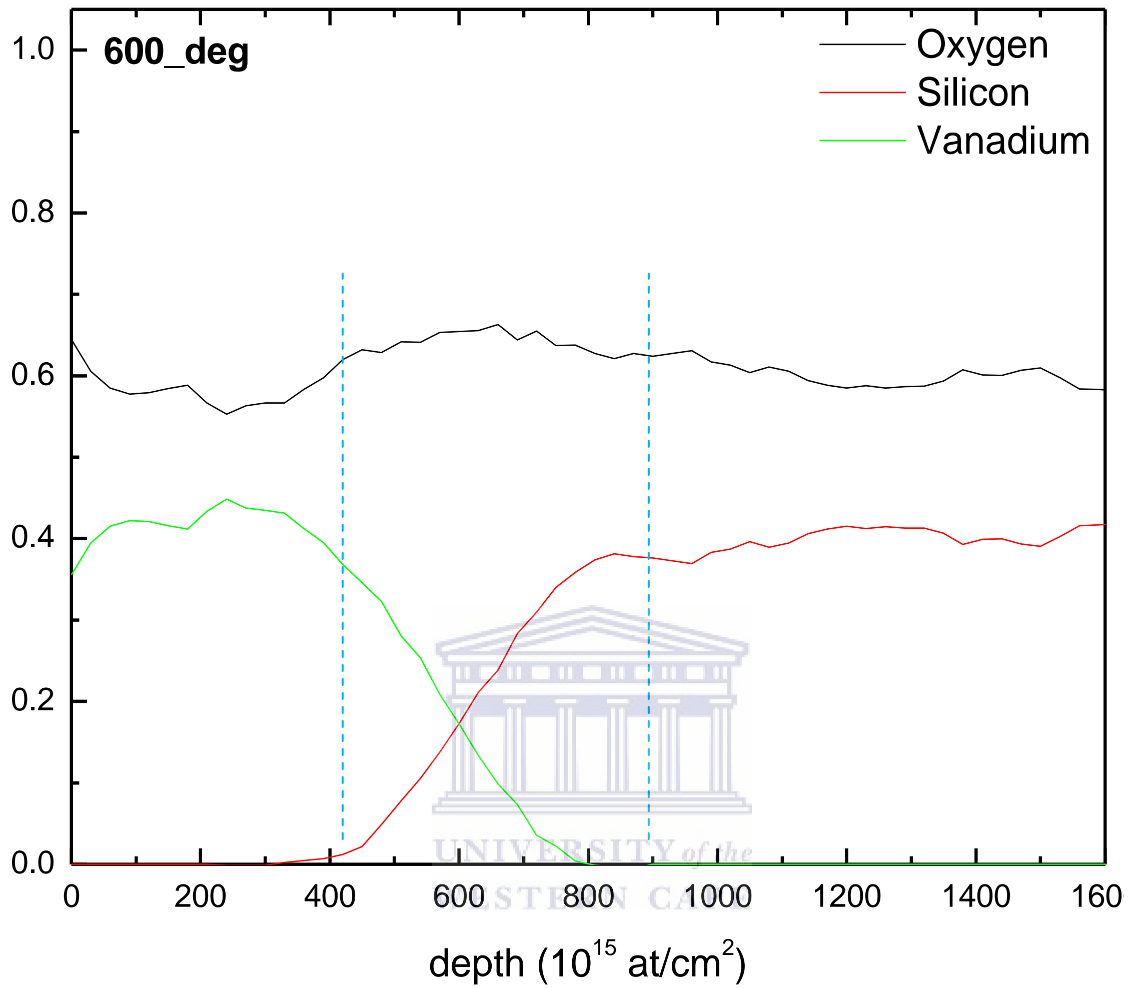

UNIVERSITY of the
WESTERN CAPE

Figure 4.13: Vanadium edge fit (557±120) x 10^{15} at/cm^2 of VO_2 film at 600^0C.

Substrate temp (°C)	RBS thickness (at/cm^2)	ERDA thickness (x 10^{15} at/cm^2)
350	530	701±110
400	1106	1067± 140
500	535	450±90
550	450	409±90
600	660	557±120

UNIVERSITY of the
WESTERN CAPE

Figure 4.2: Comparison of ERDA and RBS thickness

4.2.5 Optical properties

The optical properties were evaluated by the UV-vis at a wavelength of 1100 nm. Figure 4.20 shows the spectral transmission of VO_2 films at substrate temperatures from 350 to 600^0C, between the semiconductor (25^0C) and metallic state (100^0C). The film sputtered at 400^oC showed the best switching mechanism as it displayed a large contrast in transmittance between the semiconductor and metallic state.

The transition temperature $T_{tr,}$ temperature modulation and hysteresis loop were all investigated by the cycling process between heating and cooling branches using the UV-Vis to measure the transmission of the films.

The temperature modulation was defined as the change in maximum and minimum transmittance (ΔT%) of both the cooling and heating branches. Hysteresis loop (ΔT^oC) was defined as the temperature width of the transition temperatures between heating and cooling. The temperature corresponding to the midpoint of the hysteresis loop was then defined as the characteristic transition temperature (T_{tr}) of the SMT [9, 10, 11, 12].

Figure 4.15 shows the cycling branches of VO_2 between heating and cooling at steps of 5^oc using λ=1100 nm from 25^oC to 100^oC.

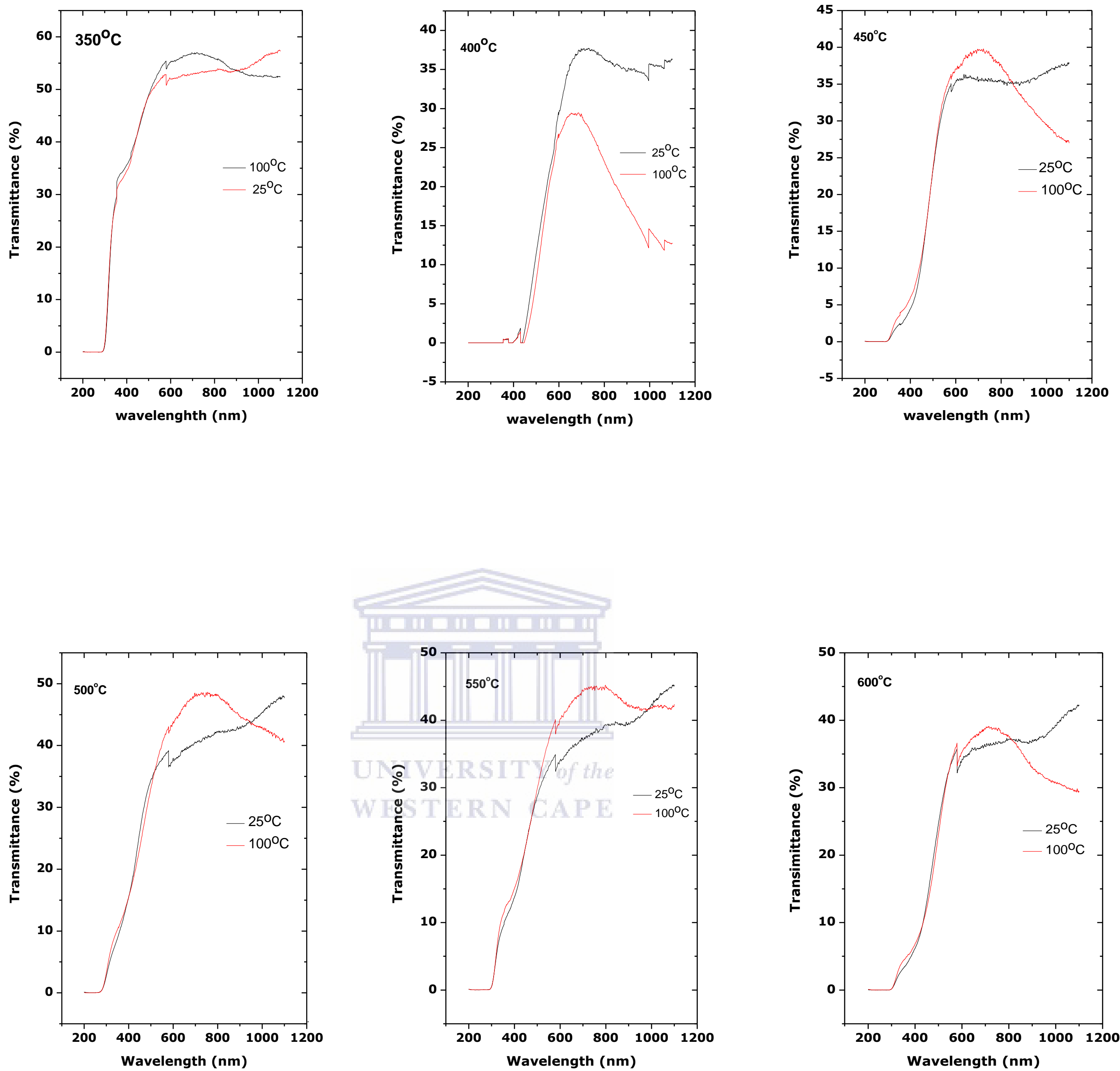

UNIVERSITY of the
WESTERN CAPE

Figure 4.14: Spectral transmission of VO_2 films at 350-600°C.

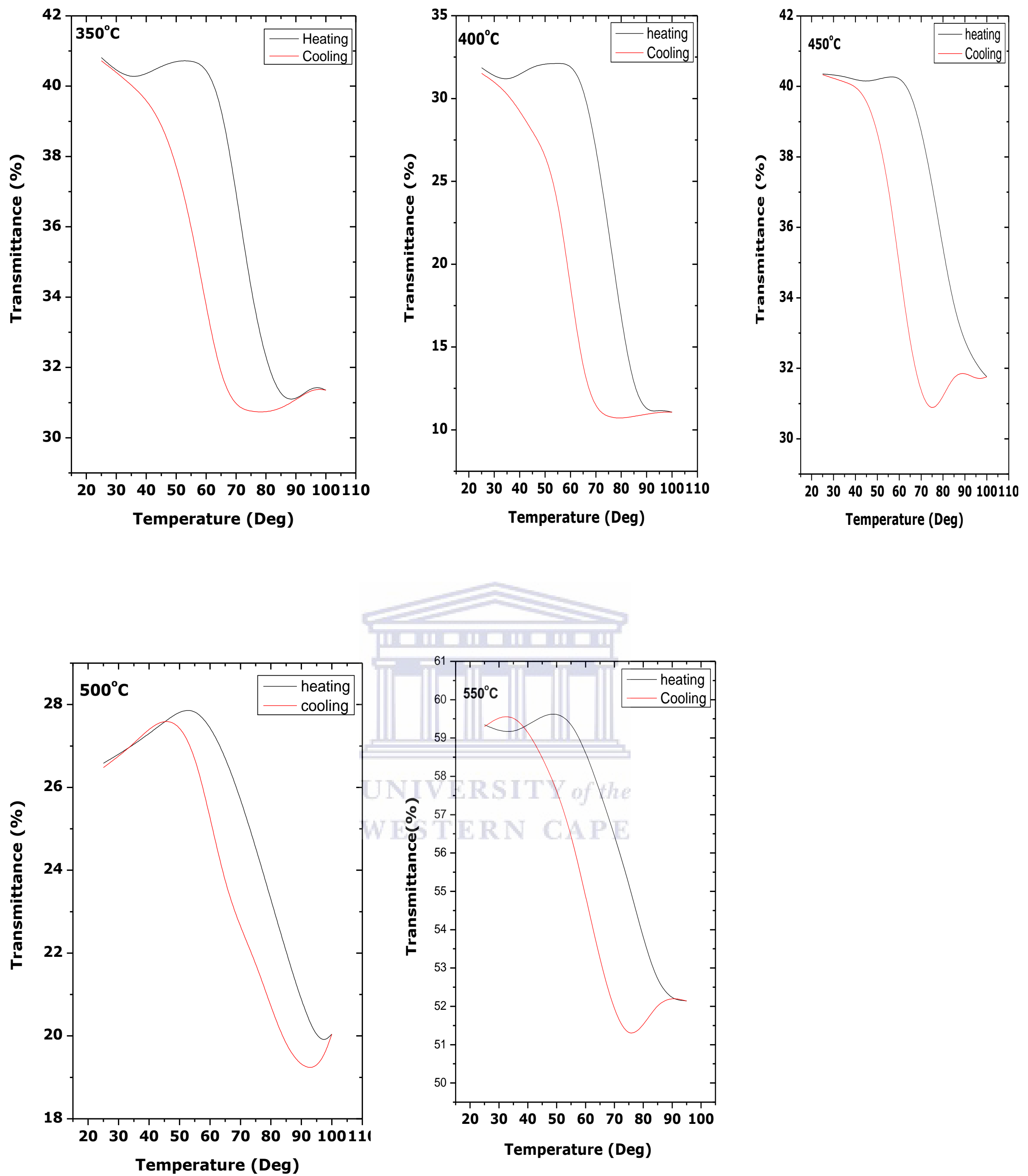

UNIVERSITY of the
WESTERN CAPE

Figure 4.15 Cycling branches of VO_2 between heating and cooling at steps of 5°c using λ=1100 nm from 25°C to 100°C.

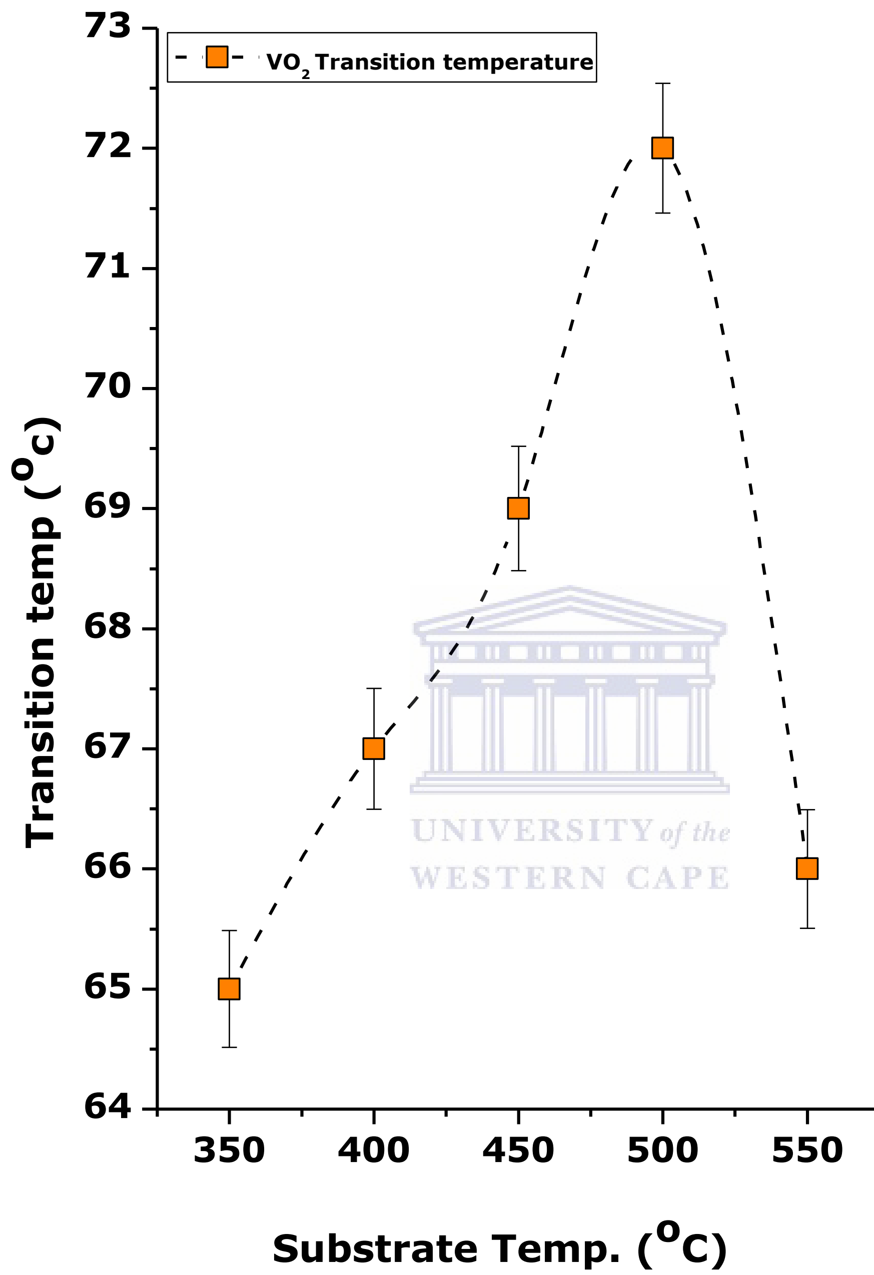

UNIVERSITY of the
WESTERN CAPE

Figure 4.16 Trend of the transition temperature (T_{tr}) with the substrate temperature.

The substrate's temperature was found to affect in a reproducible the following parameters of the VO_2 coatings; the modulation (ΔT) was found to be about 20% at λ= 1100 nm, the hysteresis width varying within the range of 12-20 ^{o}C. The films gave a transition temperature (T_{tr}) in the range between 65 –72^{0}C. High transmittance was observed in T_{tr} lower than 68^{0}C. As the temperature increases highly towards 100^{0}C, transmittance decreases to smaller percentage and remain almost constant when temperature is further increased to extreme values.

UNIVERSITY of the
WESTERN CAPE

Figure 4.16 shows the trend of the transition temperature (T_{tr}) with the substrate temperature. The behavior of T_{tr} in the SMT of VO_2 has been strongly reported to be affected by the crystallite size evolution, stoichiometry, and stress related with-in the thin films [13].

The temperature variation of the average transition temperature $<T_{tr}>$ goes through maxima at substrate temperature 500^{0}C. These maxima could be related to the growth evolution in crystallite size observed in the XRD spectra of VO_2 (011) reflection. Increase in grain distribution in vanadium dioxide thin films causes nucleation on the substrate surface, resulting in the thin films to go through maxima of at high deposition temperatures [14].

4.3 Referrences

[1] R. Carel. Grain growth and texture evolution in thin films, Phd, MIT, (1995).

[2] V. Msomi, O. Nemraoui, S Afr J Sci, Vol. 106, pg1-4, (2010).

[3] I. Petrov, P. B. Barna, L. Haitman, J. E. Greene, J.Vac.sci. Technology. A21(5), (2003).

[4] B. W. Sheldon, K. H. A. Lau, A. Rajaman. J. Appl. Phys., Vol. 90, No. 10, (2001)

[5] B. D. Ngom, M. Charker, N. Manyala, B. Lo, M. Maaza, A. C. Beye. Appl. Surface Science, 257, (2011) 6226-6232 .

[6] L. kritikos. Mater. Sci. Eng. 201,9334-9339 (2007).

[7] Yesil et. al Nucl. Instr. Meth B Vol 136-138 (1998) pg 623

[8] B. G. Chae, D. H Youn, H, T. Kim, S.L. Maeng, K. Y. Kang. J. Korean physical society. Vol 44, 4 (2004) 884-888

[9] A. R. Begishev, G. B Galiev, A. S Ignat'ev, V. G. Mokerov, V. G Poshin. Sov phys solid state. 20(6) (1978) 951

[10] P. Jin, K. Yoshimura, S Tanemura. J Vac Sci Technol A 15(3) (1997) 1113.

[11] M. A. Sobhan, R. T. Kivaisi, B. Stjerna, C. G. Granqvist. SPIE 2255 (1994) 423.

[12] M. E. Samiji. Preparation and characterization of vanadium dioxide thin films. M.Sc desertation, University of Dar es salaam. (1997)

[13] V. G. Golubev et al., Appl. Phys. Lett.,79, (2001)13

[14] R. A. Aliev, V. A. Klimov. Phys sloid state. Vol 46, 3 (2004) 532-536

UNIVERSITY of the
WESTERN CAPE

CHAPTER 5

5.1 Conclusions

Pure Vanadium dioxide thin films were successfully prepared on glass substrates by inverted cylindrical magnetron sputtering. ICMS is a good deposition technique for VO_2 thin films. The effect of the substrate temperature on the crystallinity, morphology and optical properties of VO_2 thin films was well investigated. The crystallinity of the films and the surface morphology were observed to be substrate temperature dependent.

Deposition at high substrate temperature contributed to large grains growth and textured of the VO_2 thin films. Optical transmission of VO_2 films is higher for T_{tr} < 68°C, While the various films do exhibit a good optical modulation in the NIR, there might be stress / strain phenomena related to the thin films. If so, the relaxation is taking place at about 500°C. Future investigations would focus on the possible strain/stress on the VO_2 nano-crystals and carry out the efficiency of these nano-crystals in the far infrared.

UNIVERSITY of the
WESTERN CAPE

5.2 Future work

Future work will include investigations on comparative study between two physical deposition methods; physical laser deposition method (PLD) and sputtering method carrying out optical properties in the near infrared also in the far infrared, with the objective of investigating stress/ strain phenomena in VO_2 thin films. The trend of T_{tr} is a complex phenomenon. Microstructures, crystallites and stress related to the thin films play a major role to the behavior of the characteristic temperature in the SMT of $VO_{2,}$ this comparative study will

also directly be focused on the physics and influences of T_{tr} in the reversible semiconductor-metal transition of VO_2 thin films around 68°C.

Part of future work will also include synthesizing the VO_2 thin films; carry out electrical properties investigate the trend of resistivity as a function of temperature, thereafter irradiate the thin films on different dozes, checking the effects of irradiations by protons on the thin films, comparing with the non-irradiated film to see if there will be changes observed in key factors, such as transition temperature of VO_2 thin film. Irradiation on the thin films will be based on VO_2 for space application, to see how the films will behave when damaged or subjected to harsh conditions.

UNIVERSITY of the
WESTERN CAPE